NASA CONTRACTOR REPORT

NASA CR-2145

NASA CR-2145

DEVELOPMENT OF LIGHTWEIGHT ALUMINUM COMPRESSION PANELS REINFORCED BY BORON-EPOXY INFILTRATED EXTRUSIONS

by Paul A. Roy, John A. McGinnis, and Jim Henshaw

Prepared by
AVCO CORPORATION
SYSTEMS DIVISION
Lowell, Mass. 01851
for Langley Research Center

NATIONAL AERONAUTICS AND SPACE ADMINISTRATION • WASHINGTON, D. C. • JANUARY 1973

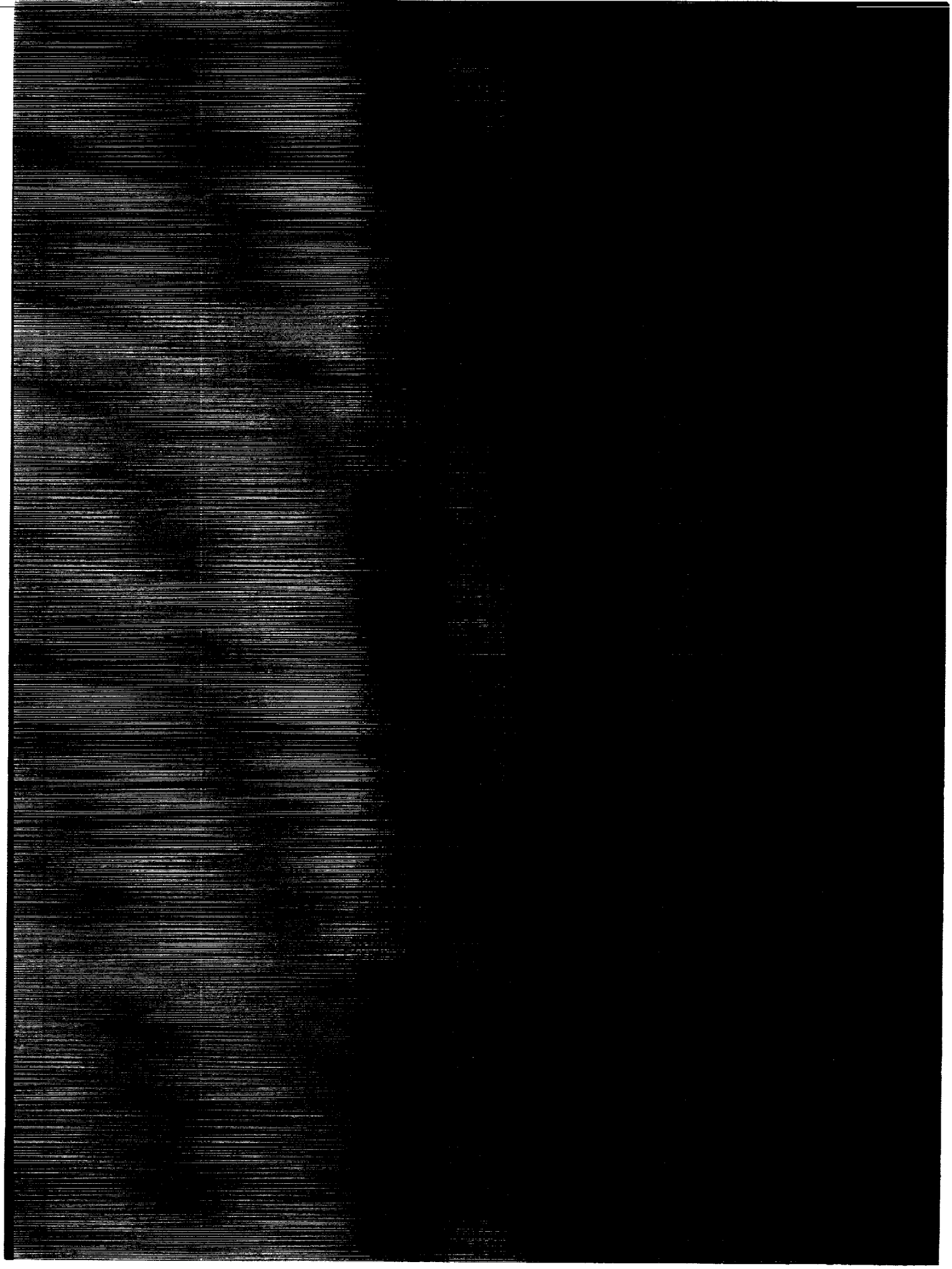

1. Report No.	2. Government Accession No.	3. Recipient's Catalog No.
NASA CR-2145		

4. Title and Subtitle	5. Report Date
DEVELOPMENT OF LIGHTWEIGHT ALUMINUM COMPRESSION PANELS REINFORCED BY BORON-EPOXY INFILTRATED EXTRUSIONS	January 1973
	6. Performing Organization Code
7. Author(s)	8. Performing Organization Report No.
PAUL A. ROY, JOHN A. McELMAN AND JIM HENSHAW	
9. Performing Organization Name and Address	10. Work Unit No.
AVCO CORPORATION SYSTEMS DIVISION LOWELL, MASSACHUSETTS 01851	114-08-01-03
	11. Contract or Grant No.
	NAS1-9938
12. Sponsoring Agency Name and Address	13. Type of Report and Period Covered
NATIONAL AERONAUTICS AND SPACE ADMINISTRATION WASHINGTON, D.C. 20546	CONTRACTOR REPORT
	14. Sponsoring Agency Code

15. Supplementary Notes

16. Abstract

Analytical and experimental studies were performed to evaluate the structural efficiencies afforded by the selective reinforcement of conventional aluminum compression panels with unidirectional boron epoxy composite materials. A unique approach for selective reinforcement was utilized called "boron/epoxy infiltration." This technique uses extruded metal sections with preformed hollow voids into which unidirectional boron filaments are drawn and subsequently infiltrated with resin to form an integral part.

Simplified analytical models were developed to investigate the behavior of stiffener webs with reinforced flanges. Theoretical results are presented demonstrating the effects of transverse shear, of the reinforcement, flange eccentricity and torsional stiffness in such construction. A series of 55 tests were conducted on boron-infiltrated rods and extruded structural sections. Test results indicate that adequate compression strength can be developed in short stiffener lengths and that longer sections possess some postbuckling strength. Agreement between buckling predictions from simplified theoretical models and experiment was fair with some discrepancies attributed to difficulties in testing.

Results obtained from optimization studies indicate that high structural efficiencies, superior to that attainable with 7075-T6 aluminum, can be realized by selectively reinforcing grades of aluminum not normally considered prime aerospace structural materials. Design trade-off studies for compression panels using selectively reinforced 6005-T5 aluminum sections exhibited weight savings ranging from a low of 6% over equivalent all 7075-T6 aluminum panels to greater than 26% when compared to equivalent 2024 aluminum designs.

The program concluded with the design and fabrication of a full-scale infiltration reinforced test panel which was delivered to the NASA Langley Research Center for final proof testing. This panel complete with load introduction bays, consisted of an aluminum skin stiffened by eleven equally space, selectively reinforced 6005-T5 aluminum NACA "Y" stiffeners.

17. Key Words (Suggested by Author(s))	18. Distribution Statement
COMPOSITE-REINFORCED PANEL STIFFENED PANEL BUCKLING COMPRESSION	UNCLASSIFIED - UNLIMITED

19. Security Classif. (of this report)	20. Security Classif. (of this page)	21. No. of Pages	22. Price*
UNCLASSIFIED	UNCLASSIFIED	126	$3.00

*For sale by the National Technical Information Service, Springfield, Virginia 22151

TABLE OF CONTENTS

	PAGE
SUMMARY	1
INTRODUCTION	1
BUCKLING OF COMPOSITE REINFORCED STIFFENERS	7
Effect of Flange Flexural Rigidity	9
Effect of Flange Transverse Shear Stiffness	11
Effect of Flange Torsional Stiffness	12
Effect of Flange Eccentricity	14
REINFORCED STIFFENER COMPRESSION PANEL DESIGN STUDIES	17
Parametric Design Studies	18
Preliminary Design Concepts	21
Design of Boron Epoxy Reinforced Proof Test Compression Panel	23
Panel Fabrication and Weight Summary	25
ELEMENT TESTING	27
Infiltration Reinforced Rod Tests	27
Reinforced Stiffener Tests	29
Experimental and Analytical Correlation	31
Proof Test of NACA Y Sections	34
CONCLUSIONS	37
APPENDIXES	39
REFERENCES	51

LIST OF ILLUSTRATIONS

Figure 1 Elastically Supported Plate - Stiffener Model 64

2 Effect of Flexural Rigidity Factor θ on Stress Factor ψ [C/Db = 2.0 Q* = 0.0] 65

3 Effect of Flexural Rigidity Factor θ on Web Buckling Coefficients K_w [C/Db = 2.0 Q* = 0.0] 66

4 Effect of Flexural Rigidity Factor θ on Stress Factor ψ [C/Db = 2.0 Q* = 0.1] 67

5 Effect of Flexural Rigidity Factor θ on Stress Factor ψ [C/Db = 2.0 Q* = 0.25] 68

6 Effect of Flexural Rigidity Factor θ on Stress Factor ψ [C/Db = 2.0 Q* = 0.5] 69

7 Effect of Flange Transverse Shear Stiffness Factor Q* on Web Buckling Coefficient K_w [θ = 50, C/Db = 2] 70

8 Effect of Flange Torsional Rigidity (C/Db) on Web Buckling Coefficient K_w [θ = 20, Q* = 0] 71

9 Effect of Flexural Rigidity Factor θ on Stress Factor, ψ [C/Db = 10, Q* = 0] 72

10 Effect of Flexural Rigidity Factor θ on Stress Factor, ψ [C/Db = 25.0 Q* = 0.0] 73

11 Effect of Flexural Rigidity Factor θ on Stress Factor, ψ [C/Db = 75.0, Q* = 0.0] 74

12 Web Buckling Coefficient for Long Stiffener Section [S = 1.0] 75

13 Web Buckling Coefficient for Long Stiffener Section [S = 2.0] 76

14 Web Buckling Coefficient for Long Stiffener Section [S = 3.0] 77

15 Flange Eccentricity Parameter 78

16 Stiffened Panel Weight versus Percent of Boron Epoxy Reinforcement 79

17 Stiffened Panel Weight versus Stiffener Pitch-Selectively Reinforced "Y" Stiffener 80

LIST OF ILLUSTRATIONS (Cont'd)

Figure 18 Stiffened Panel Weight versus Stiffener Pitch-Selectively Reinforced "T" Stiffeners 81

19 Stiffened Panel Weight versus Stiffener Pitch-Selectively Reinforced Hat Stiffeners 82

20 Comparison of Selectively Reinforced Compression Panels with Conventional Aluminum Panels 83

21 Preliminary Design Concepts 84

22 Infiltration Reinforced Proof Test Panel 85

23 Assumed Local Instability Failure Modes 86

24 Schematic Showing Local Bending in Load Introduction Fittings 87

25 Final Milling of 7075-T6 Header 88

26 Stringer Nominal Dimensions 89

27 Trimming of Stringer Flanges 90

28 Partially Completed and Completed Stringers 91

29 Skin Thickness Measurement Grid and Stringer Identification 92

30 Panel Being Prepared for Riveting 93

31 Completed Panel Showing Skin Surface 94

32 Completed Panel Showing Stringers 95

33 Compression Test Fixture 96

34 Boron Epoxy Infiltrated Thick Wall 6061-T6 Aluminum Rods t = 0.031 97

35 Boron Epoxy Infiltrated Chem-Milled 6061-T6 Aluminum Rods t = 0.015 98

36 Typical Load Deflection for Rod Flexure Specimen 99

37 Extruded 6005-T5 Aluminum "T" 100

38 Reinforced Stringer Test Sections 101

LIST OF ILLUSTRATIONS (Concl'd)

Figure 39 Typical Cross Sections for Sub-Element Test Sections 102

40 Typical Element Compression Test Setup 103

41 Load versus Strain - Specimen WR-L-1 104

42 Load versus Strain - Specimen T-S-2 105

43 Load versus Strain - Specimen T-S-2 106

44 Load versus Strain - Specimen T-L-1C 107

45 Load versus Strain - Specimen L-S-1 108

46 Load versus Strain - Specimen L-L-1 109

47 Typical Failures for 24 inch "T" and "L" Sections Showing Local Flange Buckling 110

48 Elements NACA - Y-1, -2 and -3 111

49 Element NACA - Y-4 111

50 Failed Test Sections 112

51 NACA - Y-2 Load-Strain Curve 113

52 NACA - Y-2 Load-Strain Curve 114

53 NACA - Y-3 Load-Strain Curve 115

54 NACA - Y-4 Load-Strain Curve 116

A-1 Elastically Supported Plate-Stiffener Model 117

B-1 Plate Geometry and Coordinate System 118

C-1 Plate-Stiffener Configuration 119

C-2 Plate-Stiffener Equilibrium Diagram 119

LIST OF TABLES

Table 1 Comparison of Selectively Reinforced All Aluminum Compression Panels (N_x = 7200 lb/in, Length = 48", Width = 36") 53

2 Test Panel Weight Summary 54

3 Panel Design Data Summary 55

4 Infiltration Reinforced 6061-T6 Aluminum Tubing -- Specimen Geometry 56

5 Infiltration Reinforced 6061-T6 Aluminum Tubing -- Compression Test Results 57

6 Infiltration Reinforced 6061-T6 Tubing -- Column Test Results 58

7 Infiltration Reinforced 6061-T6 Aluminum Tubing -- Flexure Test Results 59

8 Sub-Element Test Summary 60

9 Sub-Element Analytical-Experimental Correlation 61

10 Test Element Design Parameters 62

11 Summary of NACA-Y Test Data 63

SUMMARY

Analytical and experimental studies were performed to evaluate the structural efficiencies afforded by the selective reinforcement of conventional aluminum compression panels with high performance unidirectional boron epoxy composite materials. In this evaluation a unique approach for selective reinforcement was utilized; called "boron/epoxy infiltration". This technique uses extruded metal sections with preformed hollow voids into which unidirectional boron filaments are drawn and subsequently infiltrated with resin to form an integral part.

Simplified analytical models were developed to investigate the behavior of stiffener webs with reinforced flanges. Theoretical results are presented demonstrating the effects of transverse shear of the reinforcement, flange eccentricity and torsional stiffness in such constructions. A series of 55 tests were conducted on boron-infiltrated rods and extruded structural sections. Test results indicate that adequate compression strength can be developed in short stiffener lengths and that longer sections possess some post-buckling strength. Agreement between buckling predictions from simplified theoretical models and experiment was fair with some discrepancies attributed to difficulties in testing.

Results obtained from optimization studies indicate that high structural efficiencies, superior to that attainable with 7075-T6 aluminum, can be realized by selectively reinforcing grades of aluminum not normally considered prime aerospace structural materials. Design tradeoff studies for compression panels using selectively reinforced 6005-T5 aluminum sections exhibited weight savings ranging from a low of 6 percent over equivalent all 7075-T6 aluminum panels to greater than 26% when compared to equivalent 2024 aluminum designs. It was also shown that infiltration reinforced structures can be designed and fabricated using existing technology.

The program concluded with the design and fabrication of a full scale infiltration reinforced test panel which was delivered to the NASA Langley Research Center for final proof testing. This panel complete with load introduction bays, consisted of an aluminum skin stiffened by eleven (11) equally spaced, selectively reinforced 6005-T5 aluminum NACA "Y" stiffeners.

INTRODUCTION

Selective reinforcement of conventional metal structures with unidirectional boron epoxy composite materials has been gaining acceptance in recent months as providing an immediate means of achieving enhanced structural performance in weight/strength critical structures. Fundamental to the success of the approach is that it relies almost entirely upon existing design and fabrication technology. Coupling this with the fact that only limited quantities of the relatively high cost reinforcement are required makes the

selective reinforcement scheme an attractive alternative to an all composite design; particularly for the near term structures. The selective reinforcement concept as originally implemented involved bonding unidirectional composite materials onto existing metal structures at stress or stability critical locations.

A modification to this basic concept which offers numerous practical advantages over simply bonding on strips of reinforcements has been developed at Avco. The technique is called "Boron/Epoxy Infiltration" or simply "Infiltration" and consists of drawing a continuous bundle of collimated boron filaments into voids of preformed metal shapes, and subsequently infiltrating the filament filled voids with resin and curing, to form a quasi-homogeneous structure. One desirable feature of the infiltration approach is that it uses the final part as a mold thereby lending itself directly to the fabrication of complex curved shapes as well as standard straight sections.

This program was formulated to fully explore the structural merits of the infiltration method for selective reinforcement of structures. To provide a means of evaluation, a highly loaded aluminum compression panel stiffened with boron epoxy infiltration reinforced aluminum stiffeners was selected as the final proof test article to be delivered to Langley for testing at the conclusion of the contract.

To accomplish the stated objective the program scope was designed to encompass the key elements required to design and fabricate the panel. This included analytical studies dealing with the design of selectively reinforced stiffeners, parametric design studies for selectively reinforced compression panels over a range of load indicies, sub-element testing on test specimens, and typical stiffener sections, and the final design and fabrication of the test panel. These combined studies showed that infiltration reinforced compression panels were superior to their all-metal counterparts with weight savings of up to 26 percent attainable. Furthermore, it was shown that this increased efficiency can be accomplished using conventional design and fabrication practices.

Full details of the program are presented in the body of this report with detailed analytical derivations included in the Appendixes.

SYMBOLS

A_s	Area of stiffener
a	Length of plate
B	$\left(\frac{E_s I_s}{D}\right)$
b	Width of web
C	Torsional stiffness
C_1, C_2, C_3, C_4, C_5, C_6, C_7, C_8	Arbitrary constants
D	$\frac{Et^3}{12(1-\mu^2)}$ web flexural stiffness
d	Stiffener spacing
E	Young's modulus for web
$E_s I_s$	Flexural stiffness of stiffener with respect to its centroid
$E_F I_F$	Flexural stiffness of stiffener flange with respect to its centroid
$E_s A_s$	Extensional stiffness of beam or stiffener
G	Modulus of rigidity
$G_s A_s$	Transverse shear stiffness of beam or stiffener
$G_s J_s$	Torsional stiffness of beam or stiffener

$k = \frac{m\pi}{a}$	
K_w	Web buckling coefficient
L_Q	Differential operator, $\frac{\partial^2}{\partial x^2}$
m, n	Integers
$\bar{N}_x$	Applied plate load resultant
P	Load applied to beam
Q	Transverse shear parameter $\left[1 + \frac{E_s I_s}{G_s A_s} k^2\right]$
Q^*	$\frac{E_F I_F}{G_F A_F} \frac{1}{b^2}$
Q_1, Q_2	Shear forces
R_1	Outer diameter of metal sheath surrounding voids
R_o	Inner diameter of metal sheath surrounding voids
r	$\frac{Ck^2}{D}$
S	$\frac{EA\ (FLANGE)}{EA\ (WEB)}$
$\bar{S}$	$\frac{E_s A_s}{Etd}$
t	Plate thickness
U(y), V(y)	Functions of spatial coordinate "y" only
u,v,w,	Displacements in x, y, and z directions respectively
$\bar{u}, \bar{v}, \bar{w}, \bar{a}$	Constants
x,y,z	Rectangular Cartesian coordinates

$\bar{z}_s$	Distance from plate middle surface to centroid of stiffener
α	Transverse shear strain
β	$\frac{na}{mb}$
γ_{xz}	Transverse shear strain
ϵ_x	Direct strain in x-direction
η	Web flange stiffness ratio
θ	Flexural rigidity factor, $\frac{E_F I_F}{Db} - S\left(\frac{\psi}{\phi}\right)^2 Q$
λ	$\sqrt{\frac{\bar{N}_x}{Dk^2}}$
μ	Poisson's ratio
ζ	$k\sqrt{\lambda + 1}$
ξ	$k\sqrt{\lambda - 1}$
π_s	Strain energy of stiffener
σ	Stress
ϕ	Web aspect factor $\frac{m\pi b}{a}$
ψ	Web stress factor $b\sqrt{\frac{\sigma_p t}{D}}$

Subscripts

s	Stiffener
p	Plate

BUCKLING OF COMPOSITE REINFORCED STIFFENERS

The technique of selectively reinforcing the flanges of aluminum stiffeners with high strength, high modulus unidirectional boron epoxy composite materials, unquestionably provides an efficient means of increasing the total bending stiffness of a compression panel. This in turn should result in higher panel buckling efficiencies provided the stiffener itself remains stable.

An abundance of design information exists for designing sturdy all-metal stiffeners. A similar situation does not exist for selectively reinforced stiffeners; consequently, it was necessary to examine the stability characteristics of selectively reinforced stiffeners. The sections slated for consideration employed flange reinforcement only. This was predicated on the premise that with a stable skin design, the most efficient stiffeners would be those having the reinforcement as far away from the skin as possible, thereby increasing the panel flexural stiffness.

With stiffeners of this type the primary parameters of interest, as they relate to the stiffener buckling strength, are:

- flange flexural rigidity normal to the web
- flange transverse shear stiffness
- flange eccentricity, and
- flange torsional stiffness.

Premature buckling of stiffeners can occur in either of two modes or a combination thereof. The simplest mode, termed "local buckling", consists of buckling of the stiffener web or flange into a plate mode with no displacement at the flange-web juncture.

The second distinct mode is a "torsional mode" where the entire stiffener twists about its point of attachment to the skin into relatively long waves. A third potential mode and a more likely one for efficiently designed stiffeners is the coupled mode which consists of a coupling of the local and torsional modes where the web buckles in concert with lateral buckling of the flange. This mode is more complex and relies on the interaction between the web and flange for the determination of the ultimate buckling stress.

To evaluate the buckling characteristics of selectively reinforced stiffener sections in the local and combined modes, an analytical model was developed which consisted of an axially compressed plate (simulating the stiffener web) simply supported along the three edges and elastically supported by a beam (flange) along the fourth edge (Figure 1). Fundamentally, the solution obtained follows along the lines of that developed by Windenburg (Ref. 1) with modifications to account for the flange eccentricity and finite transverse shear stiffness. (See Appendix A.)

The solution for the buckling stress results in a complex transcendental expression which can best be expressed in nondimensional form in terms of a stress factor ψ and an aspect factor ϕ as given below:

$$Q\sqrt{\psi-\phi}\,[\psi+(1-\mu)\phi]^2\cot\sqrt{\phi\psi-\phi^2}\;-$$

$$Q\sqrt{\psi+\phi}\,[\psi-(1-\mu)\phi]^2\coth\sqrt{\phi\psi+\phi^2}+2\phi^{5/2}\psi\theta\;+ \qquad (1)$$

$$2Q\phi^{3/2}\psi\frac{C}{Db}\sqrt{\psi^2-\phi^2}\coth\sqrt{\phi\psi+\phi^2}\cot\sqrt{\phi\psi-\phi^2}\;+$$

$$\phi^4\theta\frac{C}{Db}\left[\sqrt{\psi+\phi}\coth\sqrt{\phi\psi+\phi^2}-\sqrt{\psi-\phi}\cot\sqrt{\phi\psi-\phi^2}\right]=0$$

where

$$\psi=b\sqrt{\frac{\sigma_p t}{D}}\;-\;\text{Stress Factor}$$

$$\phi=\frac{m\pi b}{a}\;-\;\text{Web Aspect Factor}$$

$$\theta=\frac{E_F I_F}{Db}-S\left(\frac{\psi}{\phi}\right)^2\quad Q\;-\;\text{Flexural Rigidity Factor}$$

$$Q=1+Q^*\phi^2$$

$$Q^*=\frac{E_F I_F}{GAb^2}\;-\;\text{Transverse Shear Stiffness Factor}$$

$$\frac{C}{Db}=\text{Torsional Stiffness Factor},\ \frac{G_s J_s}{Db}$$

$$S=\frac{EA\ (\text{FLANGE})}{EA\ (\text{WEB})}$$

As shown in Reference 1 this characteristic equation encompasses all solutions for buckling of the web, ranging from a completely free edge solution along the beam boundary to a totally clamped condition at this edge depending upon the beam parameters considered.

To simplify the solution of this equation, curves representing the stress factor ψ as a function of aspect factor ϕ for various values of θ were plotted holding Q^* and C/Db constant as illustrated by Figure 2. Similar curves for other values of transverse shear stiffness factor (Q^*) and torsional stiffness factor (C/Db) plotted in a similar manner are presented in later sections.

The procedure followed in using these curves for a particular case is to calculate the known parameters entering into θ using the stiffener dimensions, then assume a value for (m) the number of half waves to calculate the quantity ϕ. The corresponding value of stress factor ψ can then be determined by trial and error by taking the calculated value of ϕ and an assumed value of θ and then using the appropriate curve to determine a value for ψ. Using this value of ψ the actual θ value is calculated, this procedure is continued until the assumed and calculated values for θ converge. The above procedure is repeated by incrementing m, until the minimum value of ψ is obtained which determines the critical buckling load. Curves of this form were used to evaluate the pertinent stiffener parameters cited earlier, and these results are presented in the following sections.

Effect of Flange Flexural Rigidity

Although the results presented in Reference 1 and extended by Bleich (Ref. 2) for all metal stiffeners are, for the most part, applicable to reinforced stiffeners, they are included here for completeness. The fundamental difference between an all-aluminum flange and a selectively reinforced flange is that the latter will yield significantly higher values of the flexural rigidity factor θ than an equivalent weight all-metal flange. A selectively reinforced flange therefore is more efficient than the all-metal flange from the flexural rigidity standpoint.

To illustrate this point, consider the curves presented in Figure 2, for the case where the edge beam (flange) has infinite transverse shear stiffness ($Q^* = 0$) and a finite value for torsional rigidity factor ($C/Db = 2$). The specific values selected for Q^* and C/Db will not change the conclusions drawn here, as will be seen in later sections.

Examining these curves in detail, one notes that for values of θ above 10 all the curves have a minimum value of ψ at an aspect factor ϕ of approximately $\phi = 3.5$. This minimum value of $\psi = 7$. corresponds to a web buckling coefficient of $K_w = 5.0$, or slightly greater than that obtained for a plate simply supported on all four sides. (Note, if a value of $C/Db = 0$ had been used, indicating that the flange provided no torsional restraint, the buckling coefficient at the minimum in the curves would be equal to $K_w = 4.0$, or that of a simply supported plate. (See Reference 2.)

The general shape of the curves for $\theta \geq 10$ indicates that the buckling mode for the stiffener changes depending upon the stiffener length or more specifically the web aspect factor ϕ which is directly related to length. Taking the curve for $\theta = 20$ as a case in point, one notes that for aspect factors of $\phi > 3.5$ the stress factor $\psi > 7.0$, meaning that the web buckling coefficient will be greater than 5, or in other words, the flange will always provide adequate support to the web such that it buckles into a local mode. As the aspect factor decreases below $\phi = 3.5$, indicating an increase in plate length, web depth being held constant, the flange will still provide full support to the web but will buckle into higher wave numbers (i.e., the minimum value for ψ will remain 7.0). This behavior will continue until an aspect factor of $\phi \approx 1.0$ is reached, at which point a transition from web buckling to overall general instability of the flange normal to the web in the m = 1 mode will occur.

Additional increases in stiffener length will further reduce the buckling strength of the section, since ψ decreases, until at extremely long lengths the buckling stress will be dictated by the amount of torsional restraint provided by the flange to the plate. Theory then predicts that for $\frac{C}{Db} > 0$ the buckling stress will remain constant, and the wave number will begin to increase, however, the failure mode will still be in the beam column mode. A more detailed presentation of the behavior of long stiffeners will be found under the discussion dealing with the Flange Torsional Restraint.

Figure 3 presents a graphic illustration of the general behavior discussed above. In this figure the web buckling coefficient K_w is plotted against the web aspect ratio a/b for several values of θ. For clarity only the curve for $\theta = 50$ is shown completely including the curves for m = 1, 2, 3, ... As pointed out earlier for short stiffeners, the web is adequately supported by the flange and buckles in plate modes until a critical length is reached. At this length, the buckling mode abruptly changes its form; and further increases in length result in lower buckling loads.

The effects of flange flexural rigidity can be observed by comparing the various curves shown in this figure. At low values of flexural rigidity factor the flange does not provide adequate support to the web and the flange and web buckle laterally into the m = 1 mode. As the flexural rigidity factor increases $\theta > 20$ the flange begins to provide full support to the web up to a given critical length.

As alluded to earlier, by selectively reinforcing the flanges of stiffeners with high modulus material, improved efficiencies can be achieved. This improvement can manifest itself either in the form of lighter flanges for equivalent rigidity or increased rigidity for equivalent weight. The magnitude of the increase depends on both the amount and location of the boron epoxy reinforcement. Approximate estimates of the increase in flexural rigidity factor obtainable by reinforcing aluminum flanges with boron epoxy, are tabulated below. These values were obtained by calculating the ratio of rigidity factors for reinforced and all-aluminum flanges ($\theta_{rein}/\theta_{al}$) using a law of mixtures

relationship for the modulus of the reinforced flanges, corrected for the density differences between the two materials.

INCREASE IN FLEXURAL RIGIDITY FOR
BORON EPOXY REINFORCED ALUMINUM FLANGES

% Flange Reinforcement	Rigidity Factor Ratio
$\frac{A_{B/E}}{A_{Flange}}$	$\frac{\theta_{rein}}{\theta_{al}}$
0	1.0
25	1.8
50	2.6
75	3.4
100	4.1

Putting these values into perspective, typical percentages of flange reinforcement proposed for stiffeners designed in this program ranged around 50 percent, meaning that the flexural rigidity factors were better than twice those attainable with equivalent weight all-aluminum flanges.

Effect of Flange Transverse Shear Stiffness

Typical values for the compression modulus of the unidirectional boron epoxy reinforcement range from $E = 30 \times 10^6$ to 32×10^6 psi, whereas, the shear modulus for this material is only 1.6×10^6 psi. In other studies, particularly in shell stability calculations (Ref. 3), a large disparity between these two properties has resulted in significant errors in the predicted buckling load if proper account was not taken of the low shear modulus.

Consequently, at the outset of the program there was some concern about fact that the low transverse shear stiffness of the composite reinforcement could significantly reduce the effectiveness of the approach. Calculations for the buckling stress of the reinforced stiffeners, including transverse shear effects for the flange reinforcement, have shown that this concern was unwarranted. The term containing the transverse shear parameter appears in the factor designated Q^* and can be expressed $\frac{E_F I_F}{GAb^2}$ where $E_F I_F$ represents the flange bending stiffness normal to the web, GA is the flange transverse shear in the same direction and b is the web depth. When $GA = \infty$ the term $Q^* = 0$ and transverse shear effects are neglected as was done for the generation of many of the curves presented in this report.

It can be seen that large differences between the compression modulus and the shear modulus will tend to increase the value of Q^* which, as will be shown in the following presentation, will reduce the buckling stress for the stiffener. Prior to evaluating the significance of the transverse shear term

however it is advisable to obtain some reasonable bounds on the magnitude of the transverse shear parameter Q^*. This can be accomplished by considering the two limiting conditions of an all-aluminum flange as a lower bound and an all-unidirectional boron epoxy composite flange at the opposite extreme. Any combination of aluminum reinforced with boron epoxy should be bounded by these two cases.

Since the web depth, b, also appears in the nondimensional parameter, Q^*, it will be necessary to assume a relationship between the web depth (b) and the flange width (d). For the purposes of this evaluation a conservative estimate of $b/d = 2$ will be used. Under these assumptions the values of Q^* become .40 and .054 for the all-boron epoxy and all-aluminum flanges respectively, representing an order of magnitude difference.

Figures 4 through 6 show the effect that selected values of Q^* have on the plots of stress factor versus aspect ratio. The net result of low transverse shear stiffness shown in these curves is to bring about a reduction in the stress factor. A more descriptive plot is shown in Figure 7 where web buckling coefficient (K_w) is plotted against web aspect ratio for selected values of Q^*, holding θ and C/Db constant. As was suggested by the previous plots, this figure shows that low values of transverse shear modulus or more appropriately large differences between the shear and compressive moduli of flange material will reduce the buckling strength of the stiffener. However, the reduction is far from that which one would expect from a comparison of the two values of Q^* previously calculated. In fact, comparing the curve for infinite transverse shear stiffness $Q^* = 0$, with that of the worse case of an all-composite flange, $Q^* = .5$, one finds that the web buckling coefficient drops from 5.1 to 4.8. This is less than a 6 percent reduction and when it is noted that a reinforced flange will have a value of Q^* on the order of .25, the error is less than 4 percent if the shear term is neglected. This is reason enough to discount any detrimental effects associated with the low transverse shear modulus of the boron epoxy reinforcement.

Effect of Flange Torsional Stiffness

Until now, all of the curves which have been presented considered only nominal values of the flange torsional stiffness factor ($C/Db = 2$) where C represents the flange torsional stiffness about its longitudinal axis. During the design studies, however, it was found that the calculated value of this parameter could be as large as 50, due to the excellent torsional characteristics of the closed circular voids. In other cases, however, there was some question on how to calculate the torsional constant for the flange itself.

Basically, two different flange shapes were considered; the simplest involved using a single infiltrated rod at the base of the web as a flange. For these sections the flange torsional constant was determined using the standard circular section torsion equation, modified to account for two materials. The other shape considered, typified by the flange shown on the "T" section Figure 29, consisted of a thin metallic flange with two circular infiltrated voids at either end. For these sections a conservative approach

was adopted of dividing the flange into distinct regions of dissimilar materials and applying the equation for thin-walled, open sections for the calculations of the torsional constant of the thin metallic flange and adding to this the torsional stiffness of the circular voids, i.e., torsional stiffness equal the sum of; $\frac{t^3}{3} G_{(\text{Aluminum})}$ times the total height of the webs; $\frac{\pi}{2}(R_1^4 - R_o^4) G_{(\text{Aluminum})}$ times the number of voids in the cross section and, $\frac{\pi}{2} R_o^4 G_{(\text{Boron-Epoxy})}$ times the number of boron rods. In either case, the rotational restraint provided by the flange to the web has a positive effect on the stiffener buckling load for both the short and long stiffener buckling regimes.

Figure 8 presents typical results applicable to short stiffeners where the flange fully stabilizes the web. In this figure, showing web buckling coefficient versus web aspect ratio, several curves are shown for selected values of the torsional stiffness factor. Also shown are the curves for the limiting conditions of a simply supported edge at the beam boundary C/Db = 0, and a fully clamped edge C/Db = ∞.

The first item of note shown is that a reasonable increase in buckling stress can be achieved for nominal values of flange torsional stiffness. For example, by comparing the values for the simply supported edge with that of the case for C/Db = 2, an easily achievable value for most sections, one finds that the buckling coefficient increased by 27 percent. Additional increases in torsional stiffness, however, do not show as dramatic a result, as may be seen by comparing the values for C/Db = 2 to those of C/Db = 30, where the increase only amounts to 4 percent.

The second item of interest is that the inclusion of the torsional stiffness factor tends to reduce the critical length of the section. For the condition of no edge rotational restraint (C/Db = 0) the critical length at which the buckling mode changes from plate buckling of the web to lateral buckling of the flange is for a value of a/b = 4.8. As the torsional stiffness factor is increased, this length continually decreases until for the case of C/Db = 30 the critical length is equal to a/b = 3.8. Similar conditions exist for other values of flexural rigidity θ, however, the critical lengths will vary. These results are as expected and simply represent the plate solution with one edge elastically restrained against rotation.

For the long stiffener calculations the result is much the same, except that now the flange is being supported by the web. Some insight into the behavior of long stiffeners can be obtained by first examining the curves of stress factor (ψ) versus aspect factor (ϕ) for various values of torsional stiffener factor. Figures 9 through 11 present plots for C/Db = 10, 25 and 75 respectively. The region of interest is that for low values of aspect factor, or large a/b ratios. These curves unlike the earlier plots for C/Db = 2 have a distinct minimum for low aspect factors. Each minimum differs depending upon the flexural rigidity factor considered, implying an interaction between the flange flexure and twisting modes.

The existence of this second minimum suggests that for long sections it is possible to attain buckling strengths in the web greater than those of a free edged plate. In fact, although the ultimate failure will still be in the combined mode with the web and flange buckling laterally, there is a possibility of this taking place in higher order modes. In any event, this minimum makes it possible to develop a general design curve for long stiffener sections as shown in Figures 12 through 14.

These curves showing the web buckling coefficient plotted against the flange-web stiffness ratio, $E_F I_F / Db$, were generated by plotting the envelope of the minimum values of stress factor at low aspect factors presented in the earlier figures. Knowing the basic stiffener parameters it is a simple matter to determine the buckling coefficient for any stiffener using these curves. These figures indicate that for long stiffeners, flange torsional stiffness can be as important as flange flexural stiffness. In fact, for flanges having torsional stiffness $\frac{C}{Db}$ factors in the range of 25 or greater, buckling coefficients equivalent to those achievable in short stiffeners would be possible for extremely low values of flange web flexure stiffness ratio. Unfortunately, except for bulb flanges which have low flexure stiffness, flanges normally encountered in practice having a value for the torsional stiffness factor of 10 would be considered high, therefore, the only payoff would be in designing with higher values of $E_F I_F / Db$ which are attainable by selectively reinforcing flanges.

Changing the axial stiffness ratio, S , simply shifts the curves to the right, compounding the design problem to some extent since this term would normally increase with increased flange EI , but, fortunately not as rapidly.

This shift in the curves results from the fact that as the axial stiffness ratio gets larger the reinforcing flange assumes a greater portion of the load thereby bringing about a reduction in the overall flexural rigidity factor (θ). An examination of the flexural rigidity factor quickly bears this out if one keeps in mind that it is this parameter which controls the behavior of the combined element and not the individual terms. Taking as a simple analogy, the behavior of a beam column, it is well known that the flexural stiffness decreases as the axial load is increased.

For low values of EI/Db, all curves converge to nearly the same value of buckling coefficient, differing slightly by the amount of edge restraint considered.

Effect of Flange Eccentricity

In many applications, eccentric flanges are used in stiffeners, such as the flanges of "Z" or channel sections. For most design applications using these sections the eccentricity of the flange relative to the center line of

the web is treated in an approximate manner. One approach given in Bruhn (Ref. 4) is to account for the flange eccentricity by calculating the moment of flange about its point of attachment to the web for stability calculations. A more recent paper by Rothwell (Ref. 5), dealing with the stability of stiffened "Z" sections, uses an assumed stress distribution in the flange and accounts for the eccentricity by enforcing stress compatibility at the web flange juncture in an approximate manner.

A third approach, normally considered to be extremely conservative, is to use the moment of inertia of the flange calculated about its own neutral axis. Since none of these methods can be shown to be theoretically correct it was deemed advisable to extend the present plate-beam solution to include the effect of beam eccentricity. The only assumption entering into the solution obtained pertains to the assumption that the flange can be treated as a beam rather than a plate.

The resulting solution (see Appendix A) differed only slightly in form from that obtained for the non-eccentric flange case, with the only change appearing in the definition of the flange flexural stiffness term EI. With eccentricity effects included, the flange flexural stiffness was modified to the following form:

$$EI = EI_c + EA_s \bar{Z}^2 \bar{y}$$

where

EI_c = flange centroidal axis bending stiffness

EA_s = flange extensional stiffness

$\bar{Z}$ = distance from centroid of flange to centerline of web

and

$$\bar{y} = 1 - \frac{E_s A_s K}{Et} \left[\frac{f(Kb)}{(Kb)^2 - \frac{(1-\mu)^2}{(1+\mu)^2} \sinh^2 Kb + \frac{4 \cosh^2 Kb}{(1+\mu)^2} + \frac{E_s A_s K}{Et} f(Kb)} \right]$$

$$f(Kb) = \frac{2(3-\mu)}{1+\mu} \sinh Kb \cosh Kb + 2Kb$$

Expressed in this form the equation for the flange bending stiffness is very similar to that proposed by Bruhn with the exception of the added term included in the axis transfer term. Although similar in form, the end result can be quite different as evidenced by Figure 15 which shows plots of $\bar{y}$ versus aspect factor ϕ for several different flange-web extensional stiffness ratios. Again, the results can be related to buckled wave length or in an approximate sense to stiffener length. For short sections (i.e., $\phi > 2$) these results indicate that there is little or no eccentricity effect present and a reasonable approximation for the flange bending stiffness can be obtained by using

only the first term in the above equation. For long sections the effect of eccentricity becomes more pronounced, however, even for a/b ratios of 15, the transfer term is still 20 percent less than that proposed by Bruhn.

REINFORCED STIFFENER COMPRESSION PANEL DESIGN STUDIES

During the course of the program, parametric design studies were conducted to evaluate the structural efficiencies of aluminum compression panels stiffened with aluminum stringers selectively reinforced with unidirectional boron epoxy. The end objective of these studies was to arrive at a minimum weight design for a compression panel measuring 48 inches in length and 36 inches wide subjected to a running load of 7200 lb/in in axial compression. Ground rules for the design were that it would have stable skins to ultimate load; and for maximum efficiency, incipient failure would occur in the combined modes of local instability of the stiffeners and skin between stringers as well as overall general instability of the panel.

Materials selected for the design were 2024-T3 aluminum for the skin and extruded 6005-T5 aluminum for the stiffeners, selectively reinforced with unidirectional boron epoxy by the infiltration method. As anticipated, the limiting factor in the design was the low yield strength of the extruded 6005-T5 aluminum stringers which placed a strain limit of .0036 in/in on the entire design. This was unavoidable since at the time, this was the only structural grade of aluminum that could be extruded in the shapes required. In spite of this limitation, results obtained for the selectively reinforced designs showed acceptable weight savings over all aluminum panels.

To restrict the scope of the analytical investigation three basic stiffener shapes were selected for evaluation; namely selectively reinforced "T"'s, "Y"'s and hat sections. In all cases the reinforcement was located in the flanges only, since with the stable skin requirements this would result in the most efficient stiffener concept.

To conduct the parametric studies three preliminary design computer programs were generated, one for each section. Through a series of iteration loops the programs will generate design data for stiffener depth, thickness, spacing and skin thickness required for a given load intensity and panel size as a function of the amount of composite reinforcement. The key element in each program is its ability to parametrically evaluate the effects of various amounts of composite reinforcement in the stiffeners.

Design constraints imposed in the programs are that the panel simultaneously satisfy the condition that failure occur in the combined mode of general instability and local instability of the skins and stiffeners at ultimate load.

Eccentrically stiffened plate theory (Ref. 6) was used for the general instability calculations with the local instability of the skin and stiffener webs accounted for by using standard plate buckling theory, with appropriate plate buckling coefficients. For skin buckling between stringers, a fixity coefficient of $K_w = 4.0$ was used. Buckling coefficients employed for web stability calculations were initially taken as 5.0 for all parametric studies, but, as more data was obtained this was subsequently reduced to 4.0 for the

final design calculations. Effects of torsional buckling (twisting modes) were not included in these initial calculations. This mode of failure was only evaluated for the final design using the method presented in the RAE Data Sheets (Ref. 9).

Since one objective of these studies was to examine the design trends as a function of the amount of boron epoxy reinforcement employed, no stress constraint was introduced directly into the program, rather, stresses in the aluminum were calculated and supplied as program output. If in addition to the stability requirements a stress constraint had also been imposed on the design equations, a single real solution, or in some cases no solution at all, would have resulted for each design condition considered. Under these conditions, the design which resulted would have had fully stressed aluminum sections and a specific amount of reinforcement. This in itself, however, would not be sufficient to guarantee a minimum weight design. Consequently, stress was kept as a free parameter. Results of these studies are presented in the following sections.

Parametric Design Studies

Using the programs described above, a series of studies were undertaken to evaluate the efficiencies of each stiffener configuration as well as the effects of varying stiffener spacing and amount of flange reinforcement. To perform this evaluation, a panel 48 inches long by 36 inches wide, simply supported on all sides, under an axial load intensity of N_x = 7200 lb/in was selected as a reference element. This size and load intensity is typical of the final test article. For these calculations a value of 5 was taken for the web buckling coefficients as noted earlier; this combined with the fact that torsional instability failure which was not considered could influence the accuracy of the results. However, since the objective in these early studies was to spot trends and not arrive at a final design the method was thought to be adequate.

To determine how the amount of flange reinforcement influenced the design of the reference panel, a series of computer runs were made using different amounts of boron epoxy reinforcement. These results are shown in Figure 16 in terms of panel weight versus percent area of boron epoxy reinforced aluminum "T" and "Y" stiffeners. A stress limit of 39 ksi was used for these studies, based upon the .2 percent offset yield strength of 6005-T5 aluminum. This value was subsequently reduced to 36 ksi, or the proportional limit, for the final design calculations.

In both cases presented, the results show that there is an optimum amount of flange reinforcement above which there is no weight savings. In spite of the fact that this conclusion is based upon a specific design condition, (i.e., a 48" x 36" panel with N_x = 7200 lb/in), a similar situation will exist for other panel geometries, where the only expected change would be a shift in the optimum amount of reinforcement. Note also that the curves are relatively flat, indicating that no appreciable change in weight will result for a relatively broad range of boron epoxy reinforcement.

From a materials efficiency viewpoint, however, the obvious design point would be the minimum weight condition which requires the least amount of boron epoxy reinforcement. Of course, this must be tempered to some degree by practical design constraints. For instance, it might be desirable to reduce the section depth; consequently a higher concentration of reinforcement would be needed or for example, the minimum weight condition may be impractical from a fabrication viewpoint.

Similar trends are observed from the comparison of panel weight versus stiffener pitch as shown in Figures 17 through 19 for the T, Y and hat sections, respectively. Here again, these curves indicate that there is an optimum amount of reinforcement. The general behavior is as expected; with small amounts of reinforcement, the designs produced have closely spaced stiffeners and are essentially stress controlled. As more reinforcement is added, the panel weights decrease and stiffener spacing increases, accompanied by reduced stresses. Further increases in the amount of reinforcement beyond the optimum point continues the trend described above with increasing weight. For the particular design conditions evaluated above, the minimum weight panels were nearly fully stressed, using the allowable stress of 6005-T5 aluminum. Under different design conditions, however, this will not always be the case.

In attempting to gain a more thorough understanding of the behavior of panel weight as a function of reinforcement, results of a series of parametric studies conducted using reinforced hat section stiffeners were examined in detail. For this evaluation, the panel loading of 7200 lb/in and panel width of 36 inches were held constant, and designs were generated for panel lengths of 36, 48, 60 and 72 inches respectively. These lengths were selected in an attempt to encompass the range of design criteria from a principally stressed controlled condition to one which would be definitely stability controlled.

For all four cases there was an optimum amount of reinforcement above which the panel weight began to increase. For the 36 and 48 inch lengths the designs with small amounts of reinforcement were initially stress controlled and the minimum weight condition occurred close to the point where the 6005-T5 aluminum stringers were fully stressed. Adding more boron epoxy reinforcement beyond this point continued to reduce the stresses but in general the weight increased.

The 60 and 72 inch designs, on the other hand, were never stress critical and the minimum weight condition bore no direct relationship to the aluminum stresses; however, a minimum weight condition did occur. The general behavior exhibited by all designs as greater amounts of reinforcement were added was that the stiffener depth steadily decreased with some increase in stiffened pitch. This, as noted earlier, was coupled with a reduction in stress levels. The fact that the panel weight did not monotonically decrease as the amount of boron epoxy reinforcement was increased was attributed to the interaction of the various failure modes considered.

In other words, the addition of small quantities of reinforcement have an immediate impact on the design whether controlled by stress or general instability; however, beyond the minimum weight condition, local stability of

the skins and stiffeners begin to control. At this point, the weight introduced by the application of more reinforcement is not offset by the amount of aluminum removed.

In concluding the parametric studies, all the results obtained for the various panel and reinforced stiffener combinations evaluated in this phase were compared to typical all-aluminum compression panels. These results are presented in Figure 20 along with results obtained from Shanley (Ref. 7) for optimum all-aluminum panels in 7075 and 2024 aluminum. The data points shown for the selectively reinforced design were all normalized to an equivalent aluminum stress by dividing the applied load by the panel cross sectional area adjusted for the differences in material densities as shown below:

$$\sigma_{eq} = \frac{N_x d}{A_{al} + A_{BE} \frac{\rho_{BE}}{\rho_{al}}}$$

where

N_x = stress resultant (lb/in)

d = stiffener pitch (in)

A = cross sectional area in one bay (in^2)

ρ = material density (lb/in^3)

and subscripts

al = aluminum

BE = boron epoxy

Densities of .073 lb/in^3 and .10 lb/in^3 were used for the boron epoxy and aluminum components, respectively.

Calculating the stress in this manner makes it possible to compare these results directly on an equivalent weight basis to an all aluminum design. As can be seen from Figure 20 the reinforced designs compare favorably with their all metal counterparts in spite of the fact that a low strength alloy (6005-T5) is used as the base metal. The small amount of scatter exhibited by the various sections over the load index range can be attributed in part to the method of analysis employed. This results from the fact that the computer programs determine minimum weight designs for discrete increments of boron epoxy reinforcement with no allowance made for interpolating between each increment. Consequently, although the results plotted represent the minimum predicted weight for a given load index they could reflect slightly non-optimum quantities of reinforcement.

A second and more significant reason, however, lies in the fact that a given load index (N_x/L_o) can be arrived at by using an infinite number of combinations of stress resultant (N_x) and effective length (L_o). For example, the load index for a short, lightly loaded panel could be equal to that of a highly loaded long panel or any combination of loads and lengths in between. In spite of the equivalent load index the failure modes exhibited by such panels would be vastly different for a given material. In general one would think of short panels being constrained by material strength limitations, whereas long panels would be more susceptible to stability failure.

In evaluating the results presented with this in mind a trend develops which indicates that the selective reinforcement approach for reinforcing 6005-T5 aluminum sections is more effective for stability controlled designs than for stress controlled designs.

The results presented for the hat sections strongly reflect this trend where an examination of the loads and lengths employed for these calculations showed that all data points falling below the 7075-Y line were moderately loaded short panels (stress controlled) and those points falling above the line were for panels where general instability was the governing design criterion.

Data points in Figure 20 for a load index of N_x/L_o = 150 psi reflect the results obtained for the final test panel design. In this evaluation all three stiffener configurations, Y, T, and Hat, were considered with the reinforced "Y" section proving to be superior.

Complete details on these designs are presented in the following section.

Preliminary Design Concepts

Prior to selecting the final design for the proof test compression panel, three preliminary design concepts were prepared incorporating boron epoxy reinforced "T", Hat and "Y" shaped stiffeners. Using the optimum design features determined from the parametric design studies preliminary designs for each concept were prepared using the parametric design programs. For these calculations the skin buckling coefficient was taken as $K_w = 4.0$ but, the web buckling coefficient was reduced from the earlier studies to a value of 4.0. These preliminary designs were then checked and further refined; by addition of suitable connection flanges, making dimensional adjustments, checking clearances, introduction of fillets, etc. to arrive at the final design concepts shown in Figure 21. In addition, a torsional instability check was performed on the NACA "Y" stiffened design, but no similar check was made for the "T" stiffened panel, making the design shown somewhat marginal. A similar examination of the hat stiffened design was unwarranted.

The design conditions for each panel were:

Panel Gage Length	=	48 inches (effective length)
Panel Width	=	36 inches
Axial Compressive Load	=	7200 lb/in

Table 1 presents a summary of the panel weights and associated stresses at ultimate load. For comparison the weights of equivalent all-aluminum 7075 and 2024 stiffened panels are also presented. Weights for the 2024 aluminum panels were taken directly from the Shanley curves (Figure 20) for an axial load of 7200 lb/in and a load index of N_x/L_o = 150 psi. For the 7075 "Y" stiffened aluminum compression panels weights were determined both from the Shanley curves as well as from a design generated using design curves for curved web NACA "Y" section stiffeners (Ref. 8).

As seen in Table 1 the design obtained in this manner was slightly heavier than that obtained from the Shanley curves, despite the fact that the curved web "Y" is shown to be slightly superior to the straight web "Y" used in the Shanley presentation.

The boron epoxy reinforced compression panels all showed weight savings over their equivalent all-metal counterparts (i.e., comparing Y versus reinforced Y etc.). This resulted in spite of the fact that the reinforced hat and Y designs were limited to some extent by the strength of the 6005-T5 aluminum extrusions.

As noted before, however, the specific design conditions considered for the test panel of N_x = 7200 lb/in and length = 48 inches placed the design in the intermediate range between being stress and stability critical; based upon a strength of 36,000 psi for the aluminum as the limiting stress condition.

Consequently, for these specific design conditions no significant gains in weight reduction could be expected if a higher strength aluminum alloy were used. This is evidenced to some extent by the fact that the all-aluminum panels in 7075 were only stressed to 43,000 psi at failure, which is only 65 percent of its yield.

The reinforced "Y" stiffened panel proved to be the most efficient (lightest weight) of the three designs; with the reinforced Hat section stiffened panel running a close second. As expected the panel stiffened with the reinforced "T" section was the least efficient. Weight savings for the reinforced "Y" stiffened panel ranged from 6 percent (or 12 percent using curved and web design) over a 7075 all-aluminum "Y" stiffened panel to 24 percent for a "Y" stiffened compression panel in 2024 aluminum. For the other two stiffener sections considered, minimum predicted weight savings on an equivalent shape comparison were 15 percent for the "T" sections and as high as 27 percent for the reinforced Hat sections. (See Table 1.) Based upon these results the reinforced NACA "Y" stiffened panel design was selected for the final proof test article to be fabricated in this program.

Design of Boron Epoxy Reinforced Proof Test Compression Panel

The configuration selected for fabrication and proof testing at NASA Langley is shown in Figure 22. This panel consists of 2024-T3 aluminum skin, stiffened by 11 boron epoxy reinforced 6005-T5 aluminum NACA "Y" sections. The NACA "Y" sections were extruded to a nominal thickness of .060 inch and then chem-milled to the final thickness. Initial discussions with the extrusion vendor had indicated that it would be possible to extrude sections with wall thicknesses of .045 inch as shown and this was used as one of the design constraints employed in preparing the final design. Further evaluation however, indicated that proper dimensional control could not be maintained in these light gages, necessitating an increase in the extruded wall thickness to an .060 minimum, thereby making the secondary chem-milling operation necessary.

Detailed stress analyses of the final design indicated that the preliminary design estimates were conservative and that the panel is capable of sustaining loads up to the yield strength of the 6005-T5 aluminum stringers. These calculations, based upon assuming the panel would be simply supported on all four edges with a gage length of 48 inches are summarized below:

General Instability (Elastic Buckling)

N_{xcr} = 8,950 lb/in

σ_{al} = 42,000 psi

$\sigma_{B/E}$ = 126,000 psi

Buckling mode m = 1; n = 1

Local Instability (RAE Data Sheets)(Ref. 9)

N_{xcr} = 8,900 lb/in

σ_{al} = 41,900 psi

$\sigma_{B/E}$ = 125,700 psi

The general instability failure predictions were made for a 48 inch long panel simply supported along the edges using eccentrically stiffened plate theory assuming elastic buckling. As can be seen, the predicted buckling load for the panel is above the design load; however, at this load intensity, the stresses in the aluminum are well above yield, indicating an inelastic buckling failure will occur.

A similar situation exists for the local instability failure of the panels based on predictions made using an RAE data sheet method. In this evaluation, two local instability failure modes were postulated as shown in Figure 23. From simple plate models, it was concluded that mode 1 would result in the lowest critical buckling load. This was later substantiated in the subelement testing phase.

Using this assumed failure mode, buckling stress calculations were made for the aluminum skin and stiffeners alone, excluding the boron epoxy reinforcement. These results were then adjusted to reflect the added load carrying capability afforded by the boron epoxy reinforcement to arrive at the final buckling load reported.

Here again, the calculated buckling load of 8900 lb/in is above the 7200 lb/in design load, and again the stresses in the aluminum are above yield, suggesting inelastic buckling will occur. The predicted critical wave length for this case was 1.5 inches with failure induced by skin buckling between stiffeners.

Prediction of the precise failure load would require the use of inelastic buckling theories which is beyond the scope of this program, however, these calculations are unnecessary since the test conditions will differ somewhat from the theoretical design conditions. The test plan calls for the panel to be tested as a simply supported wide column (i.e., the unloaded edges will be unsupported) having a stiff load introduction bay at either end as shown in Figure 22.

To account for these differences it was decided to adjust the overall panel length including load introduction bays to fail in general instability at the design load of 7200 lb/in. This will result in a small margin of safety on the stress in the aluminum stringers and a large margin on local instability since these earlier calculations will remain virtually unchanged.

The panel length was determined using Euler column theory for a column having a nonuniform cross section without any corrections for wide column effects. The nonuniform cross section solution was required to account for the differences in stiffness between the load introduction bays and the center test section. Using the buckling equation for a nonuniform moment of inertia column (Ref.12) the length of the center section was determined for given end bay length, such that general instability failure of the entire panel would occur at the 7200 lb/in design load. Results of this analysis indicated that the center bay length should be 28.6 inches, which when combined with the length of the end bays gave an overall panel length of 52.6 inches. This length was chosen for the final test article.

To arrive at a conservative estimate for the panel efficiency it was further decided to calculate the panel buckling load assuming a constant cross section over the entire 52.6 inch test length, and use this load for efficiency comparisons. The predicted buckling load for this condition was N_x = 6750 lb/in. Comparing these results with an equivalent all-aluminum NACA "Y" design in 7075 taken from the Shanley curves increases the projected weight saving from the 6 percent obtained from preliminary design calculations to 13 percent or a more respectable increase in efficiency.

As noted earlier, unlike most static compression test panels, the design shown in Figure 22 also includes load introduction fixtures at either end. Similar panel tests conducted in the past have used load introduction schemes which do not fully represent aircraft structural design. Typically, the

compression panels are squared off at the ends, potted in a matrix of a low melting temperature alloy and loaded flat ended between platens of a test machine.

These end fittings are an important part of this program since they will demonstrate that standard attachment schemes can be employed for joining infiltration reinforced structures. In the load introduction method shown, the load is introduced into the stiffeners in the conventional manner via rivets or bolts through the connection flanges, and then into the unidirectional composite reinforcement via the bond between the resin and the aluminum sheath.

The design of an optimum/minimum weight joint would require additional detailed analysis and sub-component tests, therefore, it was decided to simply ensure large factors of safety of the load introduction length without any concern for weight.

Figure 22 illustrates this joint design where the compressive line load is applied to the "Vee" groove to simulate simply supported edges and then is distributed by the load introduction member (splice plate) through shear bolts to the panel. The load introduction member is fabricated from a 7075-T6 aluminum forged plate, machined to provide thick vertical flanges between each stiffener. These ensure a minimal deviation of the neutral axis of the material throughout the length of the joint, as well as providing local bending strength. The load of 7200 lb/in is transferred into each stiffener by 22-1/4 inch diameter close tolerance bolts over a length of 10 inches. The stiffeners are each reinforced by steel angles which provide additional bolt bearing strength as well as restraining the stiffeners from rotating; that is, rotation in the plane of the stiffener and bending about the panel neutral axis. This bending occurs over the length of the load introduction bays where the shear lag effect creates opposing couples at the interface between the stiffener and load introduction member. This couple is balanced by tension in the bolts at one end and compression at the other, as indicated by Figure 24, and hence dictates the local design of the reinforcing angles. As shown in the section view of Figure 22, these angles are relatively thick, being designed to resist web bending stresses imposed by the load offset between the vertical web of the stiffener and the center line of the bolts. This offset is probably one reason for the general lack of use of the NACA "Y" stiffener, which in theory is considered the most effective compression shape.

Panel Fabrication Procedure and Weight Summary

The test panel was fabricated utilizing common aircraft processes which included numerical control machining, chemical milling, riveting, etc. The two end pieces (headers) were machined from a single 7075-T6 (QQ-A-250) aluminum plate using a tape controlled milling machine. The first step in their fabrication was to rough cut them to .100 inch over size. The two pieces were then stress relieved in a temperature controlled and monitored oven at $375^{o} \pm 10^{o}$ F for five to six hours and then slowly (overnight) cooled to below 100^{o} F. This stress relief cycle was included so as to minimize subsequent distortion due to normal aging of the material, which may be more

pronounced with this material (7075) than with some others. After this cycle the individual end pieces were numerically control milled to final thickness with particular attention being given to squareness of the load surfaces, and inspected. See Figure 25. The "Y" stringers were chemical milled from the as extruded thickness to the final thickness as shown in Figure 26. After infiltrating they were cut to length and the outstanding legs drilled and machined to width, again through the utilization of tape controlled machining. (See Figures 27 and 28.)

Figure 27 shows the numerically controlled machine performing the final cuts on the stringer flanges. Note that the thin webs were supported by tooling blocks for machining. In Figure 28, two stringers at various stages of completion are shown. The section on the right has been drilled and rough cut, and the section on the left is complete. In this view the two steel doublers required to ensure proper support for the webs are also shown. Four of these doublers (two at either end) are required per section. The skin (.063 thick 6061-T6 aluminum) was inspected with the thickness being checked and recorded on a four inch square grid; this along with other information including stringer identification is depicted on Figure 29. Steel doublers are used to induce the load from the end plates to the stiffened skin test section. These were fabricated by bending .250 inch thick AISI 1010 steel strips to the general configuration of the outer surface of the "Y" stiffener. This mating surface was then machined to ensure proper fit and support to the "Y" configuration. These steel plates can be seen in position at the stringer end to the right of Figure 30. Tapered aluminum wedges were machined to form the transition between skin joggle at the end plates and the base leg of the stiffener. At this point in the fabrication process, all detail parts were weighed, with the data tabulated in Table 2. Remaining detailed information such as a materials list, quantities of materials and panel weight per unit area are given in Table 3.

The headers and boron reinforced stringers were then anodized; the exposed surface of the boron/epoxy matrix being sealed as a precaution since it is doubtful that any serious effect would result. The steel load plates were cleaned (grit blasted) and sprayed with a protective coat of zinc chromate primer. The steel load plates were then assembled to their respective stringers through the installation of high strength internal wrenching aircraft bolts and self-expanding drive rivets. (See Figure 30.)

The panel was assembled on a surface plate with the end plates jigged parallel and square and all remaining bolt and rivet holes drilled in this position. Locating and alignment pins were inserted to insure proper reassembly for final assembly. The panel was then disassembled, deburred, and all remaining aluminum parts anodized and once again assembled (Figure 30) utilizing the alignment pins, dimensionally checked and final assembly accomplished. The completed panel is shown in Figures 31 and 32.

ELEMENT TESTING

In this phase of the program a total of 55 fully instrumented boron epoxy reinforced aluminum sections were destructively tested. All sections were reinforced with boron epoxy using the infiltration method.

Standard reinforced tubular aluminum sections were tested in axial compression and flexure to obtain basic design information. Selectively reinforced stiffener sections were compression tested to evaluate the stability characteristics of reinforced sections. The test phase concluded by testing in axial compression four (4) reinforced NACA "Y" sections used in the final test article fabricated in this program. The following experimental results are arranged in this order.

Infiltration Reinforced Rod Tests

Mechanical property determinations and simple Euler column analytical correlations were made using standard infiltration reinforced aluminum test coupons. These coupons consisted of small diameter drawn aluminum tubing infiltrated with boron epoxy. Two different wall thickness aluminum tubes were tested. The control specimens used standard 6061-T3 drawn tubing with an I.D. of .1875 inch and an O.D. of .25 inch, giving a wall thickness of .031 inch. The thinner tubes obtained by chem-milling the O.D. of the original tube had a wall thickness of .015 inch. The purpose of the thinner specimens was to determine if the thickness of the aluminum sheath surrounding the boron epoxy reinforcement had any effect on the strengths achieved in the reinforcement. In both cases the amount of reinforcement remained the same with filament volumes in the core held at 53 percent as determined from an exact count on the number of .004 inch diameter filaments used.

Tests were performed to determine stiffness compressive strength, and column behavior of both specimens. In addition, flexure properties were determined for the thick-walled specimens. The compressive test fixture utilized for the axial compression and column buckling tests is shown in Figure 33. The lower specimen in the photo illustrates how hardened steel balls are placed over the ends of the sample. The sample is then placed between two end plates having conical cavities as shown by the upper specimen. The actual test procedure followed was to first align the two end plates in the Baldwin Model FGT test machine, then the test specimen was inserted. This procedure assured the best possible axial alignment. Failed specimens are shown in Figures 34 and 35 with Table 4 summarizing the specimen geometry test results.

In the test program specimens were selected at intervals along the infiltrated rods in order to ascertain if there was any detectable variation in properties and a specimen numbering sequence was adopted to reflect the specimen location. In all cases the prefix L1 refers to the thick wall tubing, and L2 refers to the thin wall tubing. The 12 foot length of infiltrated thick walled tubing was marked off in one foot lengths and specimens were cut from each length, hence the final integer in the specimen numbering sequence refers to

those one foot intervals. In the case of the thin walled tubing two six foot lengths were infiltrated and samples were taken at the ends and mid point of one and from the ends of the second. Therefore, specimens L2-1, -2, and -3 were taken from the first thin wall rod and L2-4 and L2-5 from the second.

Compression Test Results. - A total of seven thick-walled and five thin-walled (see Table 4) .6 inch long specimens were tested to determine their compressive strengths. The results obtained from these tests are summarized in Table 5. The compressive strengths obtained when translated into stress in the boron epoxy are not as high as those previously obtained which approached 400 ksi (Avco Funded Research). The calculations are based upon a typical yield strain of .42 percent in the 6061-T6 aluminum sheath. The second notable factor is that the average boron epoxy strength of the thick-walled specimens is higher than that for the thin-walled specimen which may suggest a minimum thickness for the metallic sheath. More testing will be required to substantiate this fact however.

In addition to obtaining compressive strengths several of the compression specimens were instrumented with strain gages in an attempt to obtain the axial modulus. In both cases the measured modulus was higher than predicted, i.e., 23×10^6 psi as opposed to a predicted 21.3×10^6 psi for the thick-walled rods and 27.5×10^6 as opposed to 24.8×10^6 psi for the chem-milled specimens.

Short Column Buckling Tests. - Four thick and four thin wall (Table 4) short columns were tested. The lengths of these specimens was selected on the basis that the stress in the aluminum sheath be at its yield point of approximately 45 ksi at the incipient Euler column buckling load of the rod. Instrumentation consisted of three mid length axial strain gages arranged at 120 degrees apart for two specimens of each lot and two mid length dial gages at 90 degrees to monitor the lateral deflections on all specimens tested. Strain gages were used to predict the axial modulus and to detect the buckling stress. The dial gages were used to generate Southwell plots as an alternate means of predicting the buckling loads. Results of these tests are summarized in Table 6. For the most part the failures were precipitated by elastic buckling at about the prescribed failure stress and the specimens ultimately failed in a shear mode well above the buckling stress. (See Figures 34 and 35.) Again, the initial moduli obtained were consistent with the compression test specimens and were slightly higher than predicted values.

Long Column Buckling. - Three thick-walled and four thin-walled (Table 4) long column specimens were tested. Column lengths (6.0 inch) were selected to fail elastically in the classic Euler column manner (Figure 33). The instrumentation provided was similar to that employed for the short column tests; two specimens of each type having axial gages and all specimens using dial gages.

Test results are summarized in Table 6. In all cases the rods buckled elastically and in fact, when the load was relaxed (which was done on several specimens) they returned to within .0001 inch of their original position as measured by the lateral dial gages. Upon reloading they again buckled at the

same load level. The Southwell plots consistently predicted higher buckling loads than did the strain gages. Using the gage readings, the buckling stress was determined at the point strain of reversal.

Flexure Test Results. - Six flexure tests were performed using 10 inch long thick-walled (see Table 4) specimens. Of these specimens three center point loading and three quarter point loading tests were performed. The primary purpose of these tests was to determine the rod flexural stiffness (EI). Test results are presented in Table 7. These results compared very favorably with the predicted EI which was obtained using a 30×10^6 modulus for the boron epoxy core and a 10×10^6 modulus for the aluminum sheath as was used for all other predictions.

In the summary table, the failure stress has been separated into three columns; the first two columns represent the calculated stresses at ultimate load assuming that the aluminum remained in tact to failure giving conservative estimates for the boron epoxy stresses. What actually happened however was that the aluminum yielded with some slight necking and ultimately cracked clear through to the beam mid point prior to the failure of the boron core. Figure 36 showing the load deflection curve for specimen L1-6 illustrates this fact. The curve is linear up to a load level of 55 lb. which is equivalent to a stress level in the aluminum of 47.8 ksi or above its yield point. Beyond this point the curve is nonlinear, suggesting progressive fracture of the aluminum sheath. To obtain an upper limit on the failure stress in the boron epoxy core it was assumed that at ultimate load the core alone sustained the entire load. These results are tabulated in the final column of Table 5.

Reinforced Stiffener Tests

In this phase of the program a total of 27 infiltration reinforced stiffener elements were tested in axial compression. Twenty-three of these tests were designed to evaluate the structural behavior of stiffeners reinforced with boron epoxy and the latter four tests were for qualification of the "Y" section used in the final test panel.

Since the infiltration reinforcement method relies on using extruded shapes having preformed circular voids, it was decided to purchase a single extrusion and cut various shapes from it for structural evaluation. The section for this purpose was the "T" section shown in Figure 37, extruded in 6005-T5 aluminum.

By removing various parts of this section it was possible to obtain three basic shapes, and then by chem-milling, variations in web depth to thickness ratio (b/t) were also obtained for two of these shapes. This resulted in the five test elements shown in Figure 38 with typical cross sectioned views shown in Figure 39. In addition to shape variations, all specimens were tested in six and 24 inch lengths. The six inch specimens were designed to evaluate the local instability characteristics and the 24 inch specimens were designed to examine the long column behavior of the sections with particular emphasis in detecting the twisting mode of failure cited by Peterson (Ref. 10).

Filament volumes were held constant at 55 percent, requiring the infiltration of 1250, four mil diameter filaments in each void.

Compression testing was accomplished using a Baldwin Model FGT test machine capable of developing loads to 50,000 lb. A typical test setup is shown in Figure 40. Prior to testing all the specimen ends were ground flat and parallel. They were then placed flat ended between two specially prepared diboride platens shown in the figure. The need for these platens resulted because earlier tests on short reinforced specimens using steel platens indicated that the boron filaments penetrated the platens causing the surrounding aluminum to plastically deform at the ends. Using the harder diboride platens eliminated this problem.

To simulate a simple support condition the edge of the web opposite the flange was supported in a "V" groove along its entire length as shown in the figure. A cross sectional view of this groove is shown in the lower left of the figure, and was used for the short element testing.

The "V" groove support worked successfully for all elements except the 24 inch long "T" and "L" shapes, where calculations showed that the failure mode would be overall buckling of the entire section causing the section to pull away from the "V" groove. To prevent this potential failure mode and thereby obtain a failure more representative of stiffeners attached to a panel. three intermediate tie straps were provided to hold the section in the "V" groove. These are shown in the figure and consisted of standard high strength steel shim stock attached by small bolts to the web of the section and fastened to the steel "V" groove bracket. Reasonable results were achieved using this technique, although at failure some pulling away of the web from the support was noted.

Instrumentation consisted of axial strain gages located at critical points along the flanges and webs of the specimens, with a minimum of 8 gages used in each test. The test procedure called for initially loading the sample to a nominal load allowing for settling in of the specimen and gages. The load was then relaxed and the gages were then balanced and the sample loaded in increments to failure.

Gage readings were examined at a load level equivalent to 10 percent of the predicted failure load, and if gage readings varied by more than 10 percent the specimen was removed and reground.

A summary of the test results obtained from this series of tests is presented in Table 8. Buckling loads were determined from the load-strain curves for each section with the exact buckling load determined at the point of strain reversal. Typical stress-strain curves obtained are shown in Figures 41 through 46. Note that most of these curves show that the sections exhibited reasonable post buckling strength. Furthermore, in no case did a catastrophic failure of the boron reinforcement occur, but rather, the aluminum sheath seemed to retain the boron even after large deformations had occurred.

The results obtained from the web and rod tests were as expected where failure occurred by buckling of the rod normal to the web. The only exception to this was the short length (6 inch) chem-milled web and rod sections where the web initially buckled into three half waves followed by lateral buckling of the rod section as predicted.

Similarly for the "T" and "L" sections all failures but one were initiated in the flanges. This is contrary to the predicted failure mode expected to be either local buckling or yielding of the web. The exception was the 6 inch chem-milled "T" which failed by local buckling of the web into the m = 3 mode - attributed to the high stress at failure as indicated in Table 8.

For the long "T" and "L" sections, however, the failure mode was definitely in the elastic range and is characterized by local failure of the flange as illustrated in Figure 47 for a "T" and an "L" section. The buckled half wave length in each case was approximately 7 inches long which could explain why the shorter 6 inch sections approached the yield stress of the aluminum prior to failure. Initial examination of these failed 24 inch sections indicated that the failure mode was a torsional or twisting mode and was not detected by the plate-beam model. Additional calculations however suggested that the failure mode may simply be local flange buckling and is discussed in more detail in the following sections.

Experimental and Analytical Correlation

The stiffener compression tests were designed to examine several aspects of failure of selectively reinforced stiffeners. Specifically tests were performed to evaluate the following items:

- Stiffener axial stiffness (EA)
- Web-flange interaction
- Local instability of web
- Failure modes when aluminum is stressed to yield, and
- Torsional (twisting) failure of reinforced flanges

Axial stiffness (EA) comparisons were made for all sections tested with the experimental and analytical results comparing very closely as shown in Table 9. The experimental values were determined from the initial portions of the load-strain curves. Analytical predictions were made using the law of mixtures approach assuming a modulus of 10×10^6 psi for the 6005-T5 aluminum and a modulus of 30×10^6 psi for the boron epoxy reinforcement. This boron epoxy modulus was based upon a typical value attained for 50 percent by volume unidirectional boron epoxy composites. All section properties were determined using actual test specimen dimensions as shown in Figure 39, with Table 10, presenting a summary of the more pertinent parameters.

The close correlation obtained for the axial stiffnesses of each section was as expected based upon previous test results and supports the conclusion that a law of mixtures approach is suitable for these calculations.

Earlier analytical results indicated the buckling behavior of stiffeners with flanges could be characterized in general by either buckling of the web supported by the flange, or buckling of the flange supported by the web. It was also shown that for short to moderate length stiffeners the former mode usually prevailed and the stiffener ultimate strength was strongly dependent upon the flange flexural rigidity, normal to the web. In fact, for very short sections the flange usually provided full support to the web and the failure mode was plate buckling of the web. Beyond the given critical length however the flange provided only partial support to the web and failure occurred in the combined mode of web and flange buckling.

The latter mode, where the web supports the flange, is associated with much longer sections and the buckling load is controlled primarily by the torsional stiffness of the flange.

To evaluate this interaction between the flange and web several tests were performed using the web and rod stiffener configuration shown in Figure 39. Buckling modes of interest were those associated with moderate to long stiffener sections. Behavior of extremely short stiffeners with web aspect ratios less than 4 were not considered as they are of little practical interest.

To examine the behavior of sections where the flange provides support to the web, 6 inch long web and rod specimens with two web depth to thickness ratios were tested. The section with the thick web buckled into the m = 1 mode where the flange (rod) and web buckled in combination normal to the web. In this case the flange provided partial support to the web and a web buckling coefficient of K = 1.57 was realized. The predicted buckling coefficient for this case using the plate-beam stability model presented earlier was K = 1.39 using an effective length of specimen of 4 inches. Comparisons of the actual buckling loads are presented in Table 9.

Test results obtained for the other 6 inch specimen with b/t = 44 differed, in that in this instance the initial failure mode was local buckling of the web into the m = 3 plate mode followed by flange buckling at a somewhat higher load. The predicted buckling coefficient for this section was K = 5.1, again using an effective length of 4 inches, whereas, the average experimental value was lower or K_w = 3.9. Again, however, the flange stabilized the web.

Both sections were also tested at lengths of 24 inches where the predicted flexural rigidity factor (θ) was negative indicating that the flange would no longer provide flexural support to the web. The only predicted increase in web buckling coefficient over the free edge plate solution was that associated with the torsional restraint provided by the flange. Predicted web buckling coefficients for these sections were K_w = .8 for the thick web section and K_w = .9 for the thinner chem-milled specimen. These values are the minimum values obtained from Figure 10 for EI/Db = 0 and represent the solution

for a plate simply supported on three edges and having only rotational restraint along the fourth edge.

The experimental results indicated that for the standard thick web section the web buckling coefficient was more nearly equal to the free edged plate value or K = .40, suggesting that the flange torsional restraint had no apparent effect on the buckling stress. The results for the thinner web section indicated just the reverse, however, where the average experimentally determined web buckling coefficient was K_w = .81, slightly lower than the predicted value but well above the free edged plate solution of K = .45.

This discrepancy between the two sections may be explained in part by comparing the flexural and torsional stiffness ratios for each given in Table 10. For the thick web specimens these ratios are relatively low suggesting weak coupling between the web and flange, whereas, for the chem-milled web and rod section both stiffness ratios are larger indicating a stronger contribution provided by the flange.

The above sections were designed to examine the behavior of stiffeners for which the flange provided partial or no support to the web. To complete this phase of the investigations a section was tested where the flange stiffness was theoretically adequate to provide full support to the web, such that, the web would develop its full buckling stress with no displacement of the flange. The section selected for this was a 6 inch long chem-milled T section. The theoretical web buckling coefficient predicted for this section was K_w = 5.1, which is slightly greater than the coefficient for a plate supported on all four edges. This increase as noted earlier is due to the rotational restraint provided by the flange. The test section failed, as predicted, with the web buckling locally into three half waves along its length. The measured buckling coefficient for the web was K_w = 5.2 or equivalent to the theoretical value.

Based upon initial calculations it was assumed that the 24 inch long chem-milled "T" section would also buckle in the same manner as noted by the predicted web buckling coefficient included in Table 9. Unfortunately, the section failed at a somewhat lower load level with the failure mode exhibited by local twisting of the flange. This mode was not completely unexpected since long specimen tests were promoted to induce this mode of failure however, preliminary calculations using the present theory did not predict this mode of failure. This failure mode was also evident in all other sections tested, including both the standard thick web 6 and 24 inch reinforced "T" and "L" sections.

The original reason for testing these thick "T" and "L" sections was to evaluate their behavior when the aluminum was stressed to yield, which occurred for both 6 inch specimens. Initial theoretical predictions given in Table 9 used the yield stress of the aluminum at σ_y = 36,000 psi as the predicted failure stress, consequently no buckling coefficient was specified.

In examining these twisting failures in more detail it was decided to eliminate the 6 inch length "T" and "L" specimens from further consideration since they achieved their intended purpose with aluminum stresses of approximately 36,000 ksi. Although limited, these short specimen tests tend to suggest that reinforced sections cannot be relied upon above the point where the aluminum reaches its yield stress. It should be noted, however, that no actual yielding was detected from the load strain curves.

Concentrating in more detail on the flange twisting mode of failure exhibited by the 24 inch chem-milled and standard "T" section and the 24 inch "L" section the following observations were made. First of all, the failure was manifested by local twisting of the flange about the web juncture with an effective length of approximately 7 inches with no lateral displacement of the flange. Web buckling was not evident either. Figure 47 illustrates typical failure obtained for the standard "T" and "L" sections.

Initially it was concluded that the failure was a torsional mode, however, further examination suggests that the failure may simply be local buckling of the flange. In attempting to correlate this observation with the theoretical predictions, it was assumed that the flange represented a plate simply supported along three edges and elastically supported by a beam simulating the infiltrated void at the opposing edge. For the "T" sections one half the total flange width was used.

Based upon this model the predicted buckling coefficient for the standard "T" and "L" section flanges was $K_f = .8$ or equivalent to that obtained for the 24 inch standard web and rod section. The average measured values were .5 and .41 for the standard "T" and "L" sections respectively. Recalling that the results obtained for the thick web and rod section were lower than the predicted values, and of the same order or magnitude, lends credence to the proposed failure mode.

Results for the chem-milled "T" section showed excellent agreement using this approach. In this instance the predicted flange buckling coefficient was $K_f = .9$ and the experimentally determined value was $K_f = .84$ again comparing favorably with the values given for the chem-milled web and rod. Predictions based upon this model are given in Table 9 below the pre-test predicted values which assume failure by buckling of the web.

Although in some instances the correlation between the experimental results and predicted values are not as precise as would be desired, the analytical model did predict general trends when employed properly. It must also be remembered that the test program was limited to some extent by its reliance on a single section from which the test sections were obtained.

Proof Test of NACA Y Sections

Four infiltration reinforced NACA Y specimens were tested in axial compression to obtain backup data prior to testing the final full scale panel. In this series of tests three specimen lengths were employed; a 1.375 inch specimen to determine the ultimate strength, two 6 inch specimens for

local crippling evaluations and a 36 inch specimen to examine the plate-stiffener buckling behavior. All specimens were tested flat ended between diboride platens in a 50,000 lb. Baldwin Model FGT test machine.

Nominal thickness (.060 inch) 6061-T6 aluminum sheet was riveted to all sections. For the three short specimens the skin was cut off at the edges of the connection flanges (Figure 48) to prevent any problems with local skin buckling along the free edges.

The 36 inch specimen was designed to simulate the panel installation and required that a full bay width of skin be included, which was supported by knife edges along both edges. The test specimen geometry chosen for this test is shown in Figure 49 along with typical specimen dimensions. Table 11 summarizes the test results obtained from these elements and failed specimens are shown in Figure 50.

Element 1 was uninstrumented, but skin and web buckling was visually observed at 37,000 lbs. with ultimate failure occurring at an axial compressive load of 42,000 lbs. as noted in Table 11. This corresponds to an ultimate (P/A) stress of 87.6 ksi. The buckling stress given in the table was calculated on the basis of an axial load of 37,000 giving a value of 58.2 ksi which is much greater than the published strength of 40,000 psi for the aluminum suggesting that the aluminum failed earlier. The boron epoxy stress reported in Table 11 was determined by assuming that the stress in the aluminum held constant at 40,000 psi and the remaining load was carried by the boron epoxy. This is a rather conservative approach since it is doubtful that the aluminum could sustain this stress level in the buckled condition. In any case the results obtained on this basis were extremely gratifying where the stress in the boron epoxy at failure was calculated to be 344.0 ksi.

The webs buckled as predicted, Mode 1 shown in Figure 23. The only departure from this mode was that the skin buckled in one half wave rather than two and no flange rotation was detected. Ultimate failure occurred by a flaring out of the voids at the specimen ends in what appeared to be a bearing failure.

Elements 2 and 3 failed in much the same manner, with initial buckling occurring in the skin and webs at load levels of 26,000 and 27,000 lbs., respectively. These buckling loads were determined from strain gage readings at the point of strain reversal. Figure 51 represents a set of typical results for gages mounted on the webs and skin of Section 2. Buckling stresses in the aluminum were in excess of the design load of 34,000 psi and slightly below the elastic analysis prediction of 41,900 as expected. Upon continued loading the webs and skin underwent excessive deformation, however, the reinforced flanges sustained the load for an additional 10,000 lbs., with ultimate failure occurring by flaring out of the ends at a load level of 36,000 lbs.

Figure 52 illustrates the load-strain behavior obtained from gages mounted on the reinforced voids. This figure shows a bilinear load-strain curve with an initial linear region having an EA = 6.65×10^6 lb., matching

closely with the predicted value of EA = 6.35 x 10^6 lb. At a load level of approximately 26,000 lbs. corresponding to the point of initial buckling of the webs the curve changes slope followed by a second linear region having an average axial stiffness slightly less than that of the boron epoxy reinforcement. This second region shows that some bending is occurring in the flanges but no buckling failure is evident. Again, exceptionally high ultimate stresses were obtained in the boron epoxy reinforcement, using as before the conservative assumption that the aluminum stress held constant at 40,000 psi, the stresses in the boron epoxy were found to be in the order of 260 ksi.

The simulated plate stiffener test on element 4 was performed using a full width skin section riveted to the stringer as noted earlier. Some difficulty was encountered because of the effective plate width chosen for the test. Rather than using an effective skin width equivalent to the edge to edge distance between adjacent stringers the center to center spacing was used. This resulted in a skin width between knife edge supports of 6.4 inches rather than a 4.2 inch width. As a result the unsupported span of skin was 1.1 inch wider than in the actual panel. This larger width caused the skin to buckle at a lower stress level than anticipated and thereby caused a greater load to be transferred into the stiffener.

Based on the section geometry the section should have achieved a load of 31,500 lbs., but due to premature skin buckling the section failed locally at 22,000 lbs. at which point the stress was 26,000 psi in the skins. At an axial load of 25,000 lbs. it was visibly evident that the skin between the connection flanges and the knife edges was completely buckled in a uniform pattern with a half wave length of approximately 1.75 inches.

Strain gage data for the webs and the skin between the legs of the Y showed no evidence of the skin buckling as seen in Figure 53, where the load strain curve is linear to failure.

Data recorded on the reinforced flanges showed some deviation at approximately 26,000 lbs. or somewhat above the point where the skins buckled as illustrated in Figure 54. The axial stiffness obtained from the initial portion of the curve is 10 x 10^6 lb. which is slightly higher than the predicted value of 9.31 x 10^6 lb., whereas the stiffness (EA) of the upper segment is 5.90 x 10^6 lb. or slightly less than the EA for the stringer and skin between the legs of the "Y" which was 6.35 x 10^6 lb.

One point of concern was the behavior of the flange relative to both lateral and rotational instability. Observations made during the test indicated that this concern was unwarranted. Furthermore, a post test examination of the section indicated that the reinforced flange suffered no damage at all, the failure was solely due to an end failure in the skin which precipitated a buckling in the webs. This is illustrated in Figure 50 where one can see an excessive bending deformation in the skin.

Based upon these results, it is relatively certain that the test panel will attain the design load of 7200 lb/in.

CONCLUSIONS

The selective reinforcement of aluminum stiffeners with unidirectional boron epoxy is an effective means of increasing the efficiency of structural sections. By locating discrete amounts of unidirectional composites at the extremeties of flanges the lateral stiffness of the flanges can be increased significantly, thereby increasing the critical buckling length and/or strength of the stiffener.

Flange torsional stiffness was also shown to be an important parameter where increases in web buckling strength of 27 percent can be achieved, if the rotational restraint provided to the web by the flange is accounted for.

Analytical results obtained for eccentric flanged stiffeners (i.e., Z sections) showed that the normal design practice (Ref. 4) for determining the correct flange proportions relative to the web geometry could be erroneous, if the proper relationship for the flange lateral moment of inertia is not utilized. These results showed that for short ($b/a > 4$) the effect of the eccentricity is negligible and the moment of inertia of the flange should be taken about flange centroid. As section length is increased the eccentricity effect becomes more pronounced.

Design tradeoff studies for stiffened compression panels showed that by selectively reinforced 6005-T5 aluminum panels their efficiencies could be improved to the point where they are superior to conventional all-aluminum designs in 2024 or 7075 aluminum. Weight savings ranged as high as 27 percent when comparing the selectively reinforced 6005-T5 designs with an equivalent 2024 design.

Results obtained for reinforced compression panels considering a range of load indicies (Nx/Lo) showed that there was always an optimum amount of reinforcement above which the addition of more reinforcement would only result in increased weight. For strength critical designs this optimum usually occurred near the point where the aluminum was fully stressed. In stability critical designs, however, the amount of reinforcement required to achieve a minimum weight was unrelated to the stress in the aluminum. The reason proposed for the existence of an optimum amount of reinforcement in these designs is that beyond a certain point the local stability requirements of the skin and stiffeners were the controlling parameters.

Final design calculations for the proof test panel fabricated in this program indicate that this design using infiltration reinforced 6005-T5 aluminum NACA Y stiffeners will be 13 percent lighter than an equivalent all-aluminum 7075 design. Although the NACA Y section has consistently been shown to be superior to all other stiffener shapes from a structural efficiency point of view, it was noted in this program that splice plate attachments to NACA-Y stiffened panels are somewhat difficult due to the local bending stresses which develop in the slant webs. The weight introduced by the additional reinforcement required to react these stresses could offset the other structural advantages afforded by the Y sections.

APPENDIX A

BUCKLING OF ECCENTRIC TEE STIFFENERS

The analysis presented here provides two extensions to the work presented in Reference 1. The first extension determines the effect of an eccentric tee in a rigorous manner (Figure A-1) while the second permits the consideration of finite transverse shear stiffness in the tee. The configuration analyzed is shown in Figure A-1. The web is considered to be a flat plate, simply supported on three sides and supported by a beam on the fourth side. The beam provides an elastic support but it is assumed that the centroid of its cross sectional area does not coincide with the middle surface of the plate permitting a coupling between bending and extension through the boundary conditions.

The equilibrium equations for a flat plate are as follows:

$$u_{,xx} + \frac{1-\mu}{2} u_{,yy} + \frac{1+\mu}{2} v_{,xy} = 0 \tag{A-1}$$

$$v_{,yy} + \frac{1-\mu}{2} v_{,xx} + \frac{1+\mu}{2} u_{,xy} = 0 \tag{A-2}$$

$$D\nabla^4 w + \overline{N}_x w_{,xx} = 0 \tag{A-3}$$

Note that equations (A-1) and (A-2) which govern the in-plane displacements u, v, are uncoupled from equation (A-3) which contains only the lateral displacement w. The boundary condition on the elastically supported edge will provide the coupling.

The variables x and y can be separated by assuming the following solution:

$$u = U(y)\cos kx$$
$$v = V(y)\sin kx \tag{A-4}$$

where U and V are functions of y only. Substituting equations (A-4) into equations (A-1) and (A-2) the following total differential equations are obtained:

$$-k^2 U + \frac{1-\mu}{2} U'' + \frac{1+\mu}{2} k V' = 0$$
$$V'' - \frac{1-\mu}{2} k^2 V - \frac{1+\mu}{2} k U' = 0 \tag{A-5}$$

Solutions to equations (A-5) can be written in the following form:

$$U = C_1 \sinh ky + C_2\, y \sinh ky + C_3 \cosh ky + C_4\, y \cosh ky$$

$$V = C_5 \sinh ky + C_6\, y \sinh ky + C_7 \cosh ky + C_8\, y \cosh ky \qquad \text{(A-6)}$$

There can only be four independent constants of the eight shown in equation (A-6). Substituting equation (A-6) into equation (A-5) yields the following relationships between the constants:

$$C_8 = C_2$$

$$C_6 = C_4$$

$$C_7 = C_1 = \frac{3 - \mu}{1 + \mu} \frac{C_4}{k} \qquad \text{(A-7)}$$

$$C_5 = C_3 = \frac{3 - \mu}{1 + \mu} \frac{C_2}{k}$$

The remaining four constants will be determined by applying the boundary conditions on the edges y = 0 and y = b.

A solution for w satisfying equation (A-3) and the boundary conditions in the edges x = 0 and x = a is given by the following: (Ref. 1)

$$w = (A \sinh \zeta y + B \sin \xi y) \sin k x$$

where (A-8)

$$\zeta = k\sqrt{\lambda + 1},\quad \xi = k\sqrt{\lambda - 1},\quad k = \frac{m\pi}{a},\quad \lambda = \sqrt{\frac{\bar{N}_x}{Dk^2}}$$

There are now six arbitrary constants to be determined from the boundary conditions on the edges y = 0 and y = b. These boundary conditions are:

$$\text{at } y = 0,\ u = 0 \qquad \text{(A-9)}$$

$$\text{and } v = 0 \qquad \text{(A-10)}$$

$$\text{at } y = b$$

$$\frac{E_t}{2(1 + \mu)}(u_{,y} + v_{,x}) - E_s A_s u_{,xx} + \bar{Z}_s A_s E_s w_{,xxx} = 0 \qquad \text{(A-11)}$$

$$Ny = 0 \qquad \text{(A-12)}$$

$$Cw_{,xxy} = D(w_{,yy} + \mu w_{,xx}) \qquad \text{(A-13)}$$

$$E_s I_s \, w_{,xxxx} + \left(1 - \frac{E_s I_s}{G_s A_s} L_Q\right) [P \, w_{,xx} - D (w_{,yyy} + |2 - \mu| \, w_{,xxy}) - \bar{Z}_s A_s E_s \, u_{,xxx}] = 0 \qquad \text{(A-14)}$$

where

$G_s A_s$ = Transverse shear stiffness of support beam

P = Load applied to beam

L_Q = Differential operator, $\frac{\partial^2}{\partial x^2}$

Applying the boundary conditions (A-9) through (A-14) to equations (A-6) and (A-8) and setting the determinant of the constant coefficients equal to zero results in the following characteristic equation:

$$[2 \lambda k^2 \eta + (1 + \lambda - \mu)^2 Q \xi \cot \xi b - (1 - \lambda - \mu)^2 \zeta Q \coth \zeta b + 2 r \lambda Q \sqrt{\lambda^2 - 1} \coth \zeta b \cot \xi b - \eta r (\xi \cot \xi b - \zeta \coth \zeta b)] = 0 \qquad \text{(A-15)}$$

where

$$r = \frac{Ck^2}{D}$$

$$\lambda = \left[\frac{\bar{N}_x}{Dk^2}\right]^{1/2}$$

$$Q = 1 + \frac{E_s I_s}{G_s A_s} k^2$$

$$\eta = \frac{E_s I_s}{D} + \frac{E_s A_s \bar{Z}_s^{\,2}}{D} \bar{y} - \frac{PQ}{Dk^2}$$

$$\bar{y} = 1 - \frac{E_s A_s k}{Et} \left[\frac{f(kb)}{(kb)^2 - \frac{(1 - \mu)^2}{(1 + \mu)^2} \sinh^2 kb + \frac{4 \cosh^2 kb}{(1 + \mu)^2} + \frac{E_s A_s k}{Et} f(kb)}\right]$$

$$f(kb) = \frac{2 (3 - \mu)}{1 + \mu} \sinh kb \cosh kb + 2 kb$$

APPENDIX B

BUCKLING OF ECCENTRICALLY STIFFENED FLAT PLATES

The present analysis follows the work presented in References 6 and 11, but refines the analyses presented therein by permitting the stiffener element to have a finite transverse shear stiffness. The geometry of the plate under consideration is shown in Figure B-1. The method of analysis is identical to Reference 1, except that the strain energy has an additional term to account for the transverse shear flexibility. The strain displacement relations for the stiffener are:

$$\epsilon_x = u_{,x} - z(w_{,xx} - \alpha_{,x})$$

$$\gamma_{xz} = \alpha \tag{B-1}$$

The shear strain α is zero if transverse shear flexibility is neglected. The strain energy for the stiffener becomes:

$$\pi_s = \frac{E_s}{2d} \int_0^a \int_0^b \int_{A_s} \epsilon^2{}_x \, dA_s dxdy + \frac{G_s}{2d} \int_0^a \int_0^b \int_{A_s} \gamma^2{}_{xy} \, dA_s dxdy \tag{B-2}$$

Substituting from equation (B-1) and integrating over the area of the stiffener the strain energy can be put into the following form:

$$\pi_s = \frac{E_s}{2d} \int_0^a \int_0^b \left[A_s u^2{}_{,x} - 2\bar{Z}_s u_{,x}(w_{,xx} - \alpha_{,x}) A_s \right.$$

$$\left. + I_z (w_{,xx} - \alpha_{,x})^2 \right] dxdy + \frac{G_s A_s}{2d} \int_0^a \int_0^b \alpha^2 \, dxdy \tag{B-3}$$

where $\bar{z}_s$ is the distance from the centroid of the stiffener to the middle surface of the plate and I_z is the moment of inertia of the stiffener with respect to the middle surface of the plate. If the energy expressed by equation (B-3) is added to the strain energy of the plate and the principle of minimum potential energy applied the following equilibrium equations are obtained:

$$\left[1 + \frac{E_s A_s (1 - \mu^2)}{Etd}\right] u_{,xx} + \frac{1-\mu}{2} u_{,yy} + \frac{1+\mu}{2} v_{,xy} - \frac{\bar{z}_s E_s A_s (1 - \mu^2)}{Etd} w_{,xxx}$$

$$+ \frac{E_s A_s \bar{z}_s (1 - \mu^2)}{Edt} \alpha_{,xx} = 0$$

$$v_{,yy} + \frac{1 - \mu}{2} v_{,xx} + \frac{1 + \mu}{2} u_{,xy} = 0$$

$$\frac{G_s A_s}{d} \alpha - \frac{E_s (I_s + \bar{z}_s A_s)}{d} \alpha_{,xx} + \frac{E_s (I_s + \bar{z}_s^2 A_s)}{d} w_{,xxx} \qquad \text{(B-4)}$$

$$- \frac{E_s A_s \bar{z}_s}{d} u_{,xx} = 0$$

$$D\nabla^4 w - \frac{\bar{z}_s E_s A_s}{d} u_{,xxx} + \frac{E_s (I_s + \bar{z}_s A_s)}{d} w_{,xxxx} + \frac{G_s J_s}{d} w_{,xxyy}$$

$$+ \bar{N}_x w_{,xx} - \frac{E_a (I_s + \bar{z}_s^2 A_s)}{d} \alpha_{,xxx} = 0$$

This system of four equilibrium equations can be solved for simple support boundary conditions by selecting the following expressions for displacement u, v, w, and shear strain α.

$$u = \bar{u} \cos \frac{m \pi x}{a} \sin \frac{n \pi y}{b}$$

$$v = \bar{v} \sin \frac{m \pi x}{a} \cos \frac{n \pi y}{b} \qquad \text{(B-5)}$$

$$w = \bar{w} \sin \frac{m \pi x}{a} \sin \frac{n \pi y}{b}$$

$$\alpha = \bar{\alpha} \cos \frac{m \pi x}{a} \sin \frac{n \pi y}{b}$$

Substituting equations (B-5) into (B-4) and setting the determinant of the coefficients of u, v, w, and a equal to zero, the following characteristic equation can be obtained after some algebraic manipulations:

$$\frac{\bar{N}_x a^2}{D\pi^2} = m^2 \left\{ (1+\beta^2)^2 + \frac{G_s J_s}{Dd}\beta + \frac{\frac{E_s I_s}{Dd} + \frac{12(1-\mu^2)\,\bar{S}\left(\frac{\bar{Z}_s}{t}\right)^2 (1+\beta^2)^2}{(1+\beta^2)^2 + \bar{S}(1-\mu^2) + 2\bar{S}(1+\mu)\beta^2}}{1+\left(\frac{m\pi}{a}\right)^2 \frac{Dd}{G_s A_s}\left[\frac{E_s I_s}{Dd} + \frac{12(1-\mu^2)\,\bar{S}\left(\frac{\bar{Z}_s}{t}\right)^2 (1+\beta^2)^2}{(1+\beta^2)^2 + \bar{S}(1-\mu^2) + 2\bar{S}(1+\mu)\beta^2}\right]} \right\} \qquad \text{(B-6)}$$

where

$$\bar{S} = \frac{E_s A_s}{Etd}$$

Equation (B-6) can be minimized with respect to m and n to determine critical values of $\bar{N}_x$ which will produce buckling. Note that as $G_s A_s \to \infty$ (infinite transverse shear stiffness) equation (B-6) reduces to that presented in References 6 and 11 where transverse shear flexibility was neglected.

APPENDIX C

BUCKLING OF A PLATE WITH SINGLE STIFFENER WITH FINITE TRANSVERSE SHEAR STIFFNESS

This analysis follows that of Reference 2 and considers the buckling of a plate with a single stiffener. The plate is of length a, width b, and thickness t (Figure C-1) and is subjected to an applied load $\bar{N}_x$.

The single stiffener is considered to have cross-sectional area A and moment of inertia I. It is assumed that the center line of the stiffener lies in the middle plane of the plate and the moment of inertia I, therefore refers to the axis of the stiffener in this plane. The investigation is limited to symmetric buckling with deflected stiffener. The deflection of the buckled plate is given by:

$$w_1 = \sin k x (C_1 \cosh \zeta y + C_2 \sinh \zeta y + C_3 \cos \xi y + C_4 \sin \xi y) \tag{C-1}$$

where w_1 denotes the deflections of the lower half of the plate, $y > 0$.

A similar expression for the deflection w_2 of the other half of the plate is not needed because of symmetry. ζ and ξ are given by:

$$\zeta = k\sqrt{\lambda + 1} \qquad \xi = k\sqrt{\lambda - 1} \tag{C-2}$$

where $k = \dfrac{m\pi}{a}$ and $\lambda = \sqrt{\dfrac{\bar{N}_x}{Dk^2}}$

The four constants will be determined from the following boundary conditions:

for $y = +\dfrac{b}{2}$; $w_1 = 0$ (C-2a)

and

$$\frac{\partial^2 w_1}{\partial y^2} = 0 \tag{C-2b}$$

for $y = 0$; $\dfrac{\partial^2 w_1}{\partial y} = 0$ (C-2c)

and

$$Q_1 - Q_2 = q$$

Q_1 and Q_2 are the shearing forces per unit length in the plates adjacent to the stiffener (Figure C-2). The last boundary condition expresses the fact that the difference of the shearing forces equal the load q which must be

carried by the stiffener. The differential equation governing the deflection of the stiffener is:

$$E_s I_s \frac{\partial^4 w}{\partial x^4} + \left(1 - \frac{E_s I_s}{G_s A_s} L_Q\right)\left(P \frac{\partial^2 w}{\partial x^2} - q\right) = 0 \qquad \text{(C-3)}$$

where $G_s A_s$ is the transverse shear stiffness of the stiffener, P is the load applied to the stiffener, and L_Q is an operator denoting $\frac{\partial^2}{\partial x^2}$. The expression for the difference $Q_1 - Q_2$ is:

$$Q_1 - Q_2 = q = -D \frac{\partial}{\partial y}\left[\frac{\partial^2 w_1}{\partial y^2} + (2-\mu)\frac{\partial^2 w_1}{\partial x^2} - \frac{\partial^2 w_2}{\partial y^2} - (2-\mu)\frac{\partial^2 w_2}{\partial x^2}\right]_{y=0} \qquad \text{(C-4)}$$

Because of symmetry we have the relations:

$$\left(\frac{\partial^2 w_1}{\partial x^2} = \frac{\partial^2 w_2}{\partial x^2}\right)_{y=0} \quad \text{and} \quad \left(\frac{\partial^3 w_1}{\partial y^3} = -\frac{\partial^3 w_2}{\partial y^3}\right)$$

and therefore,

$$q = -2D\left[\frac{\partial^3 w_1}{\partial y^3}\right] \quad y = 0$$

The deflection w of the stiffener and the deflection w_1 of the plate and their derivations must be alike at $y = 0$, or

$$w = w_1\Big|_{y=0} \; ; \; \frac{\partial w}{\partial x} = \frac{\partial w_1}{\partial x}\Big|_{y=0} \quad \text{etc.}$$

and the boundary condition (4) becomes:

$$B\frac{\partial^4 w}{\partial x^4} + \left(1 - \frac{E_s I_s}{G_s A_s} LQ\right)\left(\frac{P}{D}\frac{\partial^2 w}{\partial x^2} + 2\frac{\partial^3 w}{\partial y^3}\right) = 0$$

where

$$B = \frac{E_s I_s}{D} = \frac{12(1-\mu^2)}{t^3}\left(\frac{E_s}{E_p}\right) I_s$$

where the subscript s refers to the stiffener and the subscript p refers to the plate. Applying the boundary conditions the following characteristic equation is obtained:

$$\left[Bk^4 - Qk^2 \frac{P}{D}\right]\left[\frac{1}{\zeta}\tanh\frac{\zeta b}{2} - \frac{1}{\xi}\tan\frac{\xi b}{2}\right] - 2Q(\zeta^2 + \xi^2) = 0 \qquad \text{(C-5)}$$

where

$$Q = 1 + \frac{E_s I_s}{G_s A_s} k^2$$

the effect of the finite transverse shear stiffness is contained in Q. As $Q = 1$ is equation (C-5) it reduces to that presented in Reference 2. Equation (C-5) can be minimized to determine critical buckling stresses for various plate geometries.

REFERENCES

1. Windenburg, D. W.: Elastic Stability of "T" Stiffeners. Proceedings 5th International Congress for Applied Mechanics, 1939.

2. Bleich, Friedrich: Buckling Strength of Metal Structures. First Edition, McGraw-Hill Co., Inc. 1952.

3. Lenoe, E. M., Oplinger, D. W. and Serpico, J. C.: Experimental Studies of the Elastic Stability of Three-Dimensional Reinforced Composite Shells. Paper presented at 7th Aerospace Sciences Meeting, AIAA (New York, N.Y.), January 1969.

4. Bruhn, E. F.: Analysis and Design of Flight Vehicle Structures. Tri-State Offset Company, Cincinnati, Ohio.

5. Rothwell, A.: Coupled Modes in the Buckling of Panels with Z Sections Stringers in Compression, Paper given at the Symposium on Structural Stability and Optimum, Royal Aeronautical Society (Loughborough) March 1967.

6. Block, D. L., Card, M. F., and Mikulas, M. M. Jr.: Buckling of Eccentrically Stiffened Orthotropic Cylinders. NASA TN D-2960, 1965.

7. Shanely, F. R.: Weight Strength Analysis of Aircraft Structures. Second Edition, Dover Publications Inc.

8. Dow, N. F.: Comparison of the Structural Efficiency of Panels Having Straight-Web and Curved-Web Y-Section Stiffeners. NACA TN No. 1787, 1949.

9. Anon: Engineering Sciences Data Aeronautical Series, Structures Sub Series. Volume II, Royal Aeronautical Society.

10. Peterson, James P.: Structural Efficiency of Aluminum Multiweb Beams and Z-Stiffened Panels Reinforced with Filamentary Boron-Epoxy Composite. NASA TN D-5856. June 1970.

11. McElman, J. A., Mikulas, M. M., and Stein, M.: Static and Dynamic Effects of Eccentric Stiffening of Plates and Cylindrical Shells, AIAA Journal Vol. 4, No. 5, May 1966.

12. Timoshenko, S. P. and Gere, J. M.: Theory of Elastic Stability, Second Edition, McGraw Hill Book Company, Inc., 1961.

TABLE 1. – COMPARISON OF SELECTIVELY REINFORCED WITH ALL ALUMINUM STIFFENED COMPRESSION PANELS

N_x = 7200 lb/in, Length = 48", Width = 36"

Stiffener Shape	Aluminum Grade		Stress in Aluminum		Panel Weight				Weight Savings, %	
	Skin	Stiffener	psi	MN/m^2	Lb.	Lbs/ft^2	N	N/m^2	minimum	maximum
	BORON EPOXY REINFORCED ALUMINUM PANELS									
NACA Y	2024-T3	6005-T5	34.0×10^3	234.4	27.2	2.27	120.98	109.58	6(12)[c]	24
Hat	2024-T3	6005-T5	34.5	237.8	28.6	2.38	127.21	115.22		27
"T"	2024-T3	6005-T5	28.8	198.6	33.2	2.77	147.67	133.75		15
	ALL ALUMINUM PANELS									
NACA Y [a]	7075	7075	43.0×10^3	296.5	29.0	2.42	128.99	116.83		
Curved Web NACA Y[b]	7075	7075	43.0	296.5	31.0	2.58	137.88	124.89		
NACA Y [a]	2024	2024	35.0	241.3	35.8	2.98	159.23	164.23		
Z[a]	7075	7075	37.5	258.5			159.23	144.23		
Envelope Z, Hats, T[a]	2024	2024	32.0	220.6	39.0	3.25	173.47	156.94		

[a] Calculated from Shanley Curves (Reference 7)

[b] Calculated from NACA TN 1787 (Reference 8)

[c] Based upon curved web NACA Y weight (Reference 8)

TABLE 2. – TEST PANEL WEIGHT SUMMARY

Stringer No.	Stringer Weight		Mating Steel Dbl. wt. (4 per stringer)		Total Weight	
	lb.	g.	lb.	g.	lb.	g.
126-6	1.81	821.0	6.19	2807.7	8.00	3,628.7
126-7	1.87	848.2	6.00	2721.5	7.87	3,569.7
126-8	1.87	848.2	6.25	2839.5	8.12	3,687.7
126-9	1.81	821.0	6.19	2807.7	8.00	3,628.7
126-10	1.87	848.2	6.12	2776.0	7.99	3,624.2
126-11	1.81	821.0	6.19	2807.7	8.00	3,628.7
126-12	1.81	821.0	6.19	2807.7	8.00	3,628.7
126-13	1.81	821.0	6.12	2776.0	7.93	3,597.0
126-14	1.81	821.0	6.00	2721.5	7.81	3,542.5
126-15	1.81	821.0	6.25	2839.5	8.06	3,660.5
126-16	1.87	848.2	6.12	2776.0	7.99	3,624.2
Totals	20.15	9139.8	67.62	30680.8	87.77	39,820.6

Wt. of 6061-T6 Al Skin	9.75 lb.	(4,422.5g.)
Wt. of Taper Shims (2)	2.75 lb.	(1,247.3g.)
Wt. of 7075-T6 Al Header "A"	29.12 lb.	(13,208.5g.)
Wt. of 7075-T6 Al Header "B"	29.25 lb.	(13,267.5g.)
Total Weight of Components	158.64 lb.	(71,966.4g.)
Total Weight of Assembled Panel	185.50 lb.	(84,140.9g.)
Calculated Weight of Bolts, Nuts and Rivets	26.86 lb.	(12,174.5g.)

TABLE 3. – PANEL DESIGN DATA SUMMARY

Materials

Stringers - Extruded 6005-T5 aluminum
Skin - 6061-T6 aluminum sheet
Reinforcement - Nominal .004" boron filament in an epoxy matrix

Quantities

Number Filaments/Void	=	1550
Average Filament Diameter	=	.0039 in.
Filament Volume/Void	=	50.5%
Area Aluminum/Bay	=	.4729
Area B/E per Bay	=	.0735 in^2
Reinforcement Ratio	=	15.5%

Weights for Constant Cross Section Center Bay

Measured Weight of Stringer and Rivets	=	1.702 lb/ft^2
Calculated Weight of Skin	=	.880 lb/ft^2
Total Weight/Unit Area		2.582 lb/ft^2

TABLE 4. – INFILTRATION REINFORCED 6061–T6 ALUMINUM TUBING

SPECIMEN GEOMETRY

Item	Units	Thick Walled Rods	Chem Milled Rods
O.D.	in (cm)	.250 (.635)	.219 (.556)
I.D.	in (cm)	.188 (.477)	.188 (.477)
Wall Thickness	in (cm)	.031 (.079)	.015 (.038)
No. Filaments	-	1296	1296
Composite Filament Volume	%	53	53
Area Aluminum	in^2 (cm^2)	.0213 (.137)	.0096 (.062)
Area Boron Epoxy	in^2 (cm^2)	.0277 (.178)	.0277 (.178)
Total Area	in^2 (cm^2)	.0490 (.316)	.0373 (.240)
Percent Reinforcement	%	56	74

SUMMARY OF TEST DATA

Axial Modulus (Measured)	psi (GN/m^2)	23.0×10^6 (158.6)	27.0×10^6 (186.1)
Axial Modulus (Predicted)	psi (GN/m^2)	21.3×10^6 (146.8)	24.8×10^6 (171.0)
Flexural Modulus (Measured)	psi (GN/m^2)	17.1×10^6 (117.9)	-
Flexural Modulus (Predicted)	psi (GN/m^2)	16.3×10^6 (112.3)	-
Axial Strength (Measured)	ksi (TN/m^2)	190×10^3 (1.31)	205×10^3 (1.41)
Axial Strength (Predicted)	ksi (TN/m^2)	250×10^3 (1.72)	300×10^3 (2.06)
Composite Strength (Measured)	ksi (TN/m^2)	300×10^3 (2.06)	260×10^3 (1.79)
Composite Strength (Predicted)	ksi (TN/m^2)	400×10^3 (2.76)	400×10^3 (2.76)

TABLE 5. – INFILTRATION REINFORCED 6061–T6 ALUMINUM TUBING – COMPRESSION TEST RESULTS

Specimen No.	Failure Load		Average Stress		Boron Epoxy Stress	
	lb	kN	ksi	GN/m^2	ksi	GN/m^2
Thick Walled Specimen; L = 0.6 inch						
L1-1	9,500	42.256	194	1.337	308	2.123
L1-2	8,500	37.808	173	1.193	272	1.875
L1-5A	9,200	40.922	184	1.269	298	2.054
L1-5B	9,200	40.922	184	1.269	298	2.054
L1-8	10,300	45.814	210	1.447	337	2.323
L1-10	10,000	44.480	204	1.406	326	2.247
L1-11	9,000	40.032	183	1.261	290	1.999
Chem-milled Specimens; L = 0.6 inch						
L2-1	7,100	31.581	190	1.310	240	1.654
L2-2	8,400	37.363	226	1.558	289	1.992
L2-3	6,900	30.691	185	1.275	234	1.613
L2-4	8,600	38.253	232	1.599	296	2.041
L2-5	7,200	32.026	192	1.323	244	1.682

TABLE 6. – INFILTRATION REINFORCED 6061–T6 TUBING–COLUMN TEST RESULTS

Specimen No.	Length		Measured Buckling Stress				Ultimate Strength		Axial Modulus	
			Strain Gages		Southwell Plots					
	in	cm	ksi	MN/m^2	ksi	MN/m^2	ksi	MN/m^2	psi	GN/m^2
Standard Thick-Walled Reinforced Rod; σ_{cr} = 122.4 ksi (Predicted Simply Supported Ends)										
L1-5A	2.25	5.71	122.5	844	112.2	773	177.5	1223	23×10^6	158
L1-5B	2.25	5.71	-	-	161.2	1111	149.0	1027	-	-
L1-7A	2.25	5.71	110.0	758	-	-	157.0	1082	23×10^6	158
L1-7B	2.25	5.71	-	-	156.9	1081	155.0	1068	-	-
Chem-Milled Reinforced Rod; σ_{cr} = 149.0 ksi (Predicted Simply Supported Ends)										
L2-1	2.0	5.08	130.0	896	196.0	1351	171.5	1182	26×10^6	179
L2-3	2.0	5.08	-	-	198.0	1365	186.6	1287	-	-
L2-4	2.0	5.08	130.0	896	160.0	1103	201.0	1386	26×10^6	179
L2-5	2.0	5.08	-	-	133.0	917	134.0	923	-	-
Standard Thick-Walled Reinforced Rod; σ_{cr} = 17.4 ksi (Predicted Simply Supported Ends)										
L1-3A	6.0	15.24	16.0	110	-	-	44.9	309	22×10^6	151
L1-3B	6.0	15.24	-	-	24.3	167	34.7	239	-	-
L1-9	6.0	15.24	16.0	110	28.5	196	44.7	308	22×10^6	151
Chem-Milled Reinforced Rod; σ_{cr} = 16.9 ksi (Predicted Simply Supported Ends)										
L2-1	6.0	15.24	-	-	27.0	186	18.8	129		
L2-3	6.0	15.24	16.0	110	-	-	40.2	277		
L2-4	6.0	15.24	-	-	46.2	318	42.9	295		
L2-5	6.0	15.24	-	-	31.2	215	32.1	221		

TABLE 7. – INFILTRATION REINFORCED 6061-T6 ALUMINUM TUBING-FLEXURE TEST RESULTS

Specimen No.	Load Condition	EI		Failure Stress					
				σ_{al}		σ_{BE}		Boron Epoxy Core Only	
		$lb\text{-}in^2$	$N - m^2$	ksi	MN/m^2	ksi	GN/m^2	ksi	GN/m^2
L1-6	Center Point	--	-	78	538	176	1.21	312	2.15
L1-8	Center Point	3231	9.27	87	599	196	1.35	347	2.39
L1-10	Center Point	3266	9.37	70	483	157	1.86	278	1.92
L1-1	Quarter Point	3340	9.58	82	565	185	1.27	324	2.23
L1-2	Quarter Point	3230	9.27	87	599	196	1.35	347	2.39
L1-11	Quarter Point	3100	8.89	74	510	166	1.14	294	2.02

TABLE 8. – SUB-ELEMENT TEST SUMMARY

Element Description	Element No.	Test Length		Buckling Load		Buckling Stress in Aluminum(a)		Ultimate Load		Failure Mode
		in	cm	lb	kN	ksi	MN/m^2	lb	kN	
Standard Web and Rod	WR-S-1	6	15.24	6200	27.578	29.5	203.4	6600	29.35	Rod Buckled, m = 1
	WR-S-2	6	15.24	6200	27.578	27.0	186.2	6600	29.35	Rod Buckled, m = 1
	WR-L-1	24	60.96	1600	7.117	7.0	48.3	2250	10.00	Rod Buckled, m = 1
Chem milled Web and Rod	WR-S-1C	6	15.24	2700	12.010	18.5	127.5	5200	23.12	Web Buckled, m = 3
	WR-S-2C	6	15.24	3600	16.013	22.2	153.0	4800	21.35	Web Buckled, m = 3
	WR-L-1C	24	60.96	700	3.114	3.8	26.2	900	4.00	Rod Buckled, m = 1
	WR-L-2C	24	60.96	700	3.114	4.0	27.6	950	4.22	Rod Buckled, m = 1
Standard Reinforced T	T-S-1	6	15.24	17,200	76.505	35.0	241.3	18,000	80.06	Sympathetic buckling of flange
	T-S-2	6	15.24	17,000	75.616	35.0	241.3	18,500	82.28	Sympathetic buckling of flange
	T-S-3	6	15.24	16,000	71.167	32.0	220.6	18,000	80.06	Sympathetic buckling of flange
	T-L-1	24	60.96	14,500	64.496	31.0	213.7	15,500	68.94	Sympathetic buckling of flange, m = 3
	T-L-2	24	60.96	14,500	64.496	31.5	217.2	14,500	64.49	Sympathetic buckling of flange, m = 3
	T-L-3	24	60.96	---	---	---	---	12,200	54.26	End failed
Chem milled Reinforced T	T-S-1C	6	15.24	9600	42.700	27.0	186.1	12,500	55.60	Web Buckled, m = 3
	T-S-2C	6	15.24	10,500	46.704	29.0	199.9	12,500	55.60	Web Buckled, m = 3
	T-S-3C	6	15.24	10,000	44.480	28.0	193.0	12,400	55.15	Web Buckled, m = 3
	T-L-1C	24	60.96	7000	31.136	19.0	131.0	7600	33.80	Sympathetic Buckling of flange, m = 3
	T-L-2C	24	60.96	7000	31.136	19.0	131.0	7800	34.69	Sympathetic Buckling of flange, m = 3
Reinforced L	L-S-1	6	15.24	9500	42.256	34.0	234.4	11,000	48.92	Flange Buckled, m = 1
	L-S-2	6	15.24	11,000	48,928	36.0	248.2	11,000	48.92	Flange Buckled, m = 1
	L-L-1	24	60.96	6400	28,467	22.0	151.7	8000	35.58	Flange Buckled, m = 3
	L-L-2	24	60.96	8400	37.363	28.0	193.0	9000	40.03	Flange Buckled, m = 3

TABLE 9. – SUB-ELEMENT ANALYTICAL-EXPERIMENTAL CORRELATION

Element Description	Length		EA (Predicted)		EA (Measured)		Buckling Coefficient (k)		P_{cr} (Predicted)		P_{cr} (Measured)	
	in.	cm	lb	MN	lb	MN	Predicted	Measured	lb	kN	lb	kN
Standard Web and Rod	6	15.24	2.23×10^6	9.91	2.13×10^6	9.47	1.39	1.58	5480	24.3	6200	27.5
	24	60.96	2.23	9.91	2.27	10.1	0.80	0.40	3180	14.1	1600	7.1
Chem-milled Web and Rod	6	15.24	1.79	7.96	1.67	7.42	5.10	4.25	4380	19.4	3150	14.0
	24	60.96	1.79	7.96	1.71	7.60	0.90	0.81	860	3.82	925	4.1
Thick T	6	15.24	4.69	20.8	4.75	21.1	Stress Failure	–	16,900	75.1	17,000	75.6
	24	60.96	4.69	20.8	4.80	21.3	Stress Failure (0.80)[a]	– (0.51)[a]	16,900	75.1	14,500	64.4
Chem-milled T	6	15.24	3.63	16.1	3.60	16.0	5.10	5.16	10,200	45.3	10,000	4.44
	24	60.96	3.63	16.1	3.80	16.9	5.10 (0.90)[a]	3.50 (0.83)[a]	10,200	45.3	7,000	31.1
L Section	6	15.24	2.92	12.9	2.85	12.6	Stress Failure	–	10,500	46.7	10,250	45.6
	24	60.96	2.92	12.9	3.00	13.3	Stress Failure (0.80)[a]	–	10,500	46.7	7,400	32.9

(a) Values determined using local flange buckling model.

TABLE 10. – TEST ELEMENT DESIGN PARAMETERS

Section Description	Area of Aluminum		Area Boron Epoxy		EI/Db	C/Db	S
	in^2	cm^2	in^2	cm^2			
Standard Web & Rod	.1376	.887	.0284	.183	15.2	8.0	1.4
Chem-milled Web & Rod	.0938	.585	.0284	.183	102.0	53.0	2.6
Standard T	.0938	.585	.0568	.366	4310	15.0	3.7
Chem-milled T	.1930	1.245	.0568	.366	7189	7.7	4.5
L Section	.2072	1.335	.0284	.183	2240	3.9	1.8

TABLE 11. – SUMMARY OF NACA-Y TEST DATA

Element No.	Test Length		Buckling Load		Buckling Stress In Aluminum		Ultimate Load		Gross Stress (P/A) Ultimate		Stress in B/E		Failure Mode
	in.	cm	lb	kN	ksi	MN/m2	lb	kN	ksi	MN/m^2	ksi	MN/m^2	
NACA-Y-1	1.375	3.49	37,000	164.6	58.2	401.2	42,000	186.8	87.6	604.0	344.0	2371.0	End failure precipitated by web and skin buckling
NACA-Y-2	6.0	15.24	26,000	115.6	38.5	246.8	36,000	160.1	74.5	513.6	260.0	1792.0	End failure precipitated by web and skin buckling
NACA-Y-3	6.0	15.24	27,000	120.0	40.0	275.8	36,000	162.3	76.5	527.5	267.0	1841.0	
NACA-Y-4	36.0	91.44	20,000	88.9	26.0	179.3	29,000	129.0	36.5	251.7	96.0	662.0	Skin buckling followed by local end failure in skin only.

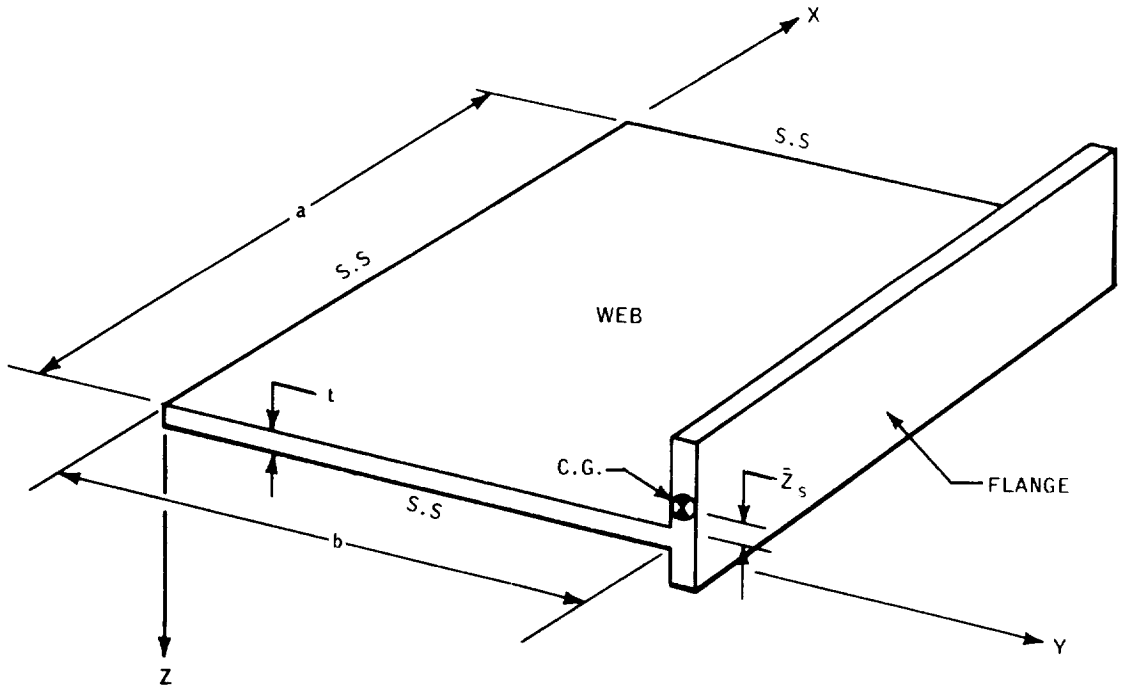

Figure 1 ELASTICALLY SUPPORTED PLATE - STIFFENER MODEL

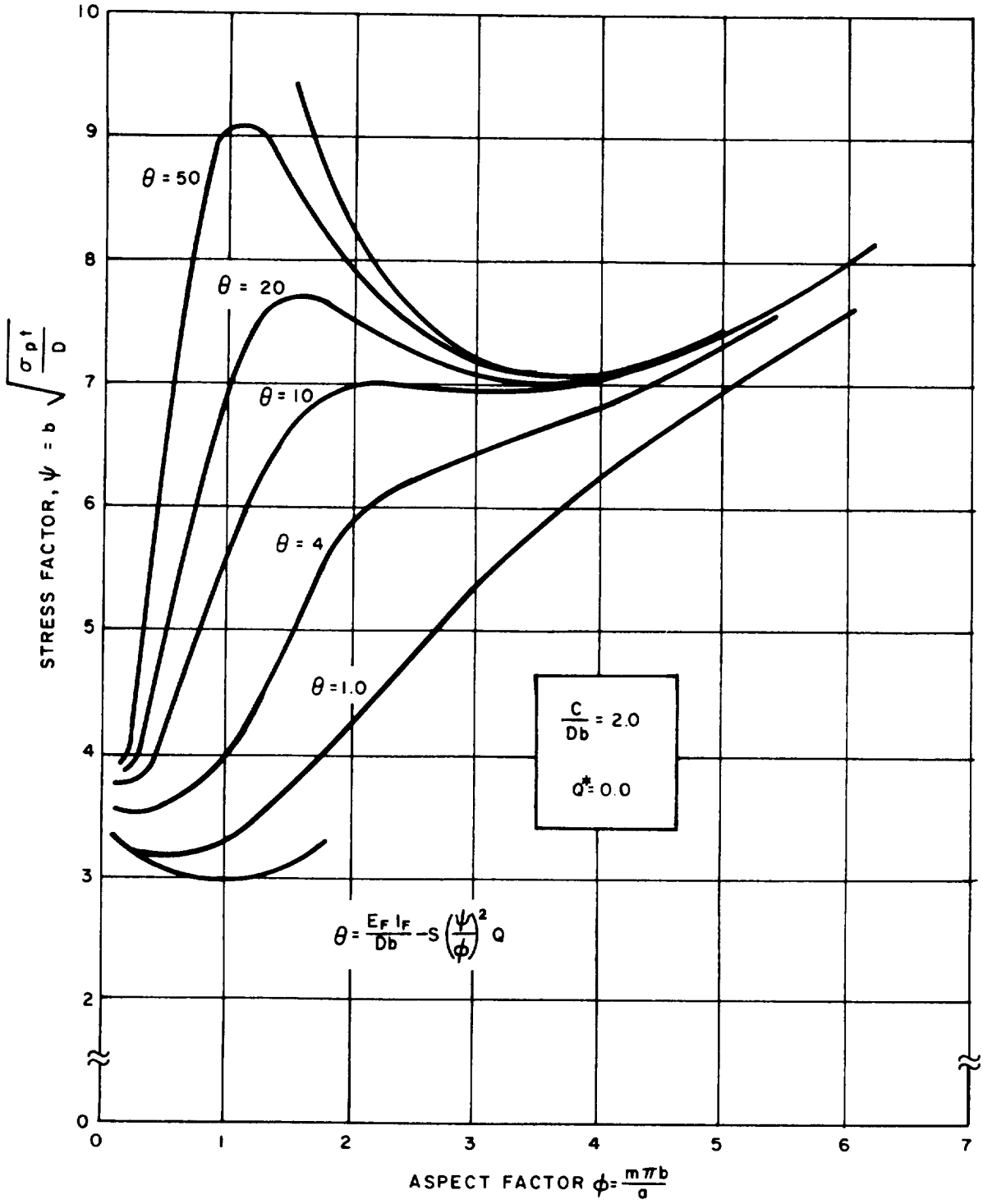

Figure 2 EFFECT OF FLEXURAL RIGIDITY FACTOR θ ON STRESS FACTOR ψ

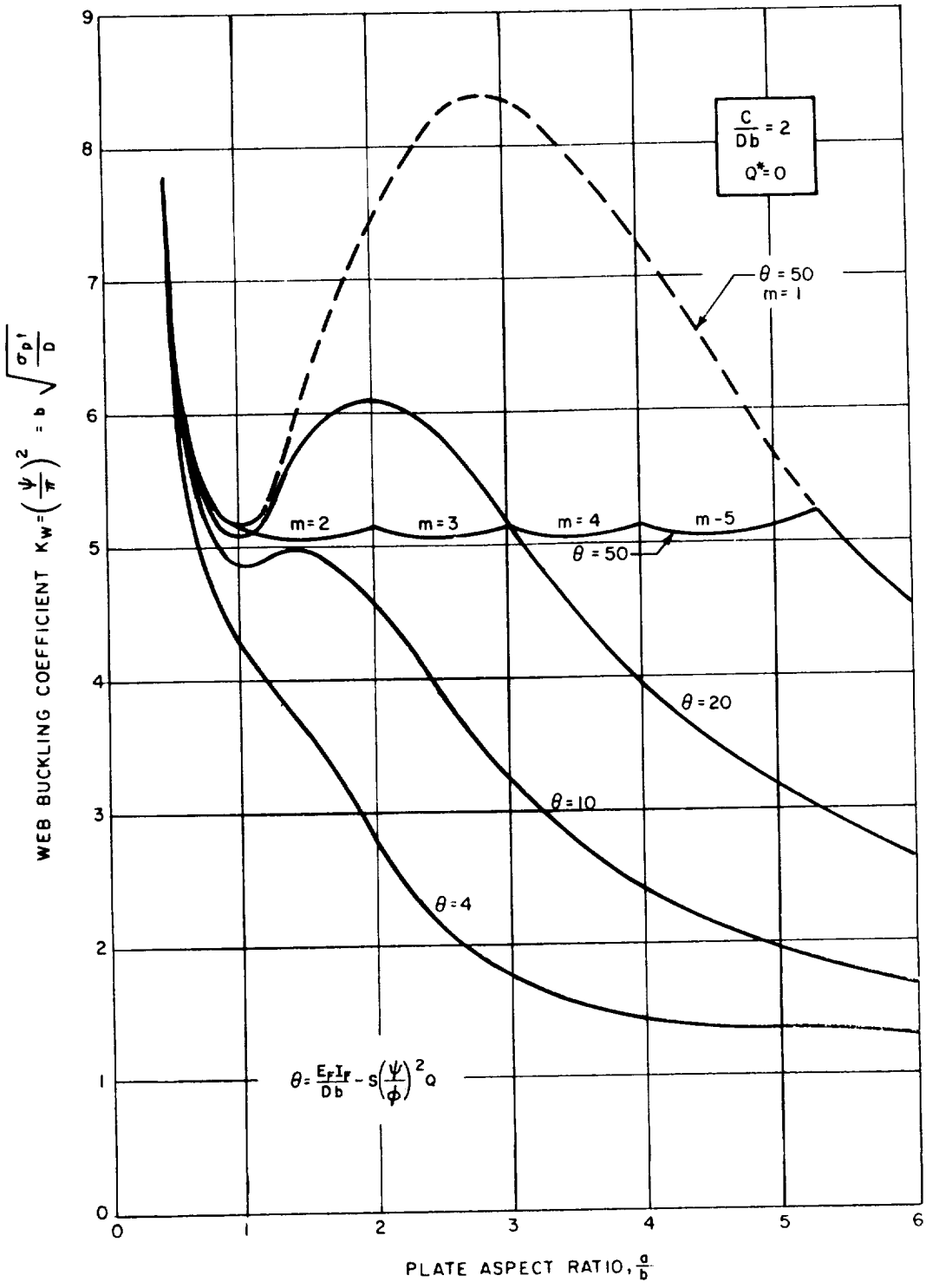

Figure 3 EFFECT OF FLEXURAL RIGIDITY FACTOR θ ON WEB BUCKLING COEFFICIENTS K_w

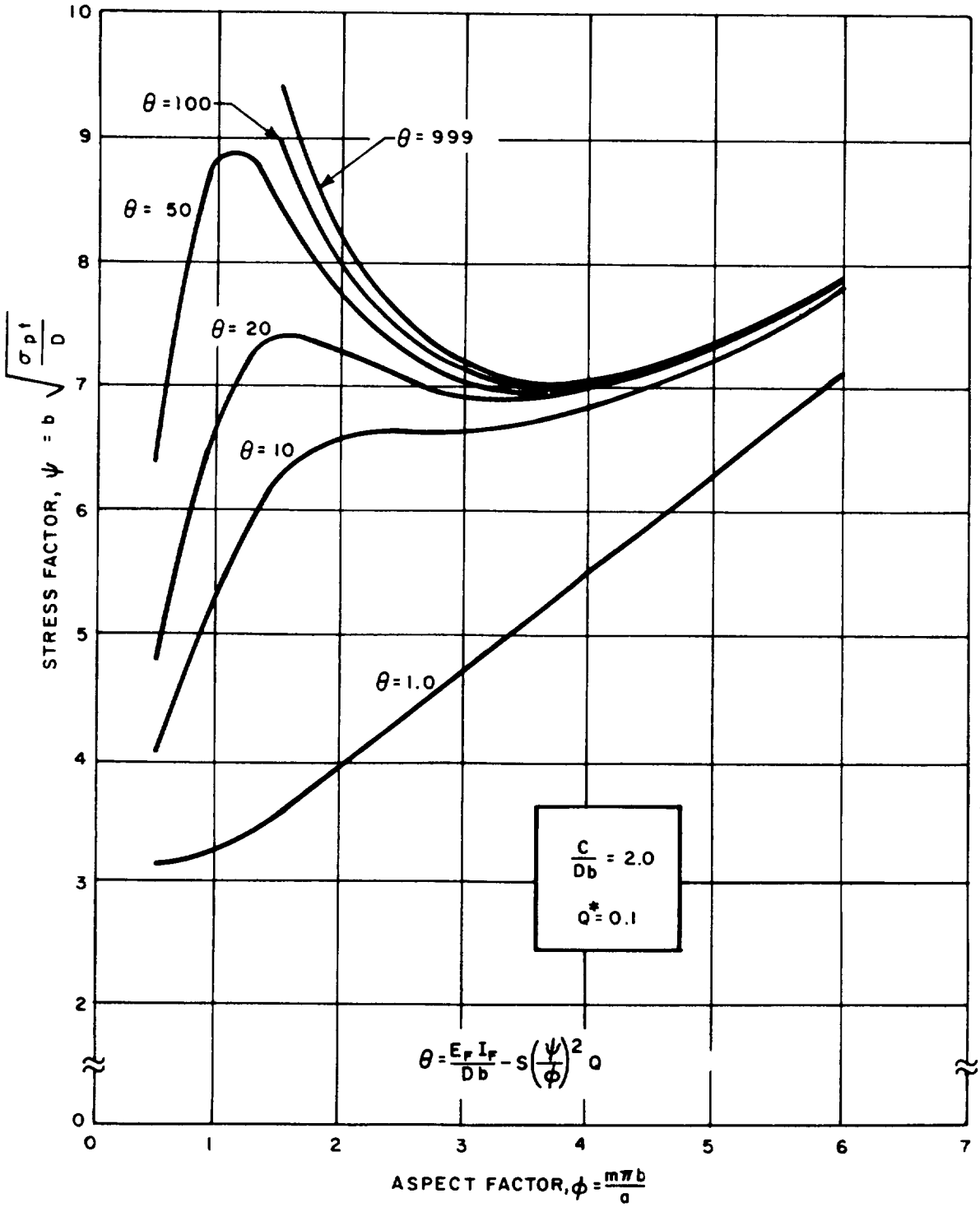

Figure 4 EFFECT OF FLEXURAL RIGIDITY FACTOR θ ON STRESS FACTOR ψ

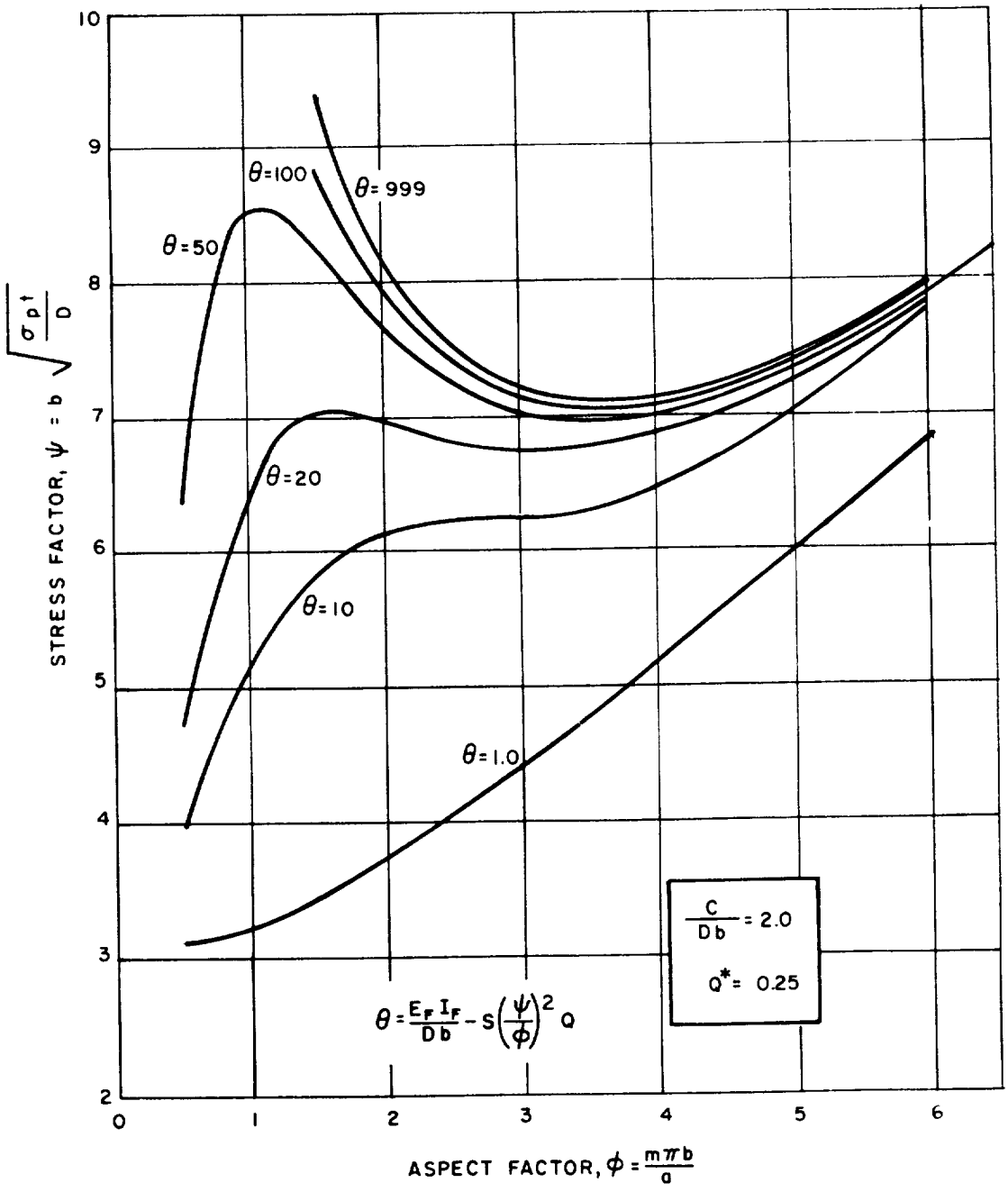

Figure 5 EFFECT OF FLEXURAL RIGIDITY FACTOR θ ON STRESS FACTOR ψ

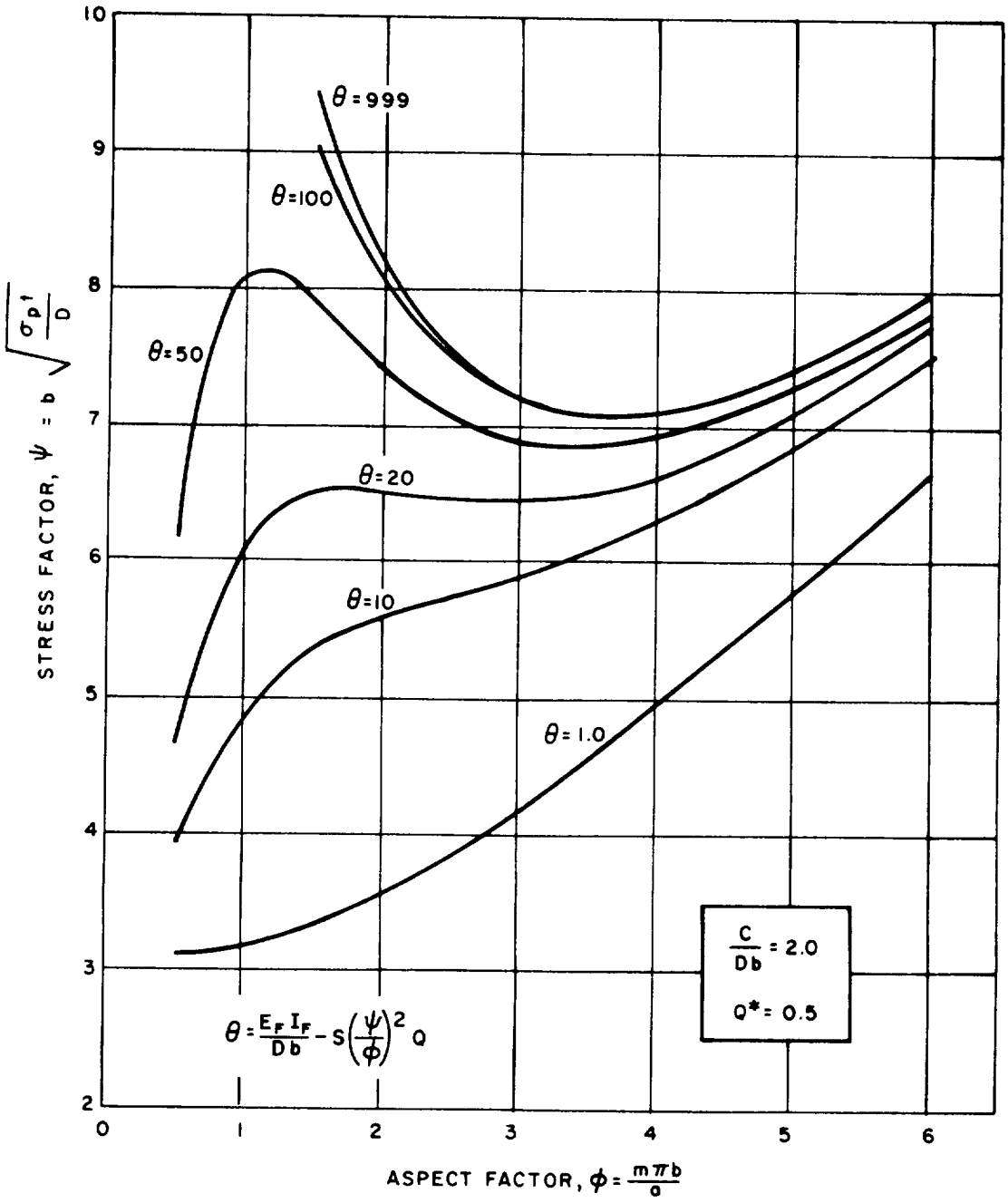

Figure 6 EFFECT OF FLEXURAL RIGIDITY FACTOR θ ON STRESS FACTOR ψ

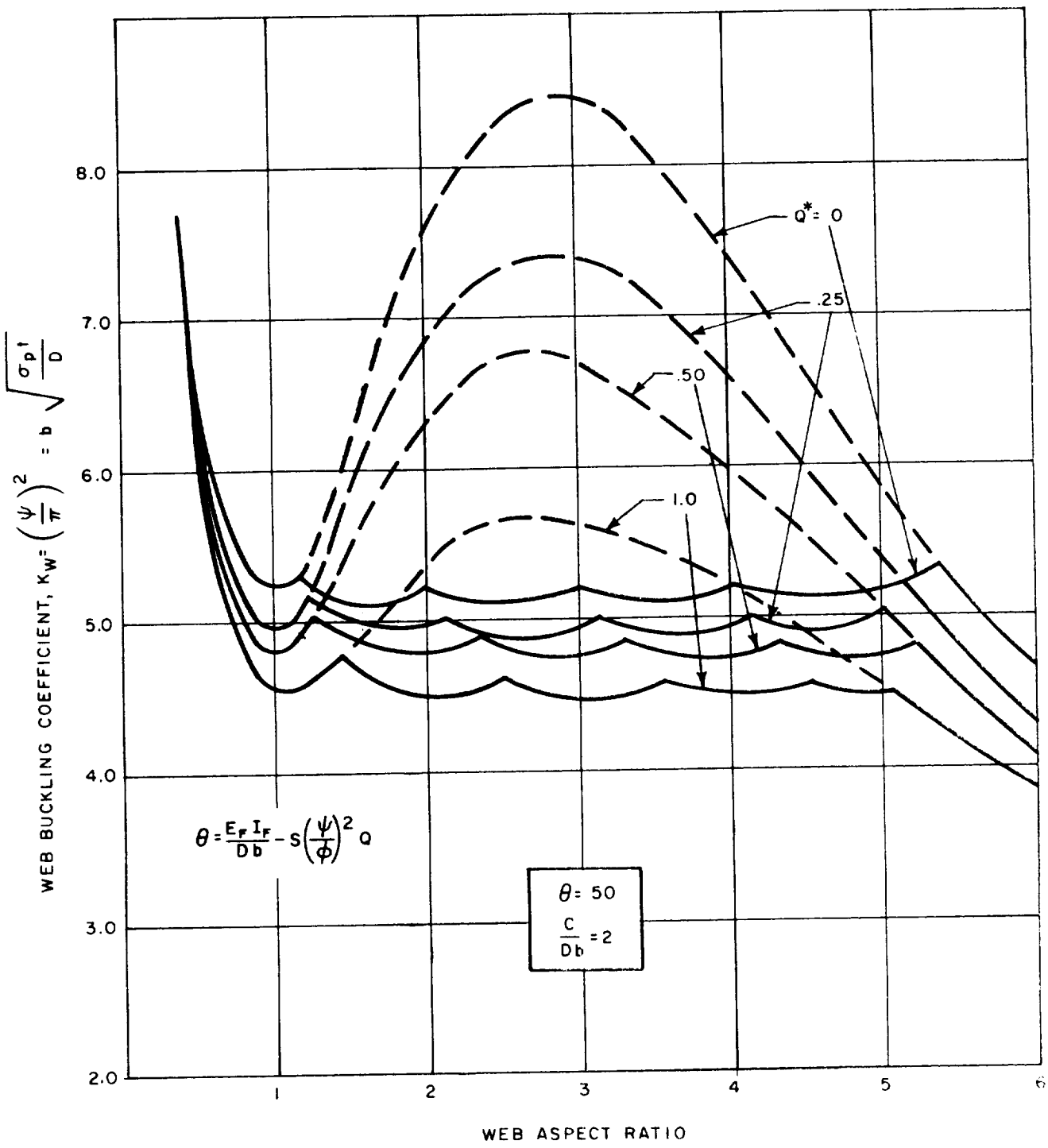

Figure 7 EFFECT OF FLANGE TRANSVERSE SHEAR STIFFNESS FACTOR Q* ON WEB BUCKLING COEFFICIENT K_w

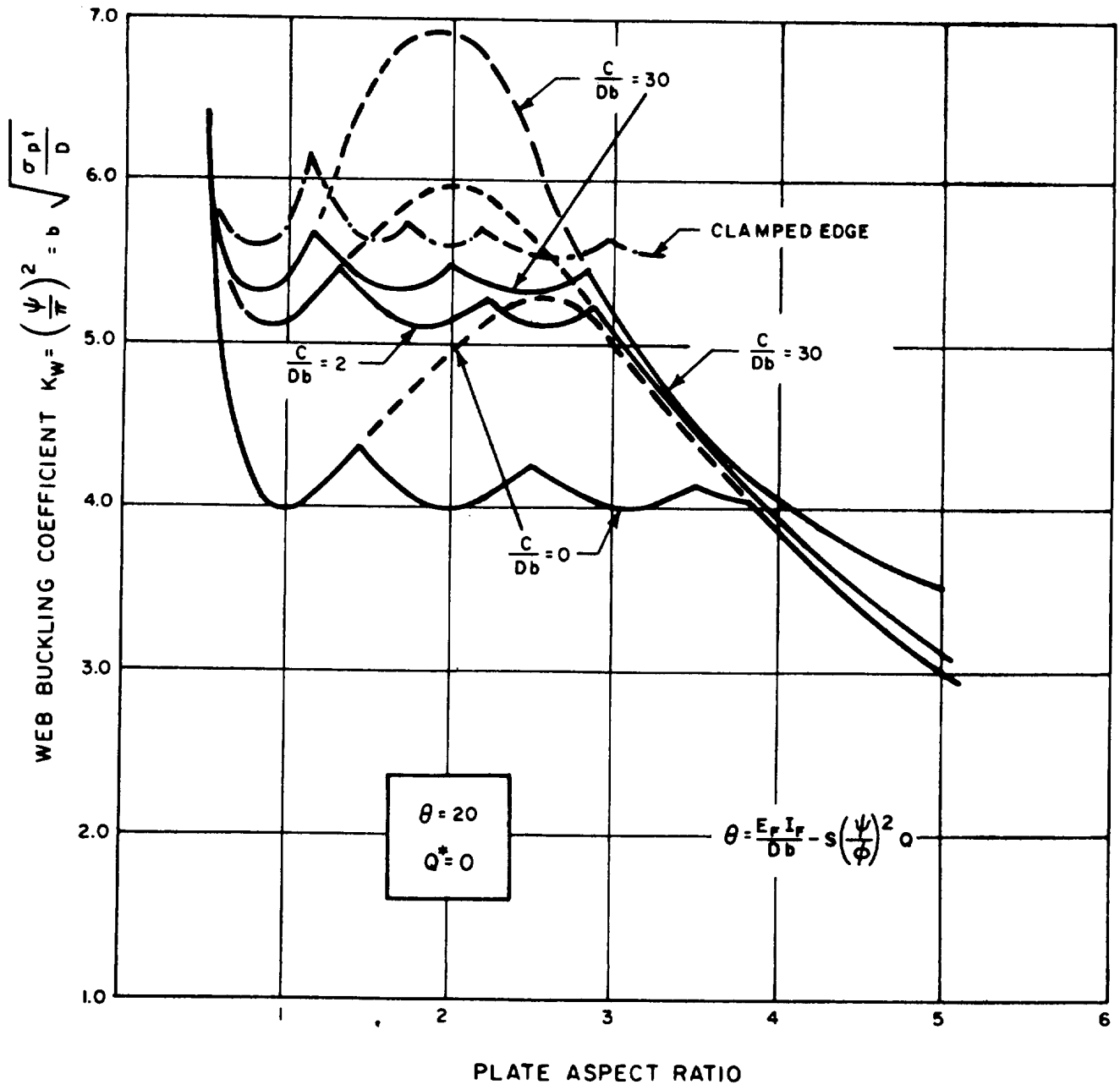

Figure 8 EFFECT OF FLANGE TORSIONAL RIGIDITY (C/Db) ON WEB BUCKLING COEFFICIENT K_w

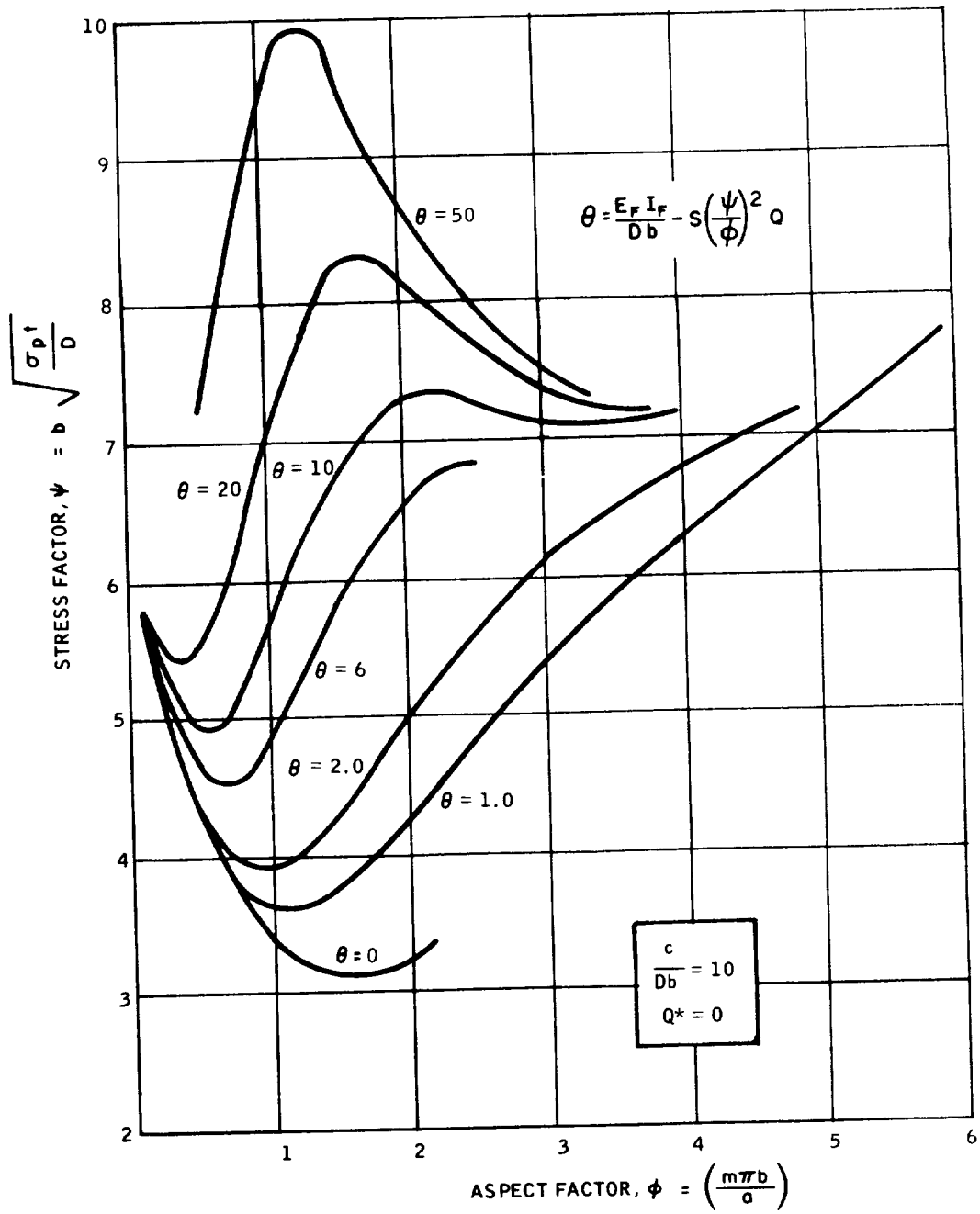

Figure 9 EFFECT OF FLEXURAL RIGIDITY FACTOR θ ON STRESS FACTOR, ψ

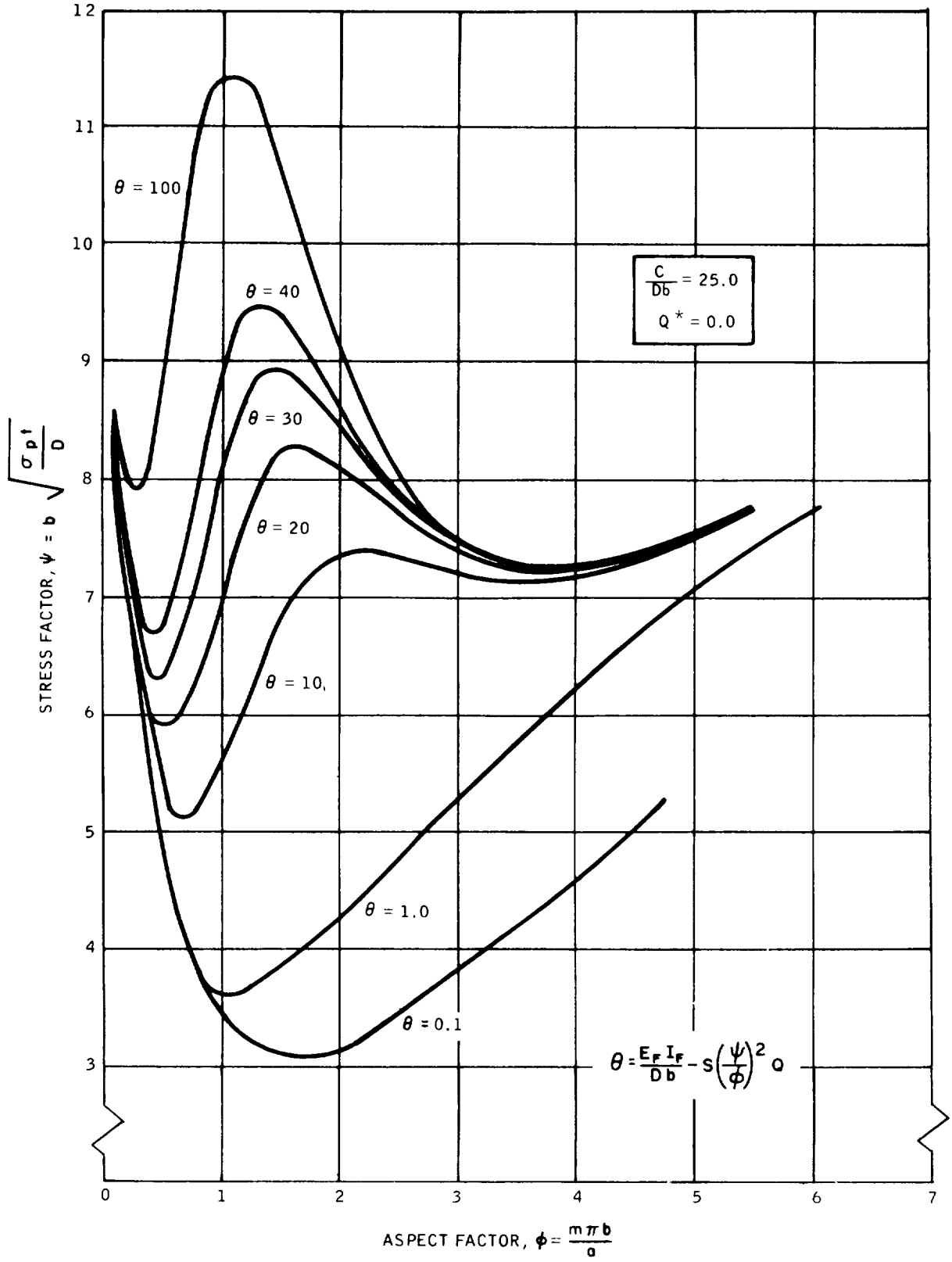

Figure 10 EFFECT OF FLEXURAL RIGIDITY FACTOR θ ON STRESS FACTOR, ψ

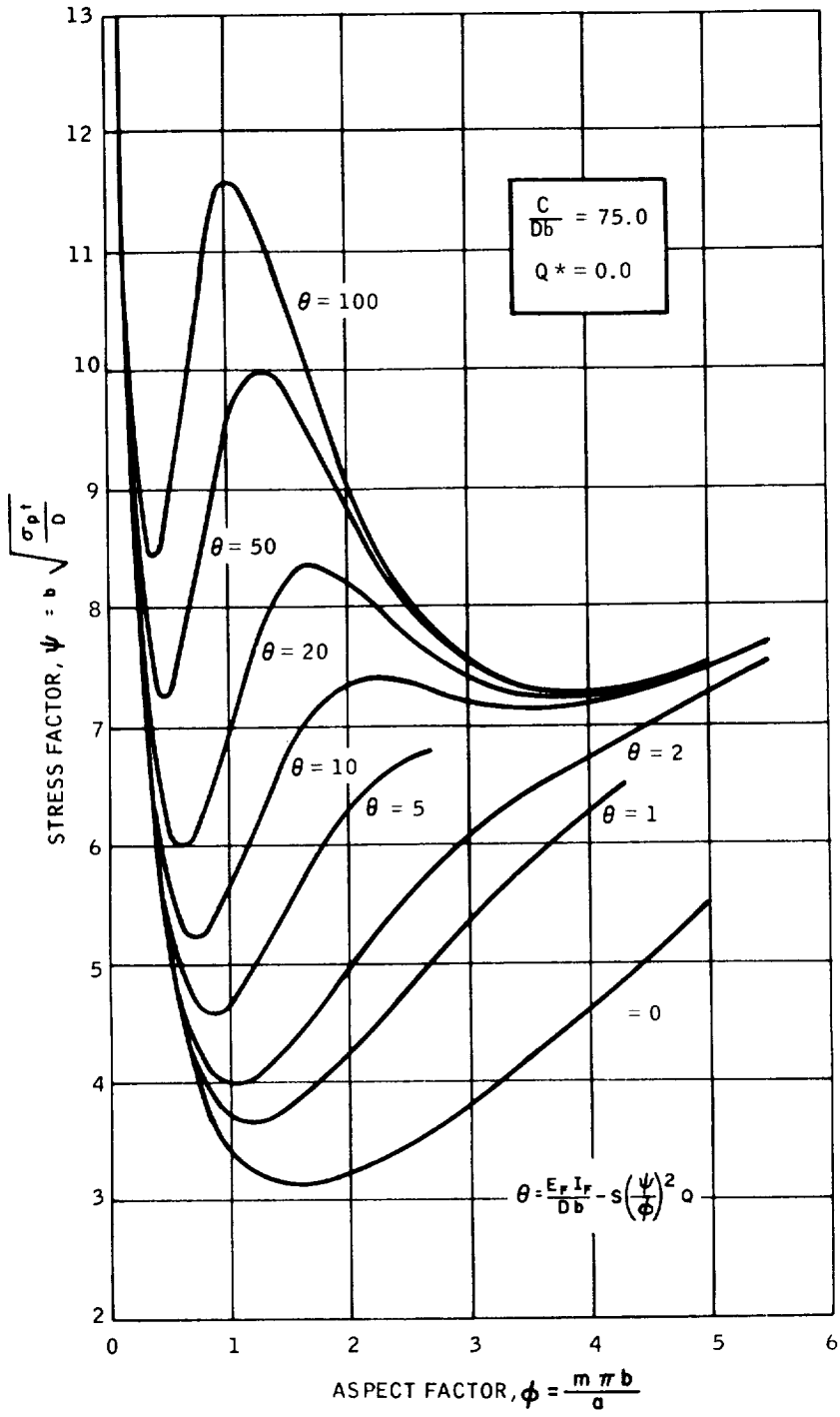

Figure 11 EFFECT OF FLEXURAL RIGIDITY FACTOR θ ON STRESS FACTOR, ψ

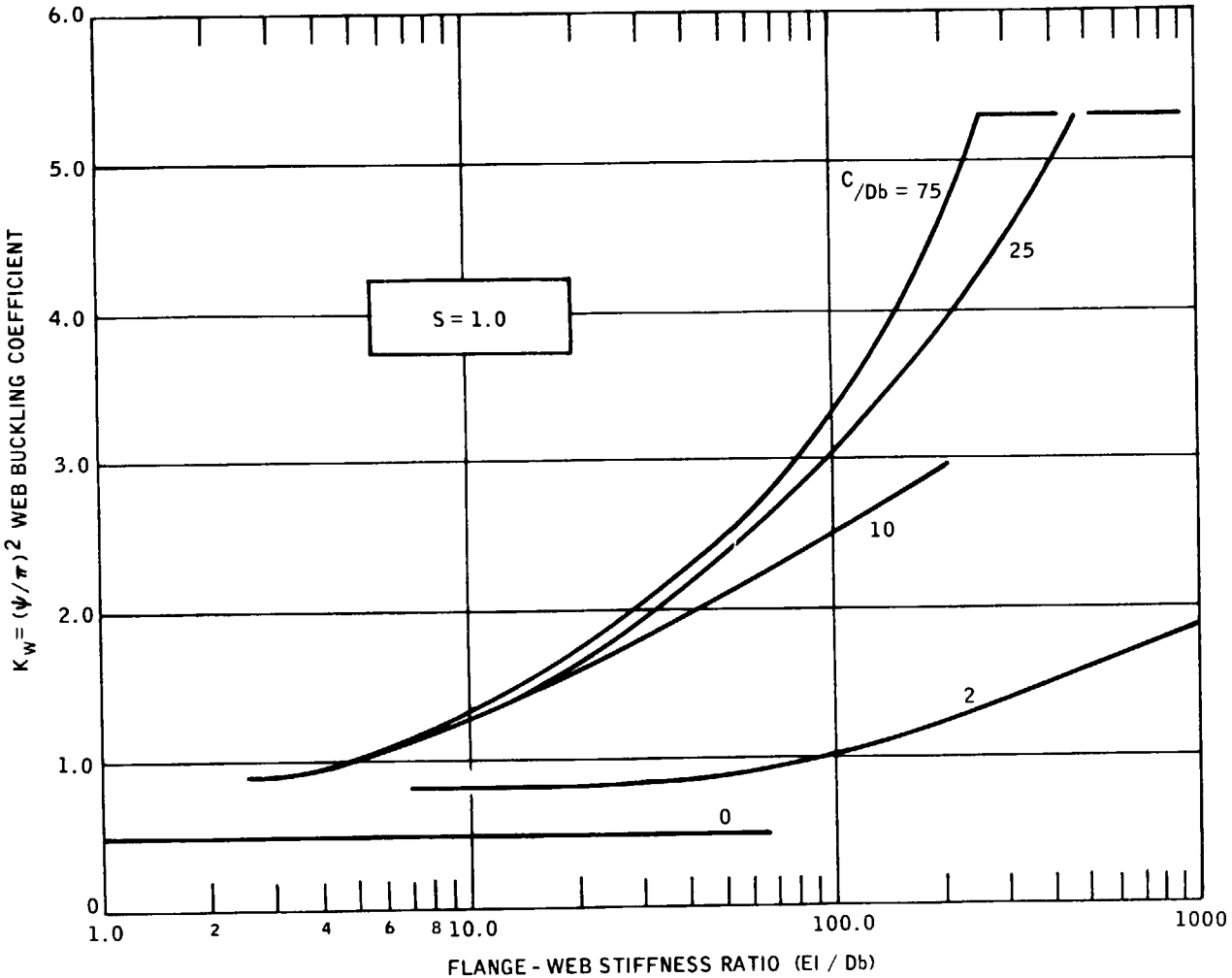

Figure 12 WEB BUCKLING COEFFICIENT FOR LONG STIFFENER SECTION

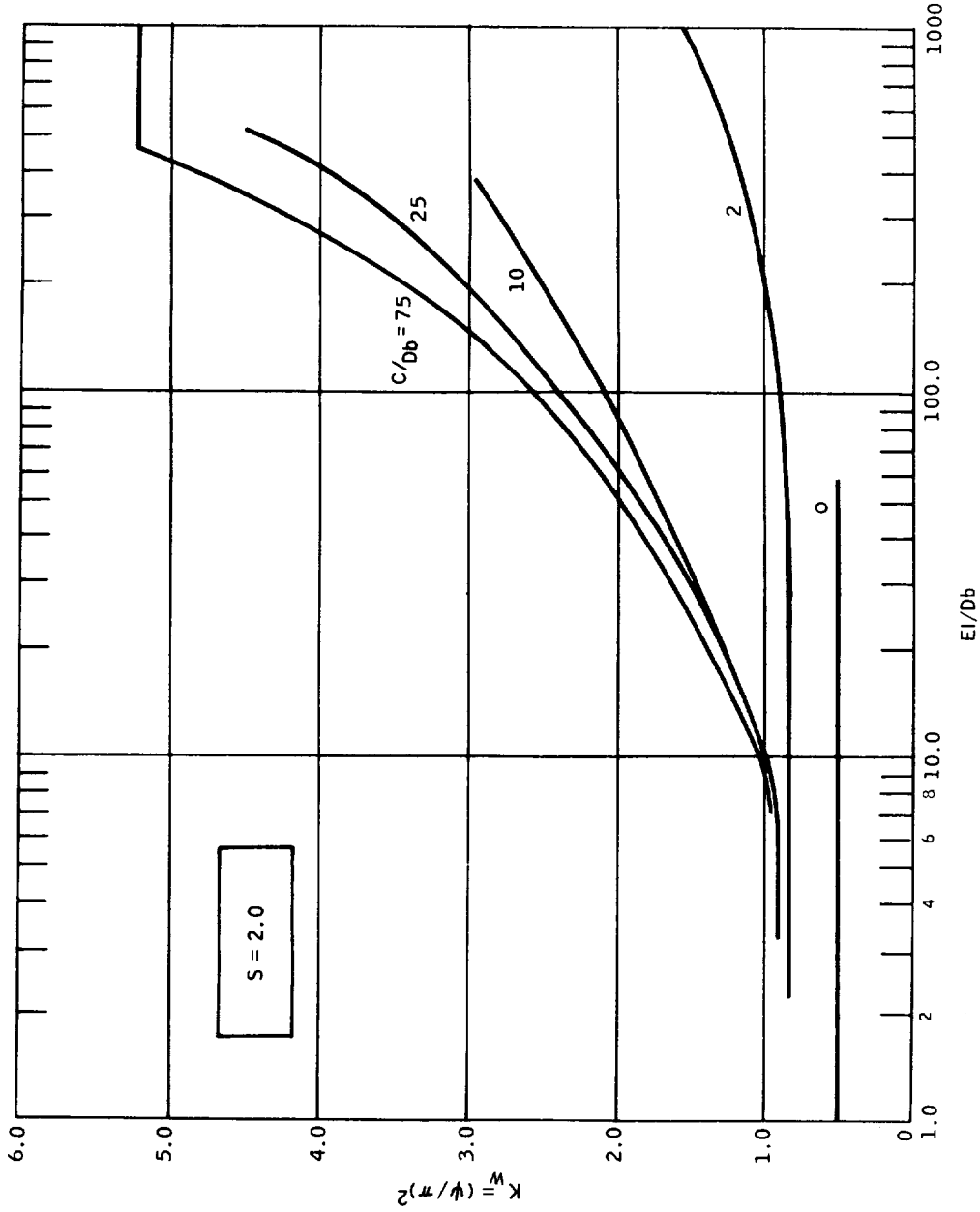

Figure 13 WEB BUCKLING COEFFICIENT FOR LONG STIFFENER SECTION

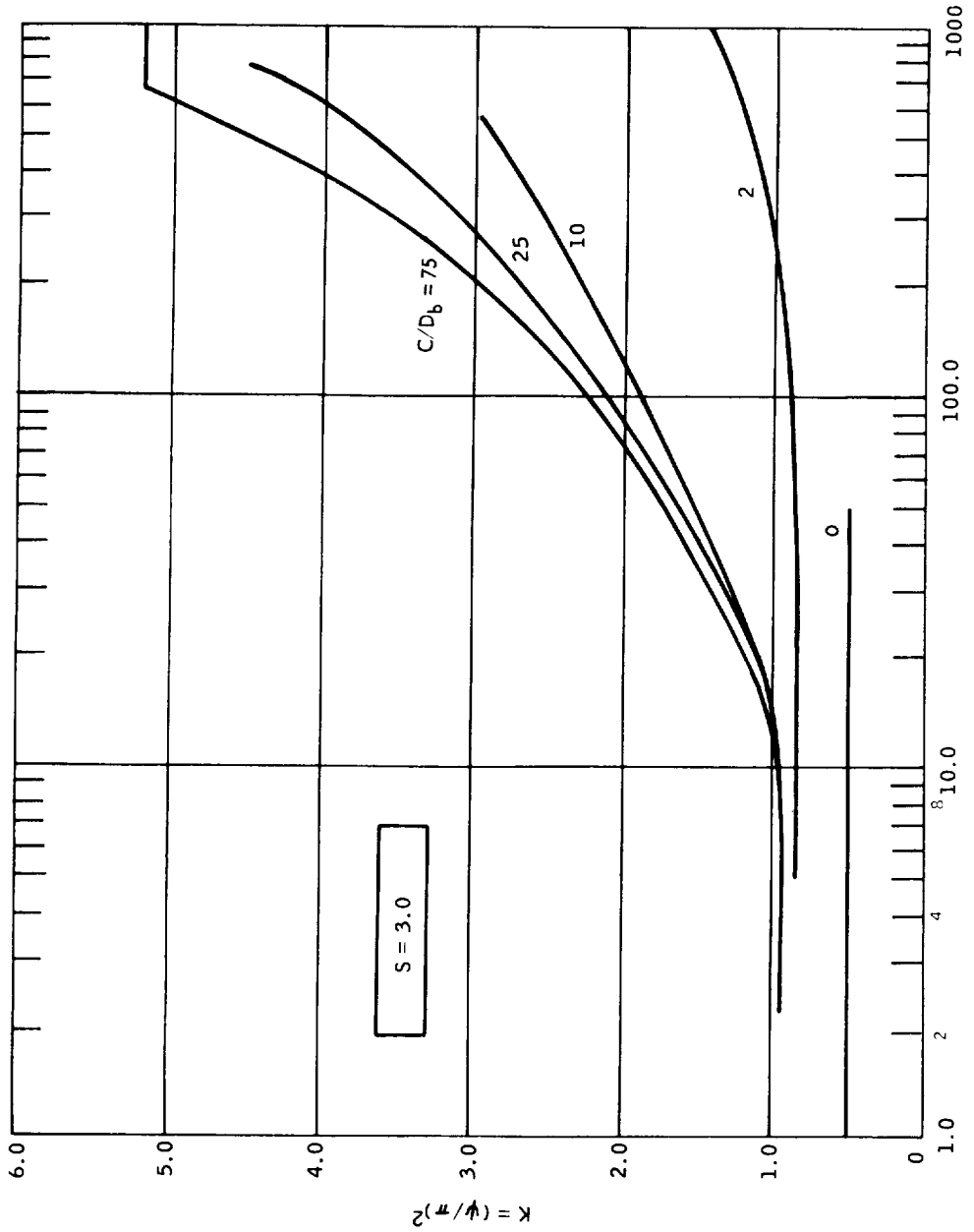

Figure 14 WEB BUCKLING COEFFICIENT FOR LONG STIFFENER SECTION

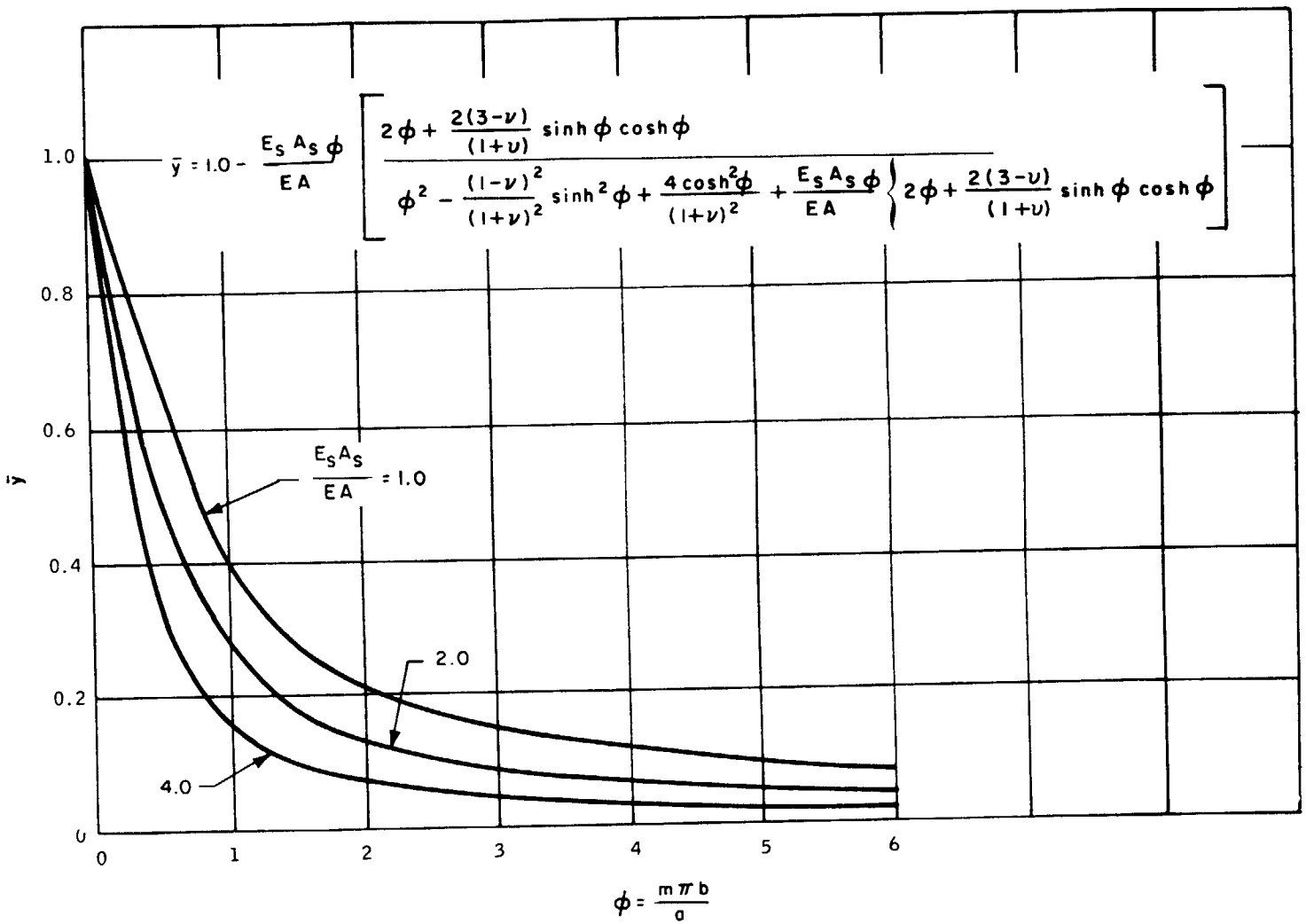

Figure 15 FLANGE ECCENTRICITY PARAMETER

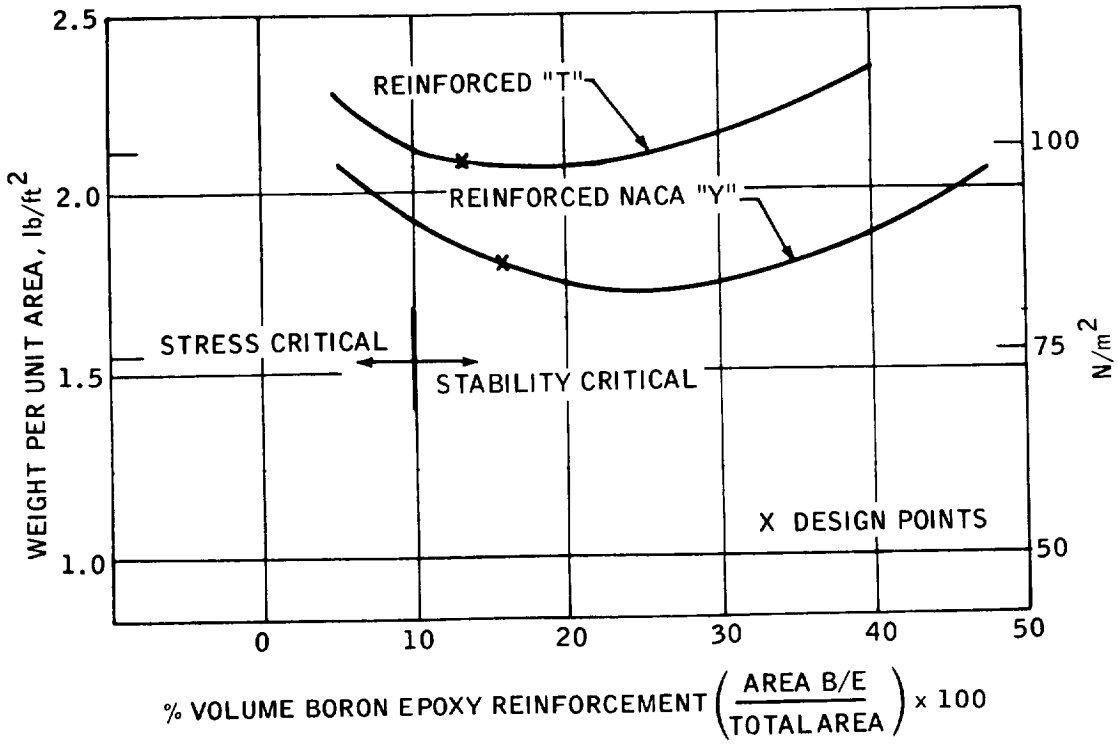

Figure 16 STIFFENED PANEL WEIGHT VERSUS PERCENT OF BORON EPOXY REINFORCEMENT

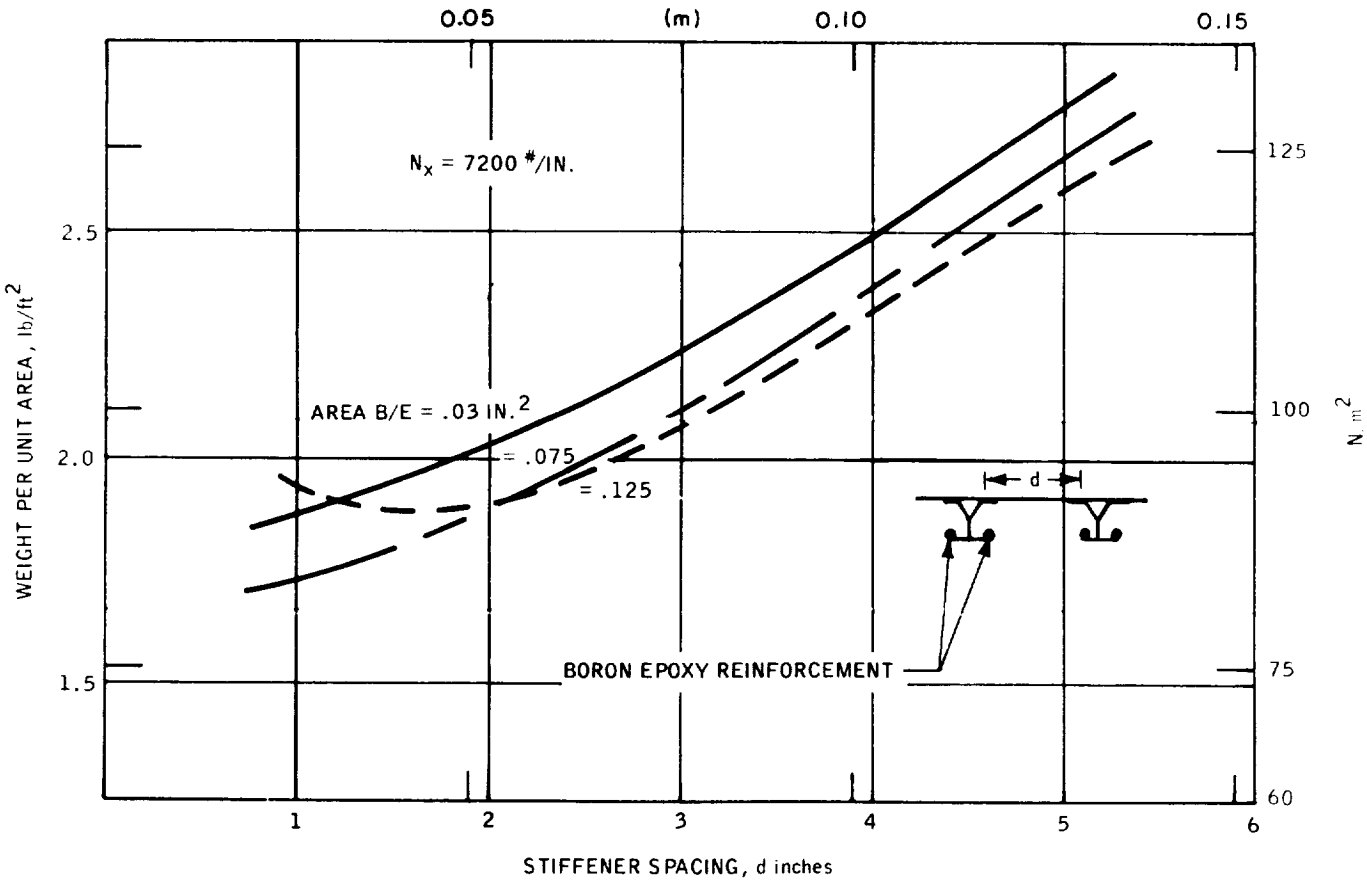

Figure 17 STIFFENED PANEL WEIGHT VERSUS STIFFENER PITCH–SELECTIVELY REINFORCED "Y" STIFFENER

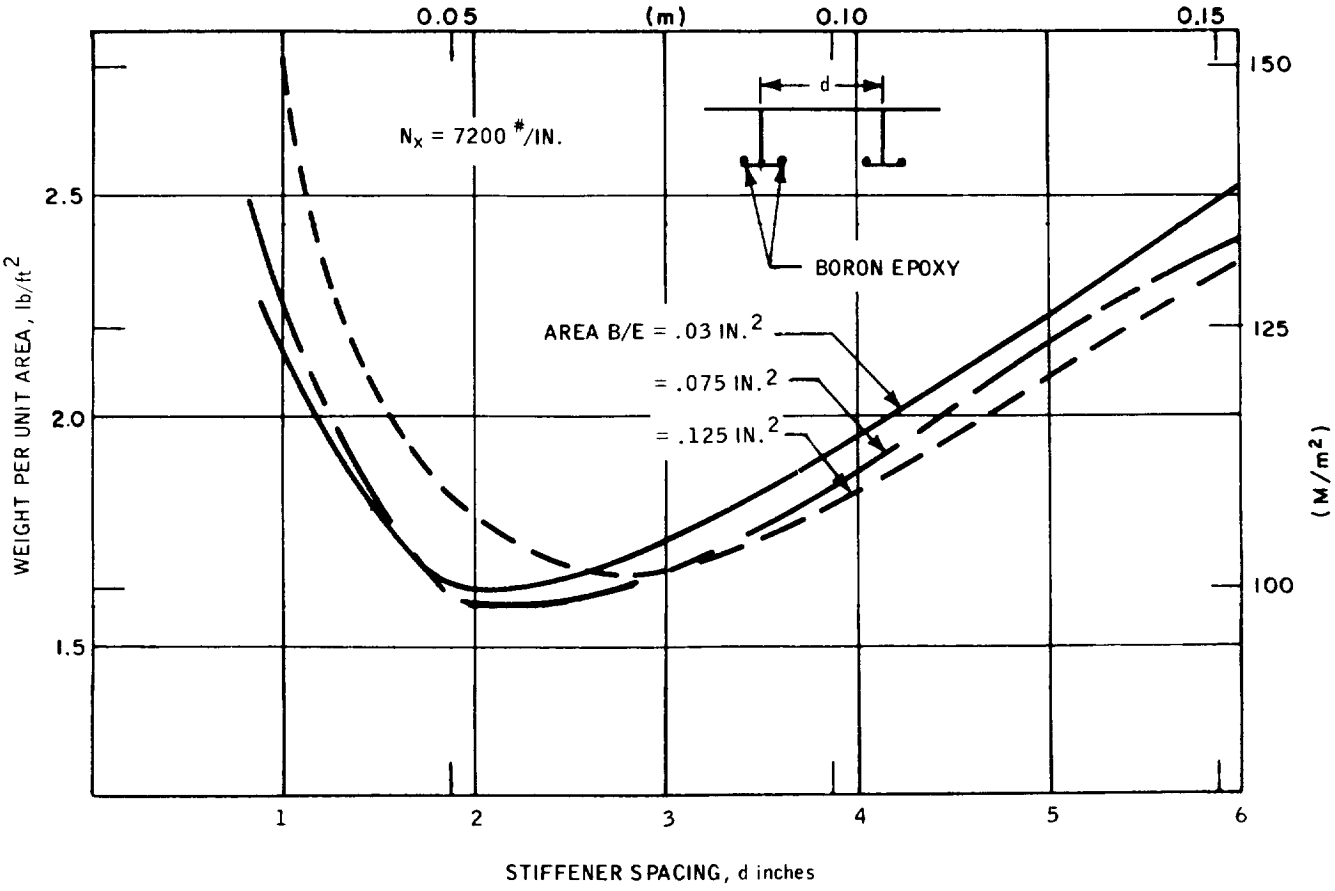

Figure 18 STIFFENED PANEL WEIGHT VERSUS STIFFENER PITCH–SELECTIVELY REINFORCED "Y" STIFFENER

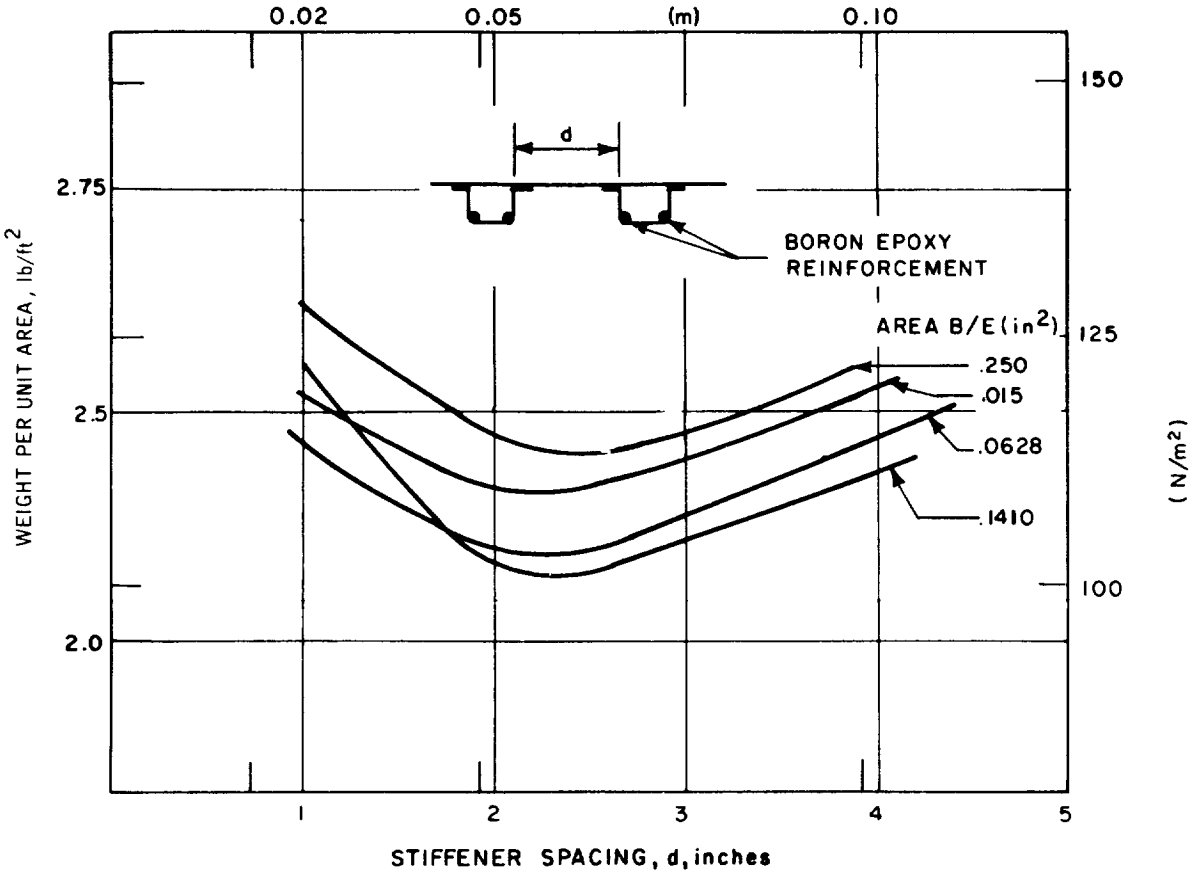

Figure 19 STIFFENED PANEL WEIGHT VERSUS STIFFENER PITCH–SELECTIVELY REINFORCED HAT STIFFENER

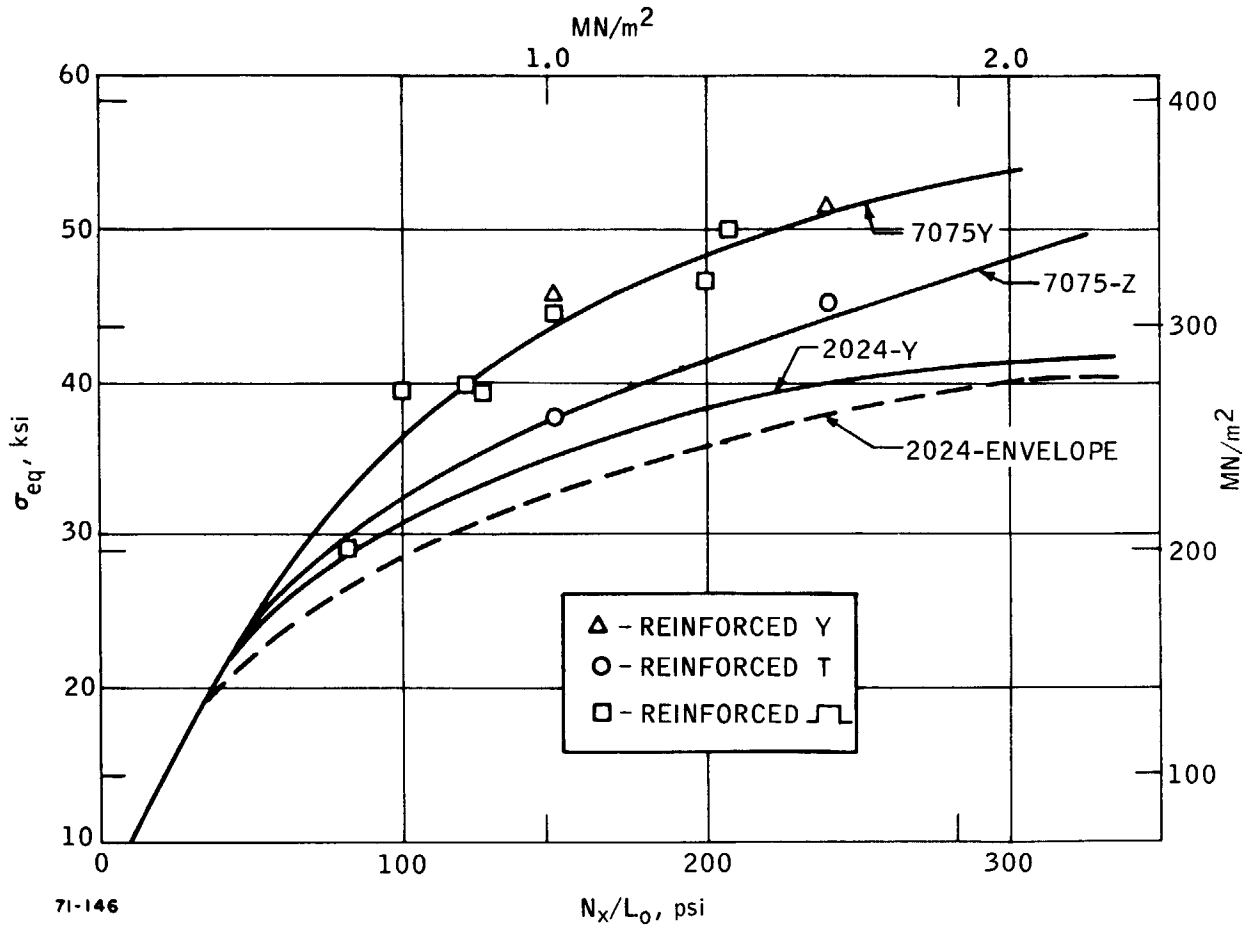

Figure 20 COMPARISON OF SELECTIVELY REINFORCED COMPRESSION PANEL WITH CONVENTIONAL ALUMINUM PANELS

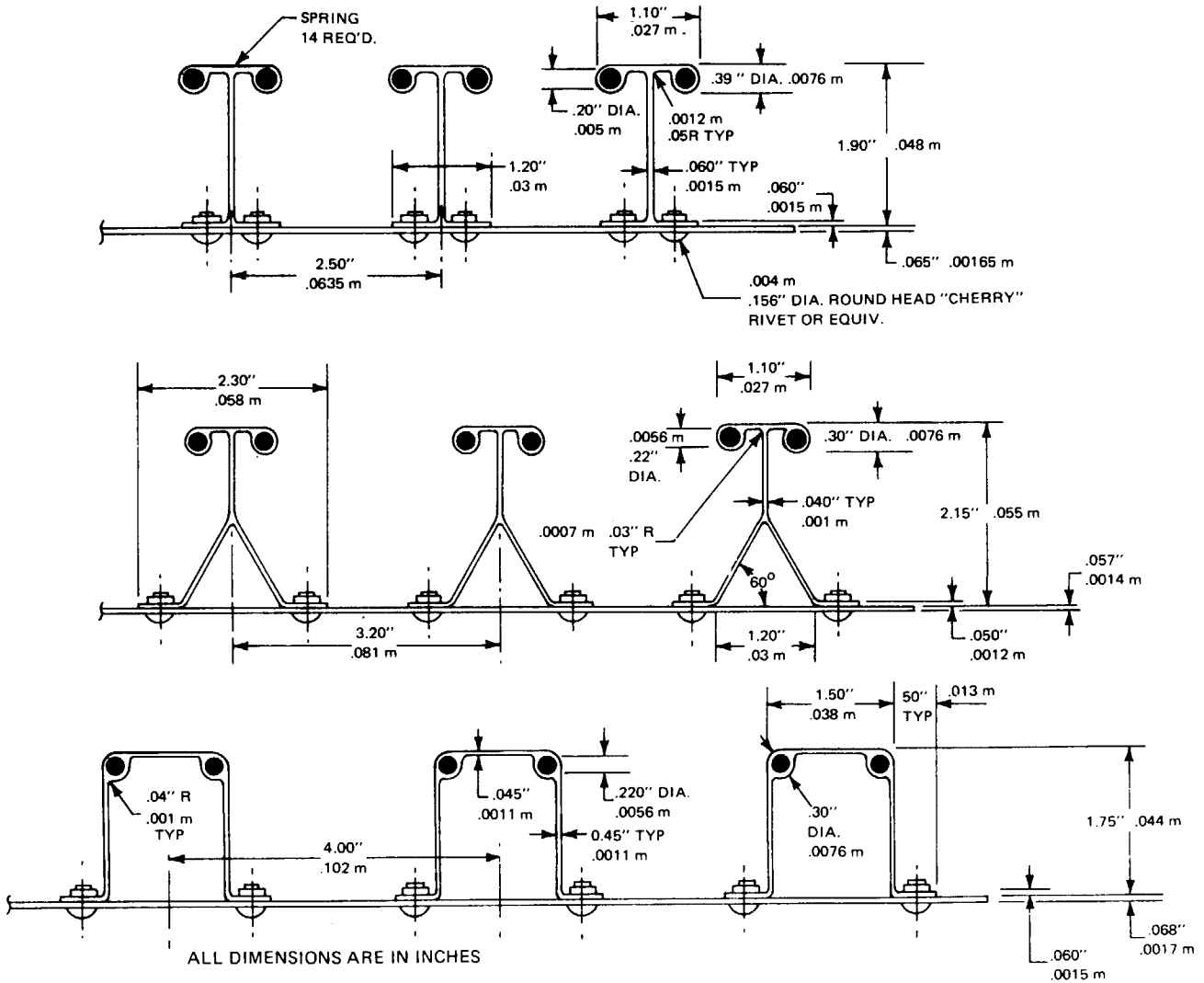

Figure 21 PRELIMINARY DESIGN CONCEPTS

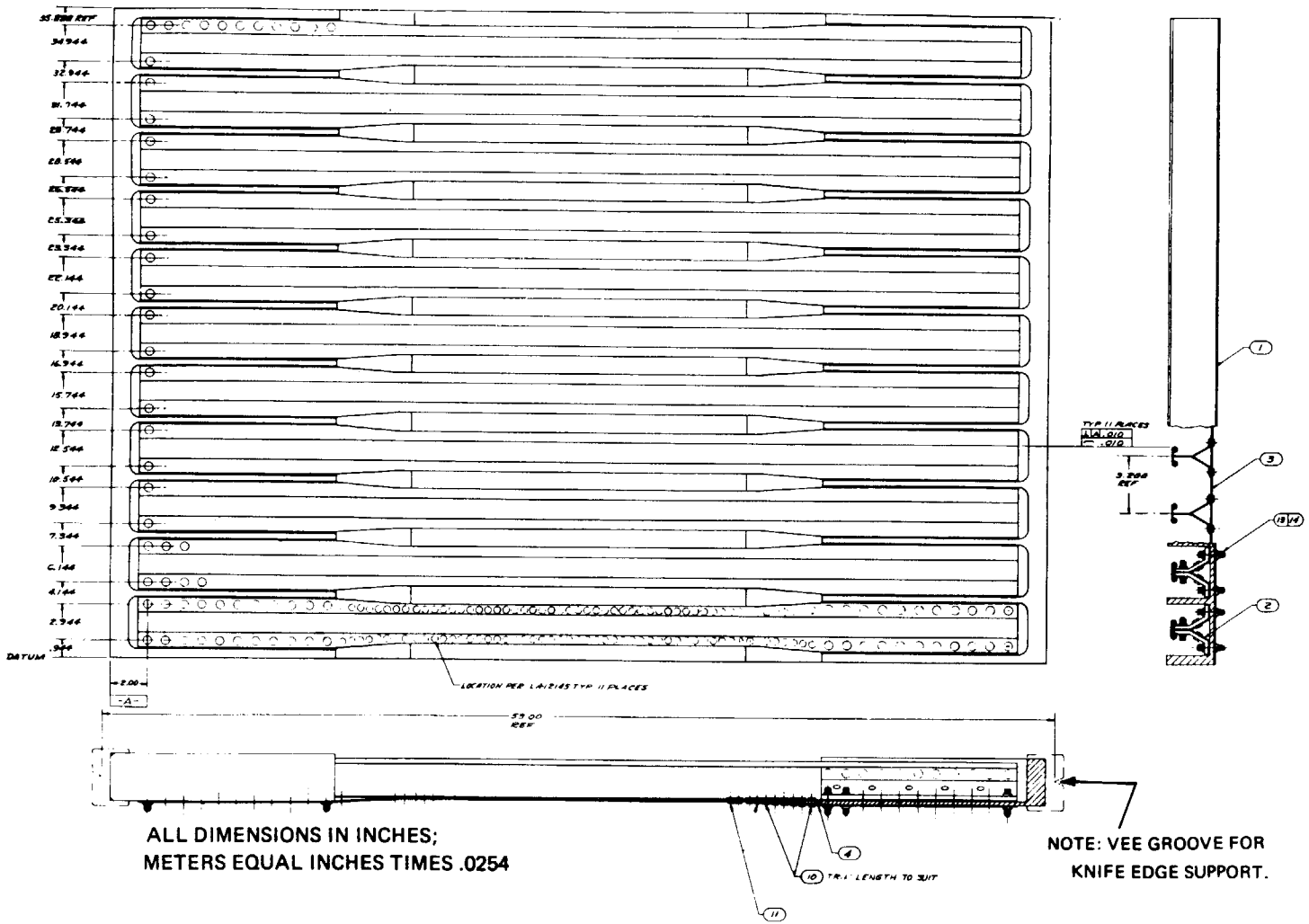

Figure 22 INFILTRATION REINFORCED PROOF TEST PANELS

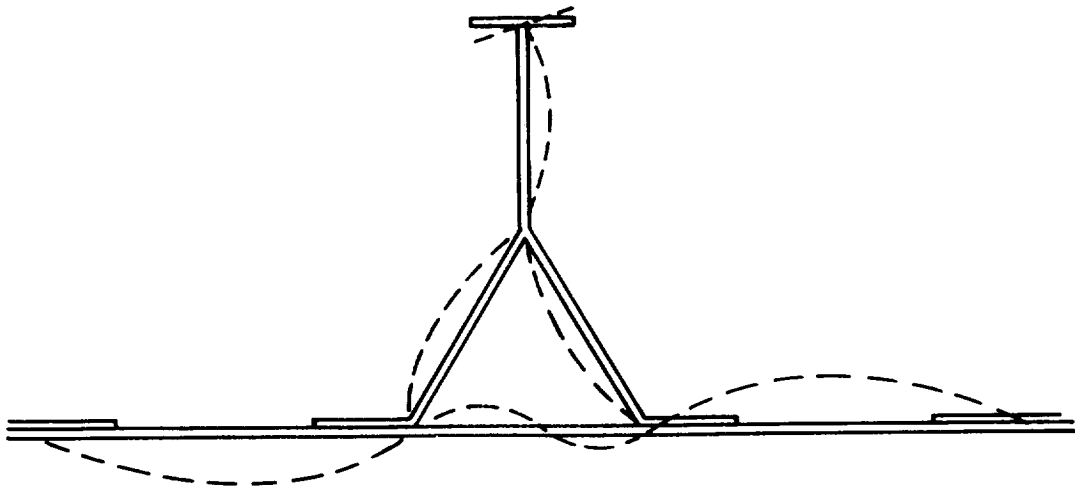

MODE 1

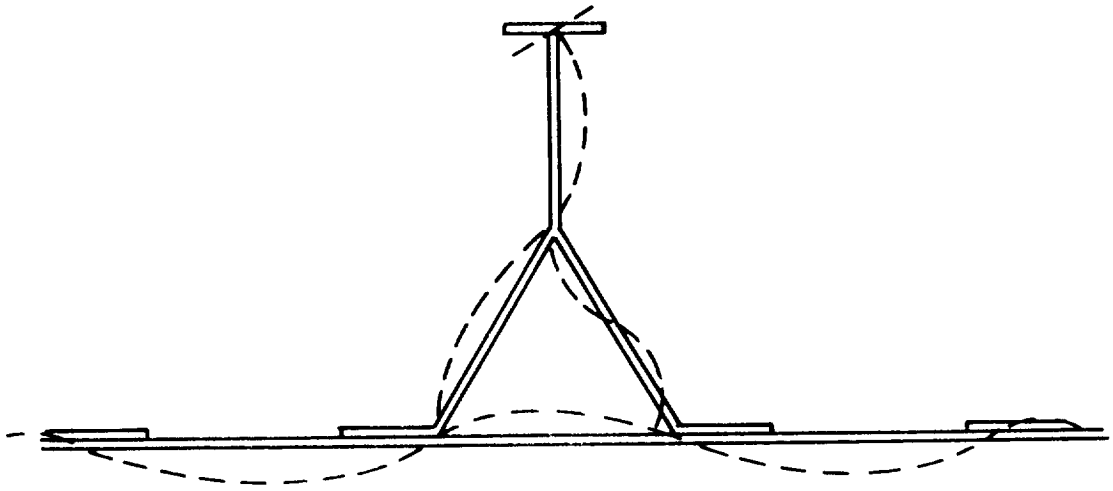

MODE 2

Figure 23 ASSUMED LOCAL INSTABILITY FAILURE MODES

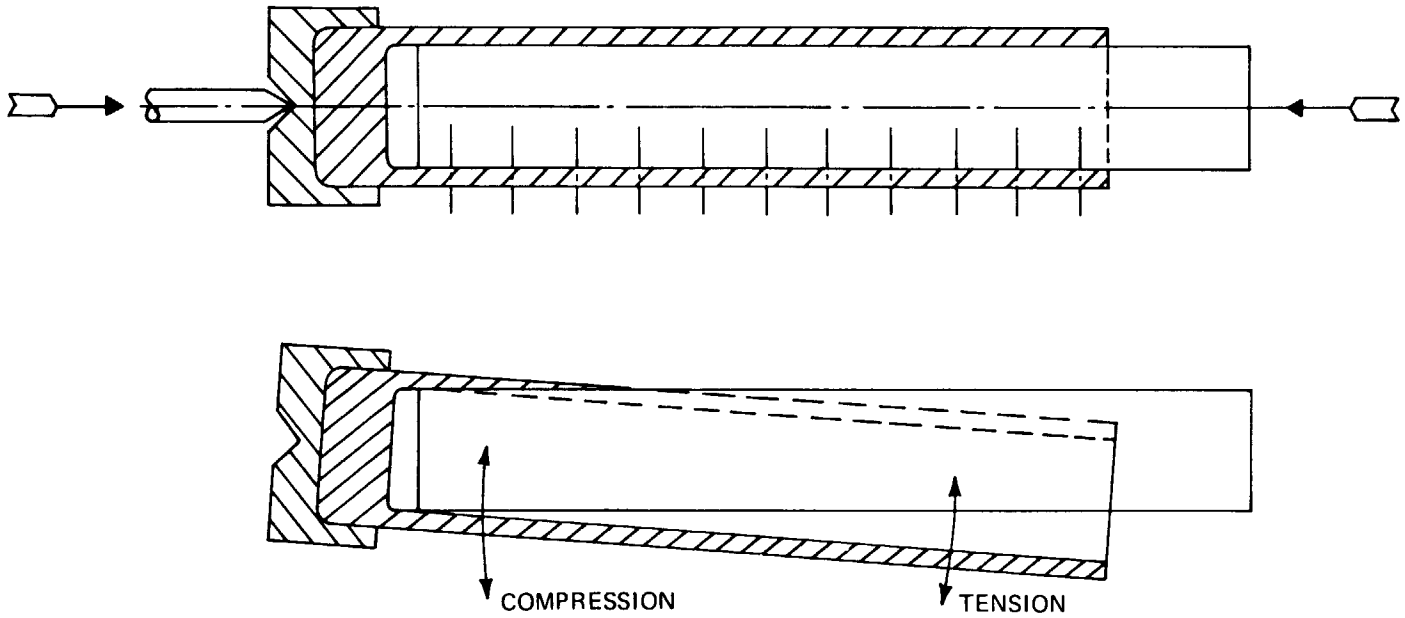

Figure 24 SCHEMATIC SHOWING LOCAL BENDING IN LOAD INTRODUCTION FITTINGS

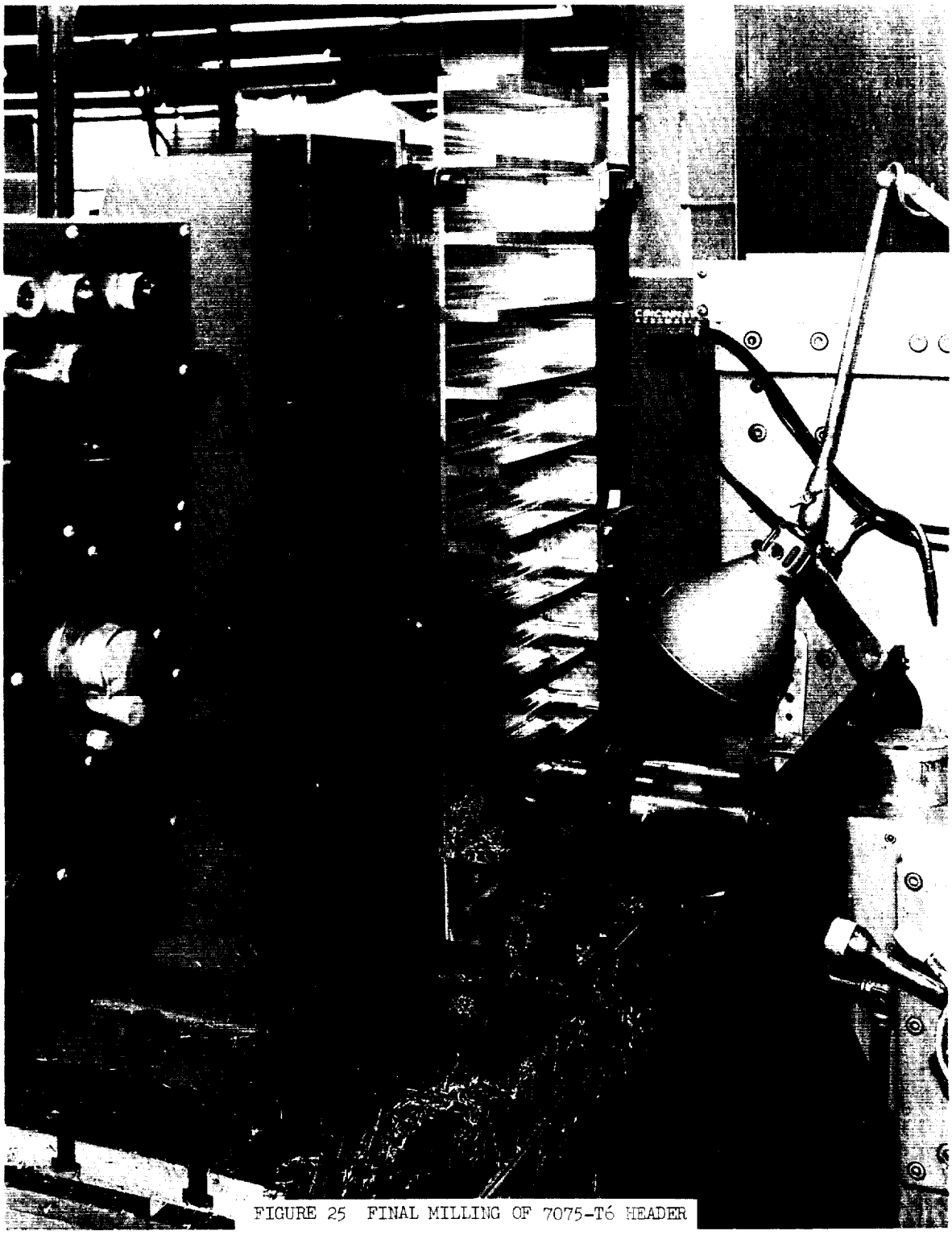

FIGURE 25 FINAL MILLING OF 7075-T6 HEADER

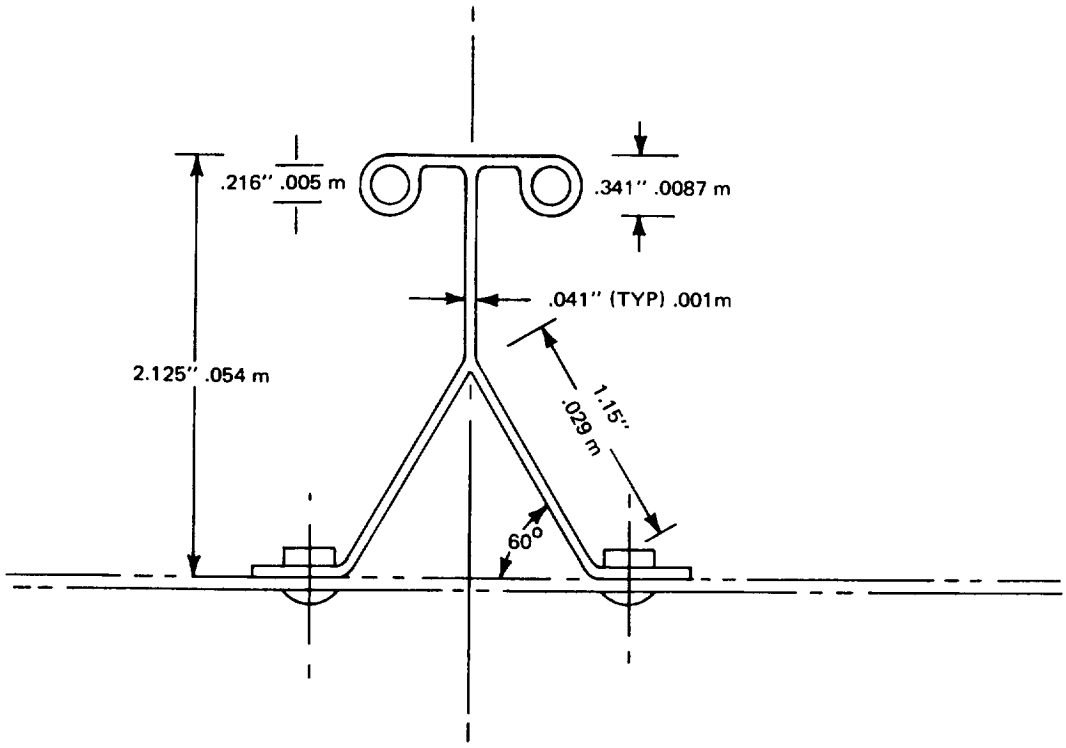

Figure 26 STRINGER NOMINAL DIMENSIONS

FIGURE 27 TRIMMING OF STRINGER FLANGES

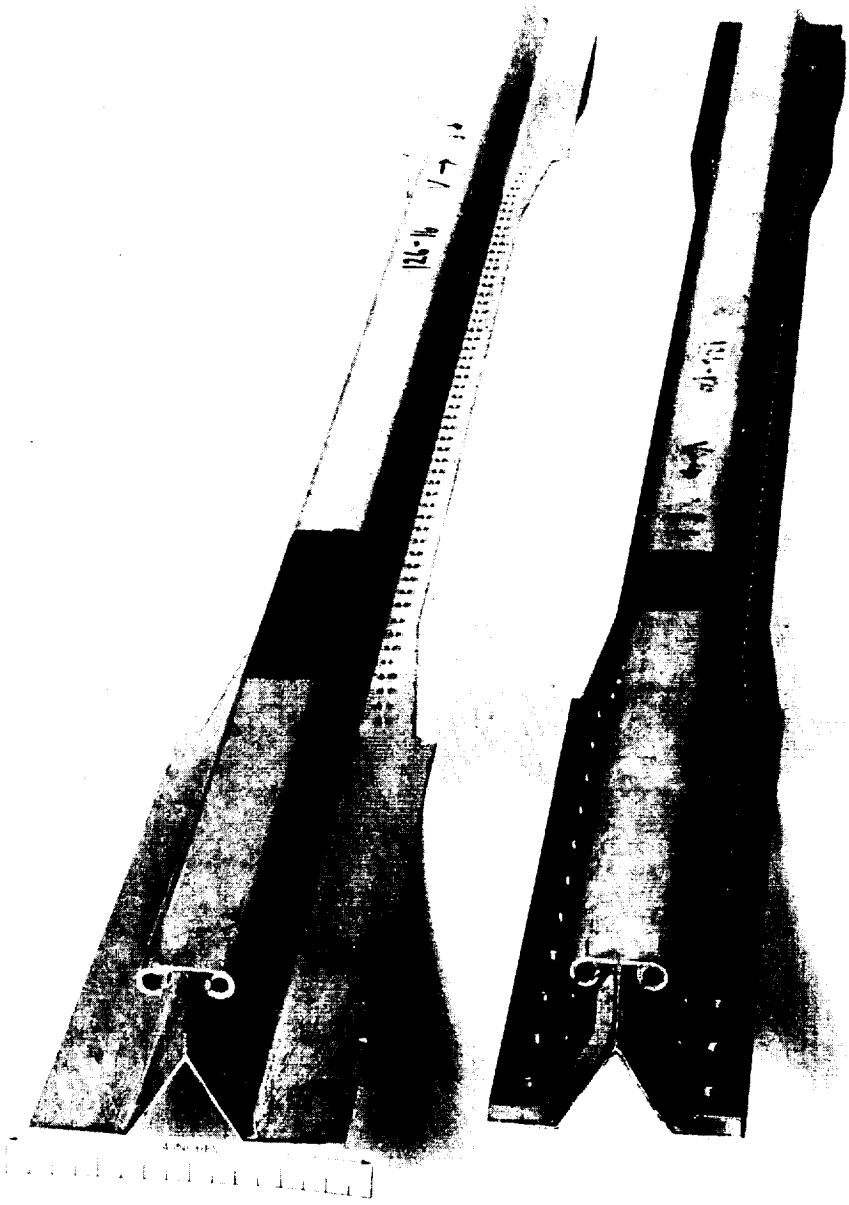

Figure 28 PARTIALLY COMPLETED AND COMPLETED STRINGERS

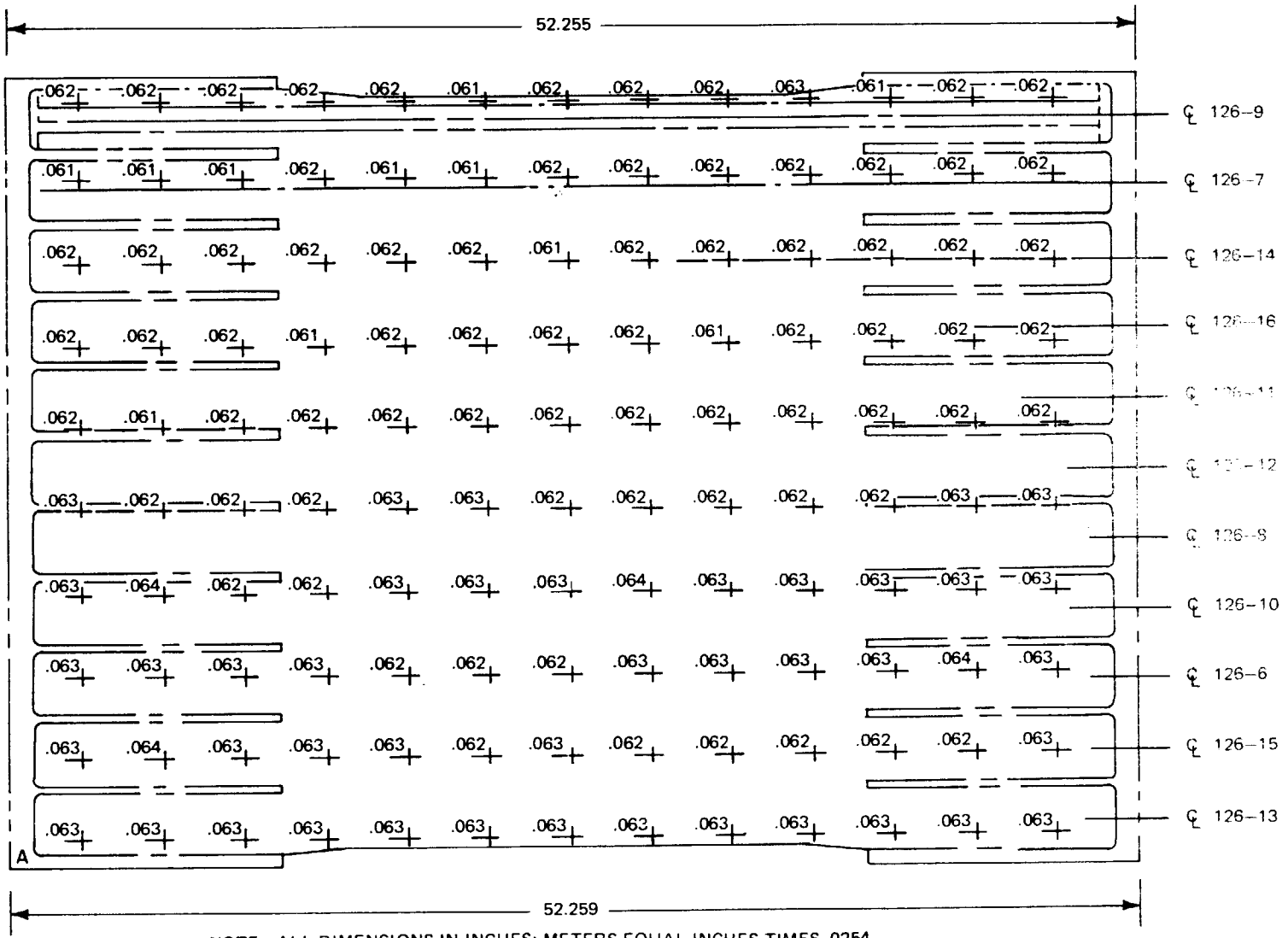

NOTE: ALL DIMENSIONS IN INCHES; METERS EQUAL INCHES TIMES .0254

Figure 29 SKIN THICKNESS MEASUREMENT GRID AND STRINGER IDENTIFICATION

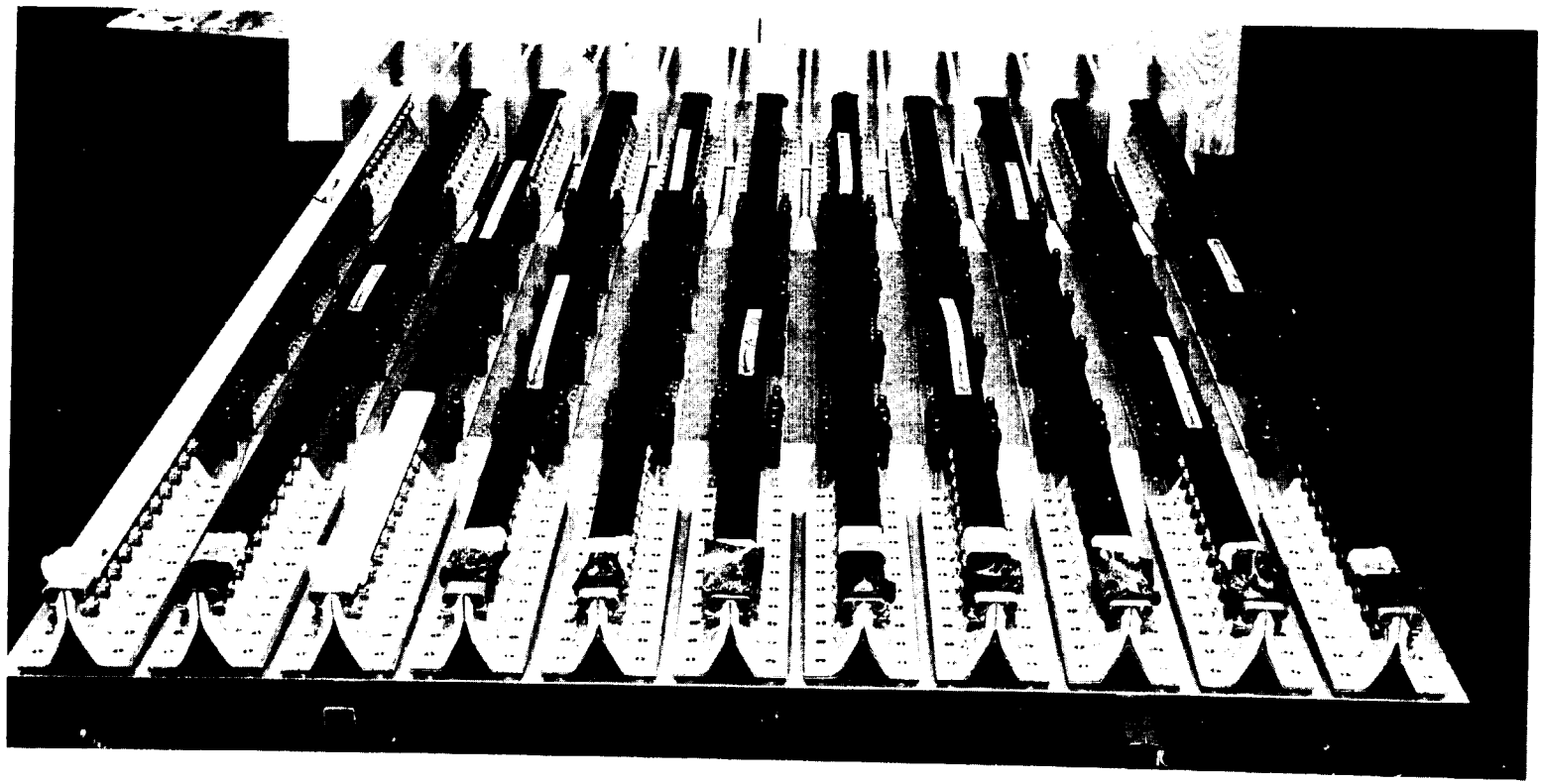

Figure 30 PANEL BEING PREPARED FOR RIVETING

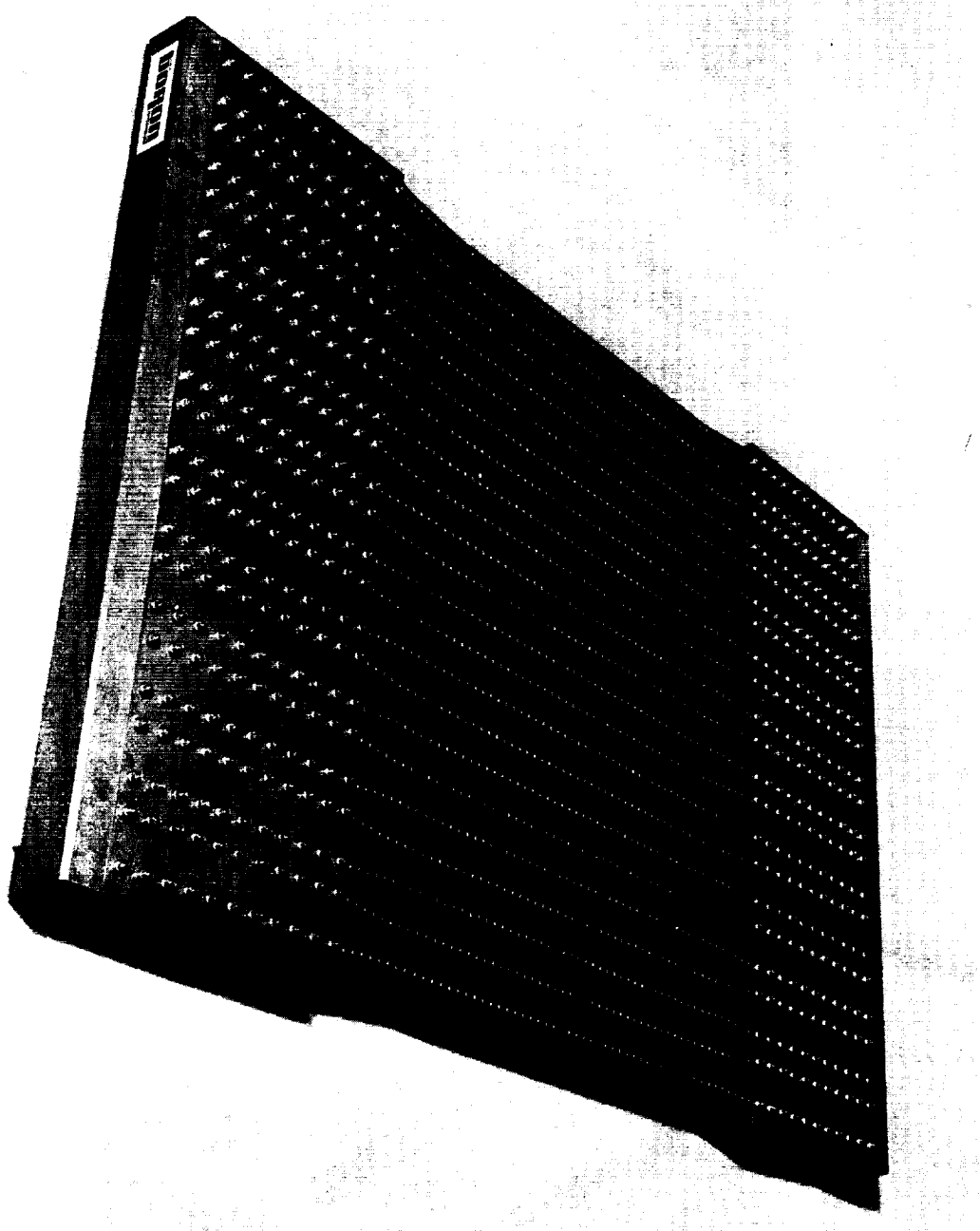

Figure 31 COMPLETED PANEL SHOWING SKIN SURFACE

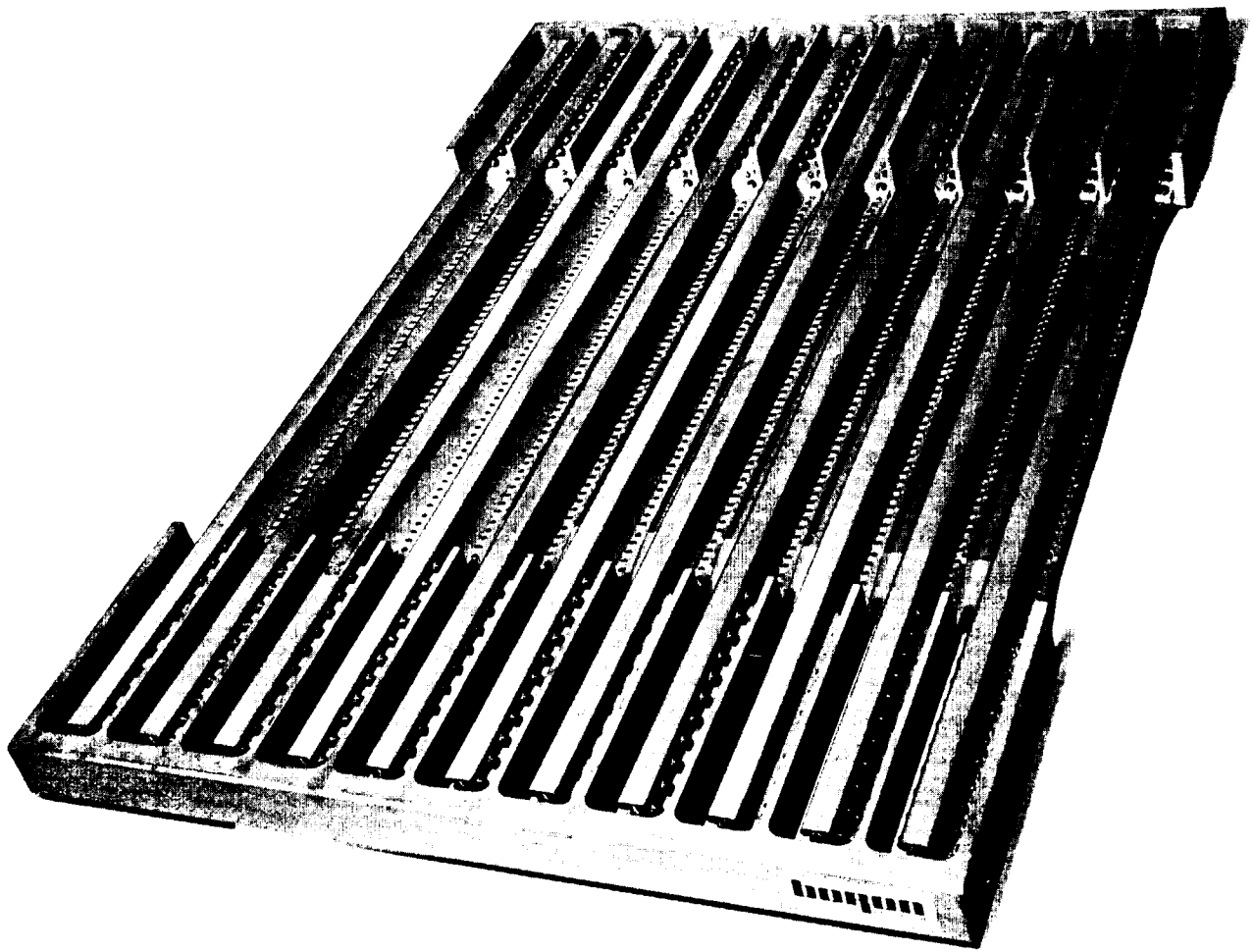

Figure 32 COMPLETED PANEL SHOWING STRINGERS

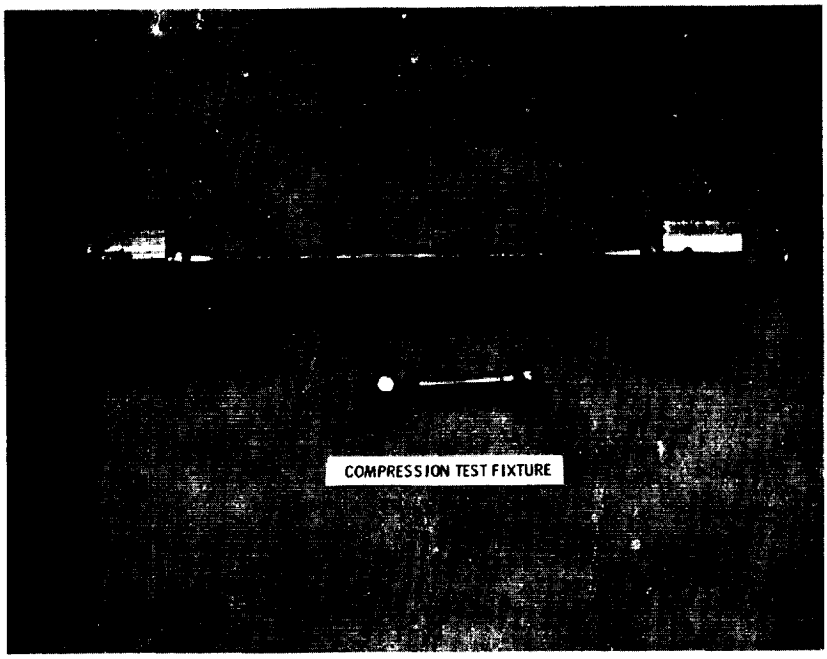

Figure 33 COMPRESSION TEST FIXTURE

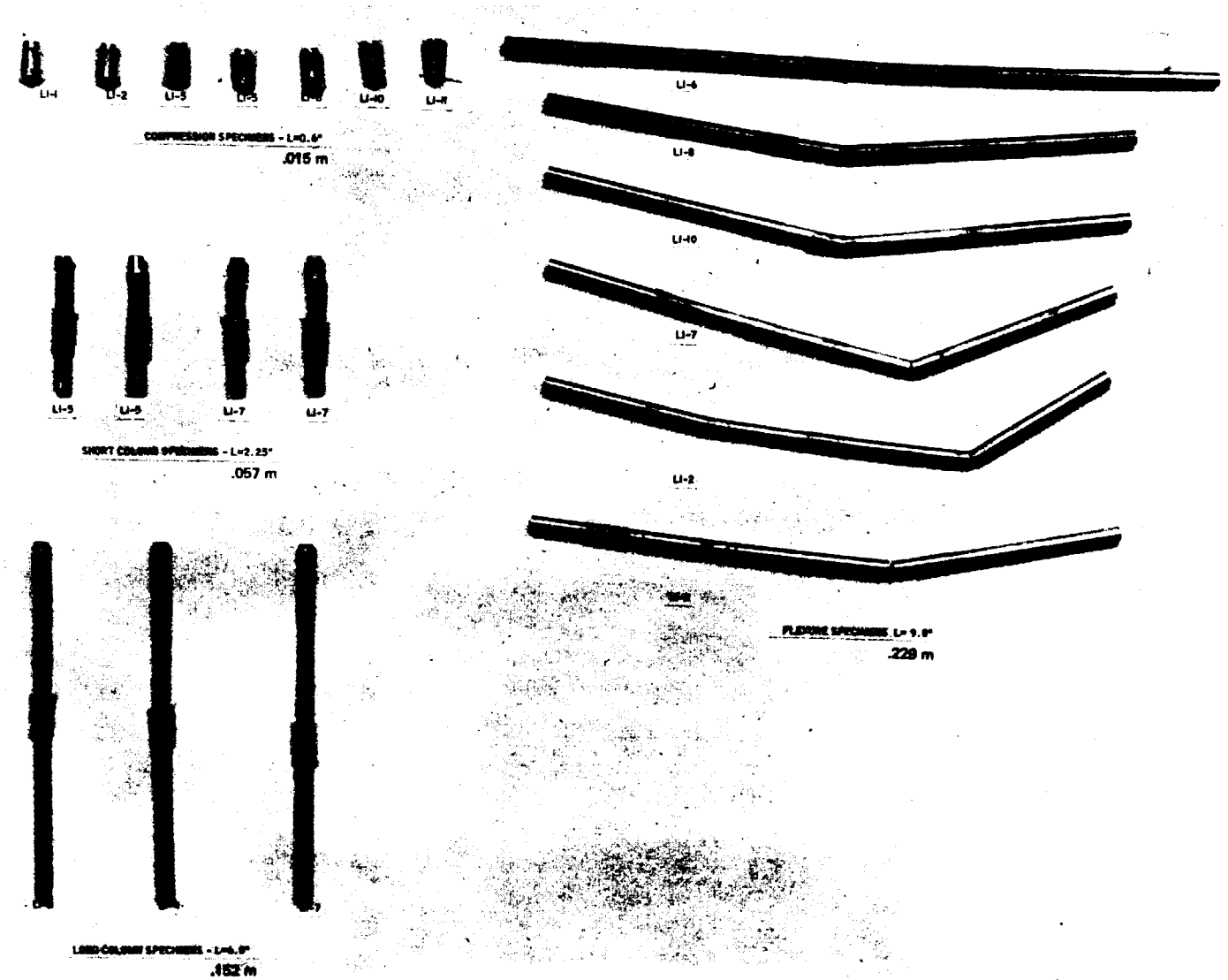

Figure 34 BORON EPOXY INFILTRATED THICK WALL 6061-T6 ALUMINUM RODS t = 0.031

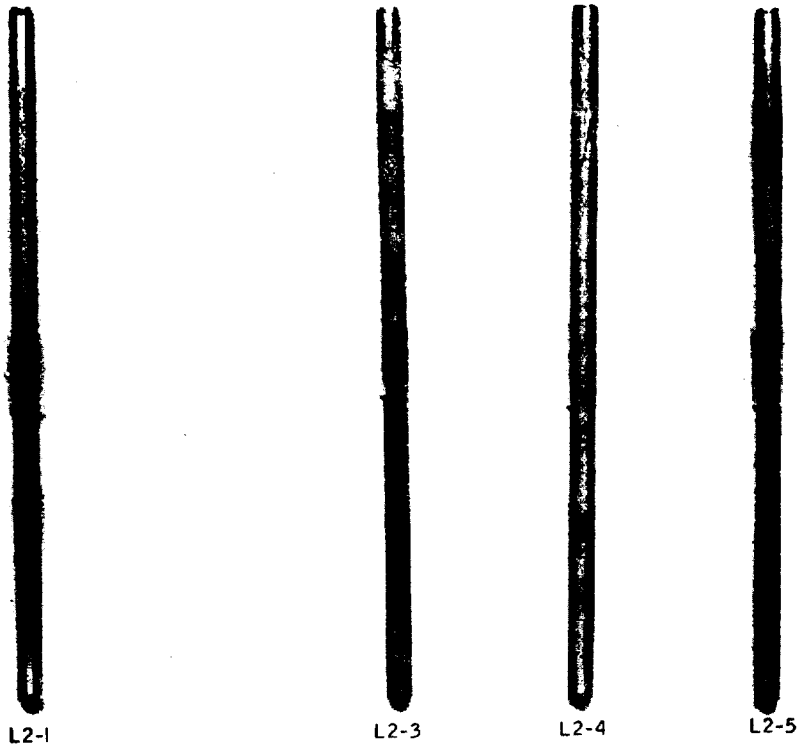

Figure 35 BORON EPOXY INFILTRATED CHEM MILLED 6062

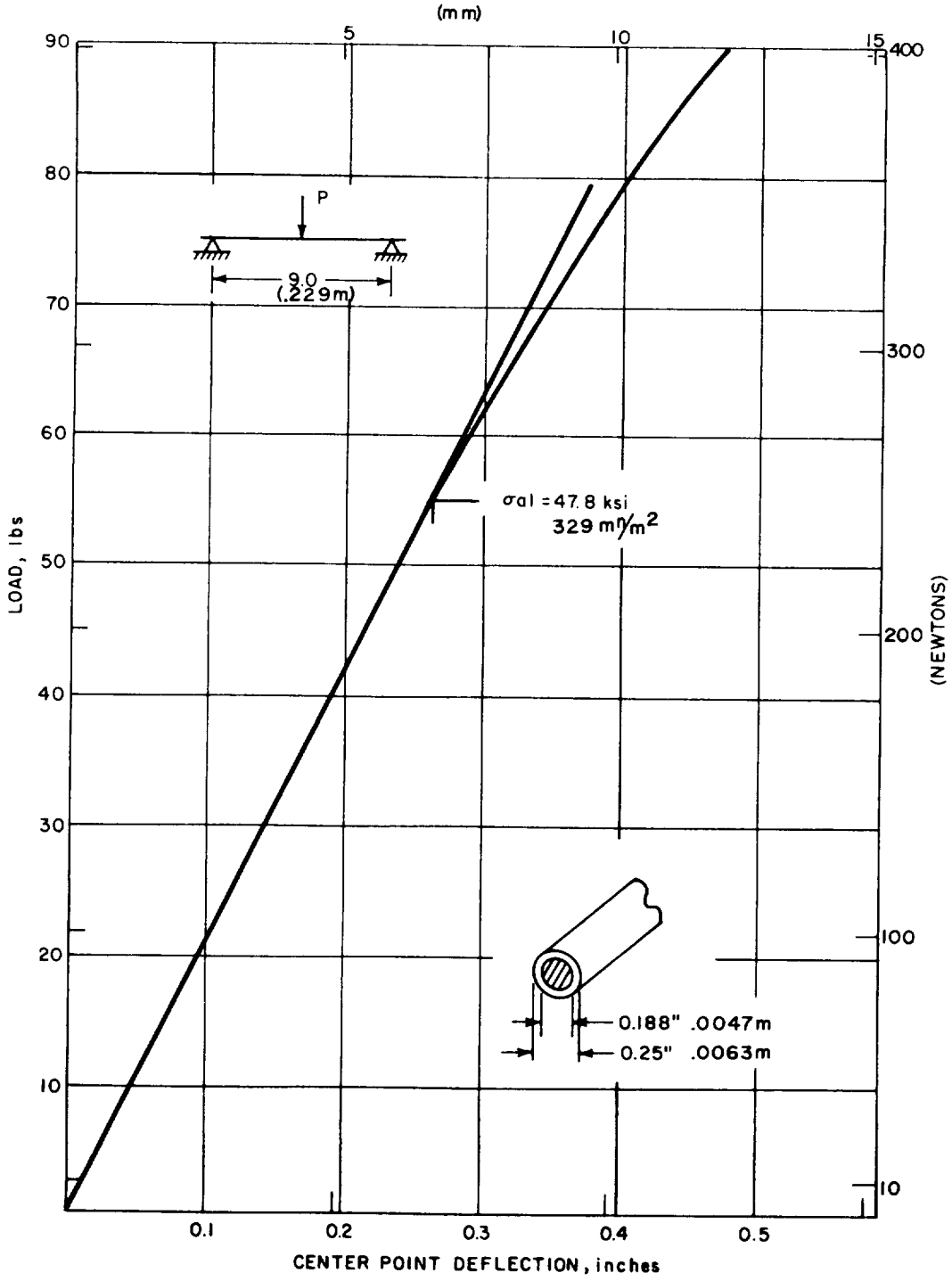

Figure 36 TYPICAL LOAD DEFLECTION FOR ROD FLEXURE SPECIMEN

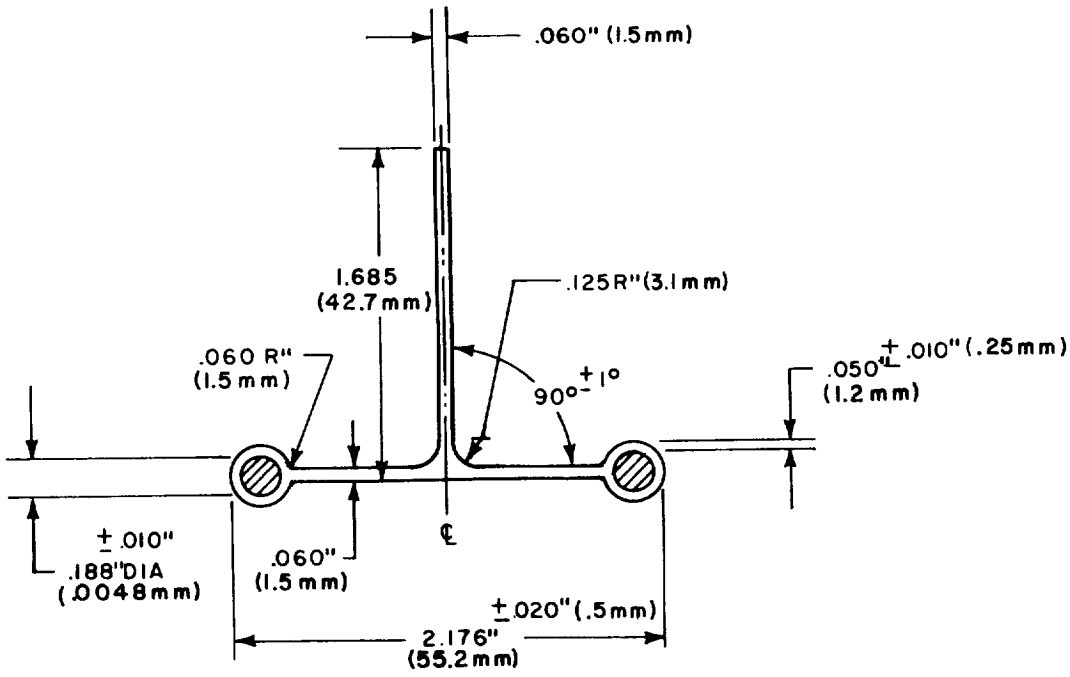

Figure 37 EXTRUDED 6005–T5 ALUMINUM "T"

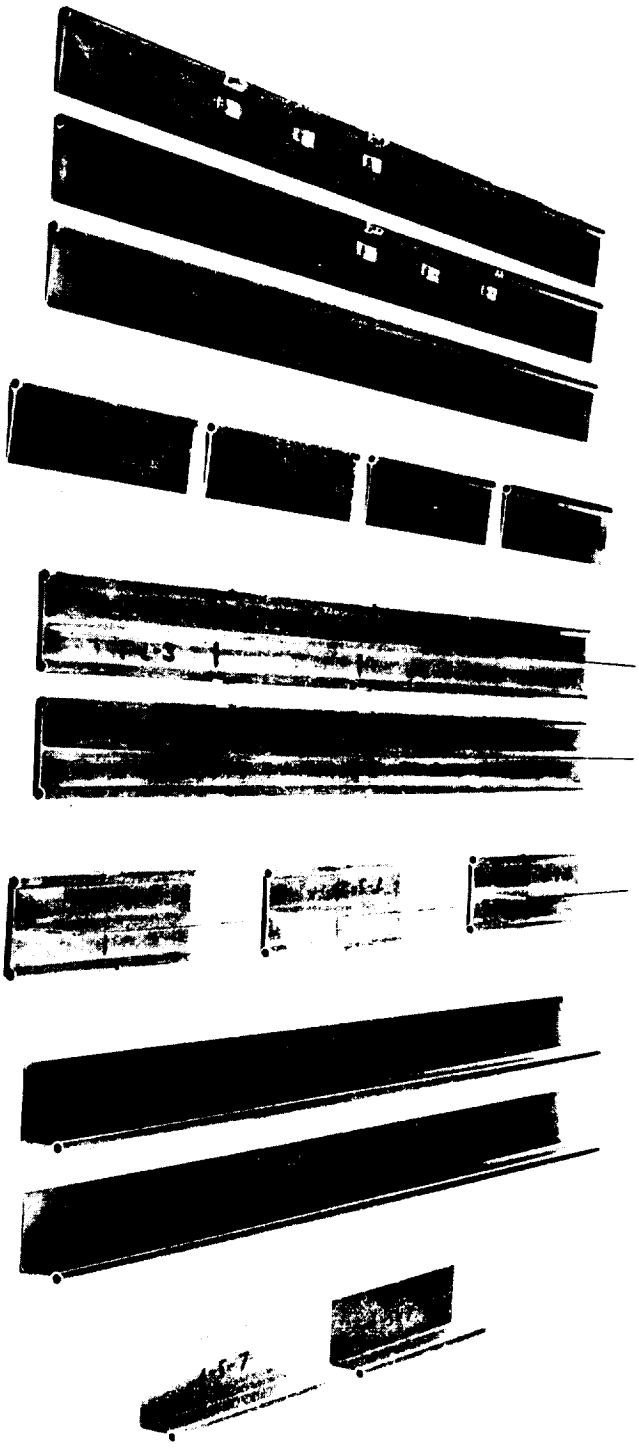

Figure 38 REINFORCED STRINGER TEST SECTIONS

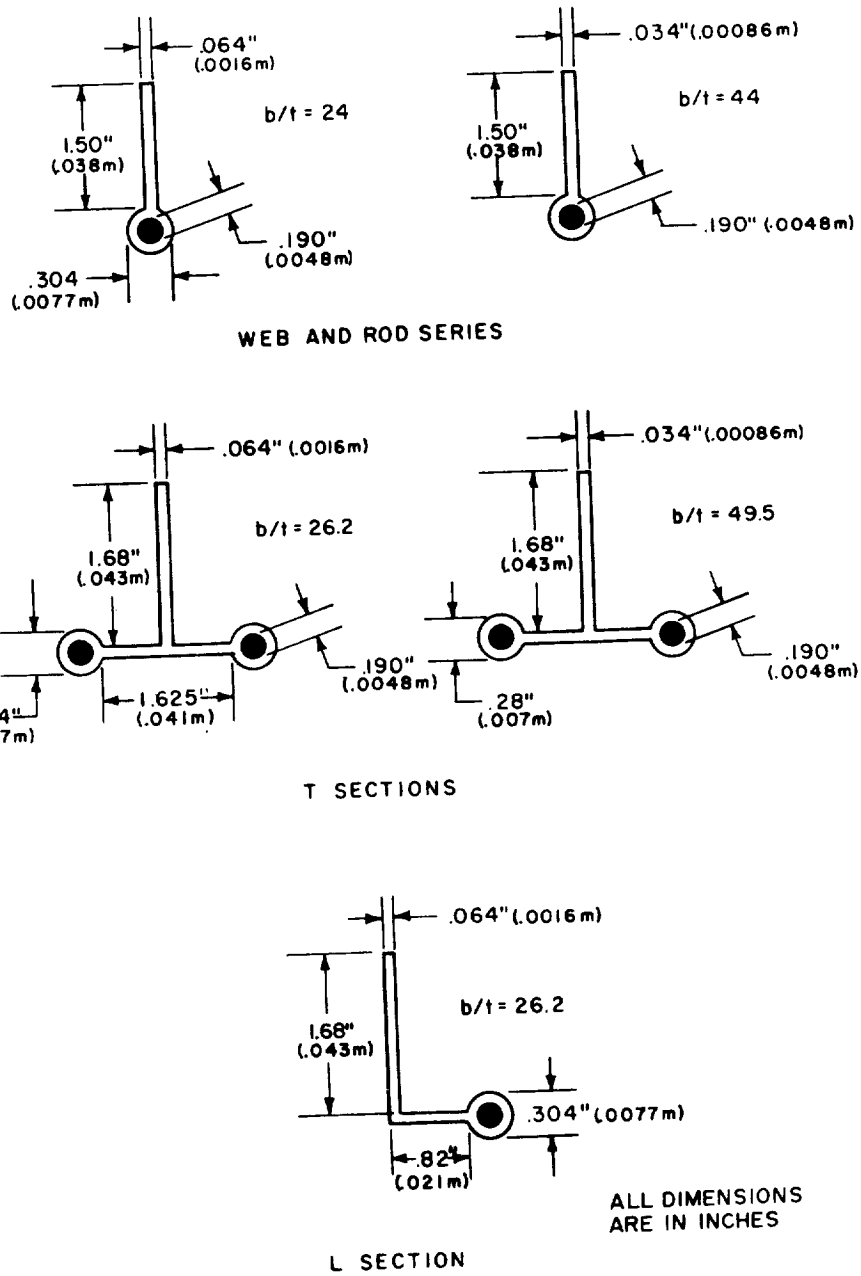

Figure 39 TYPICAL CROSS SECTIONS FOR SUB-ELEMENT TEST SECTIONS

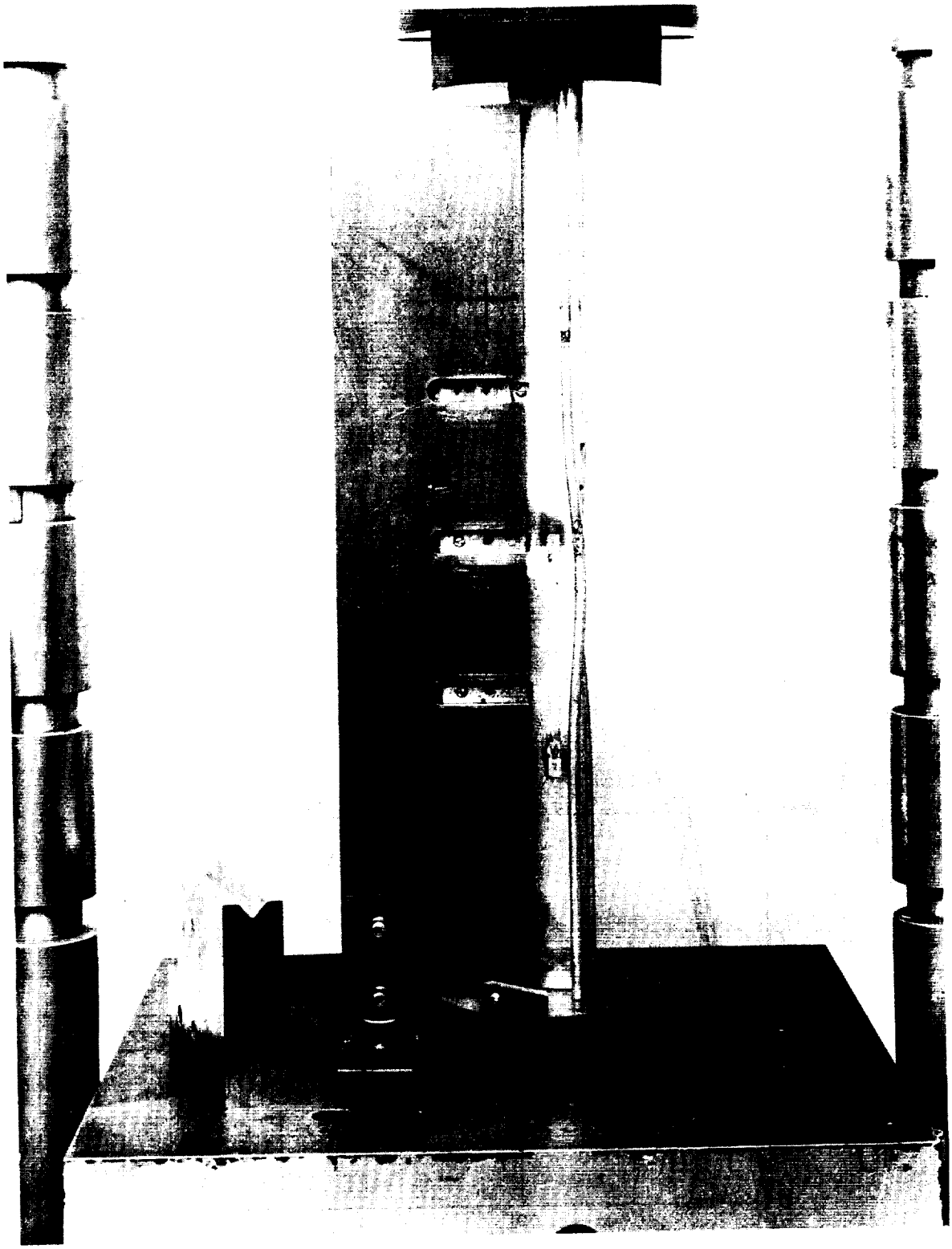

Figure 40 TYPICAL ELEMENT COMPRESSION TEST SETUP

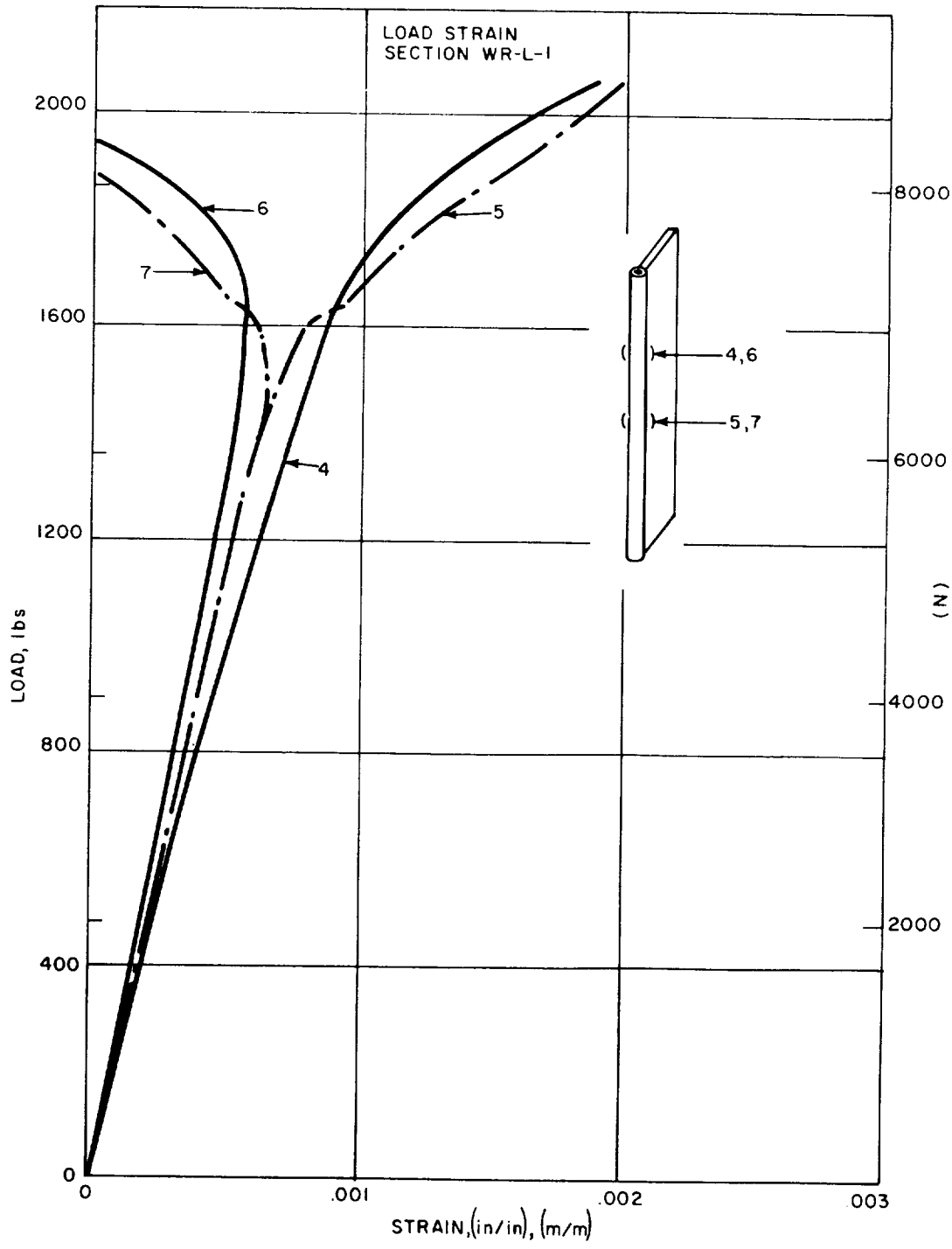

Figure 41 LOAD VERSUS STRAIN - SPECIMEN WR-L-1

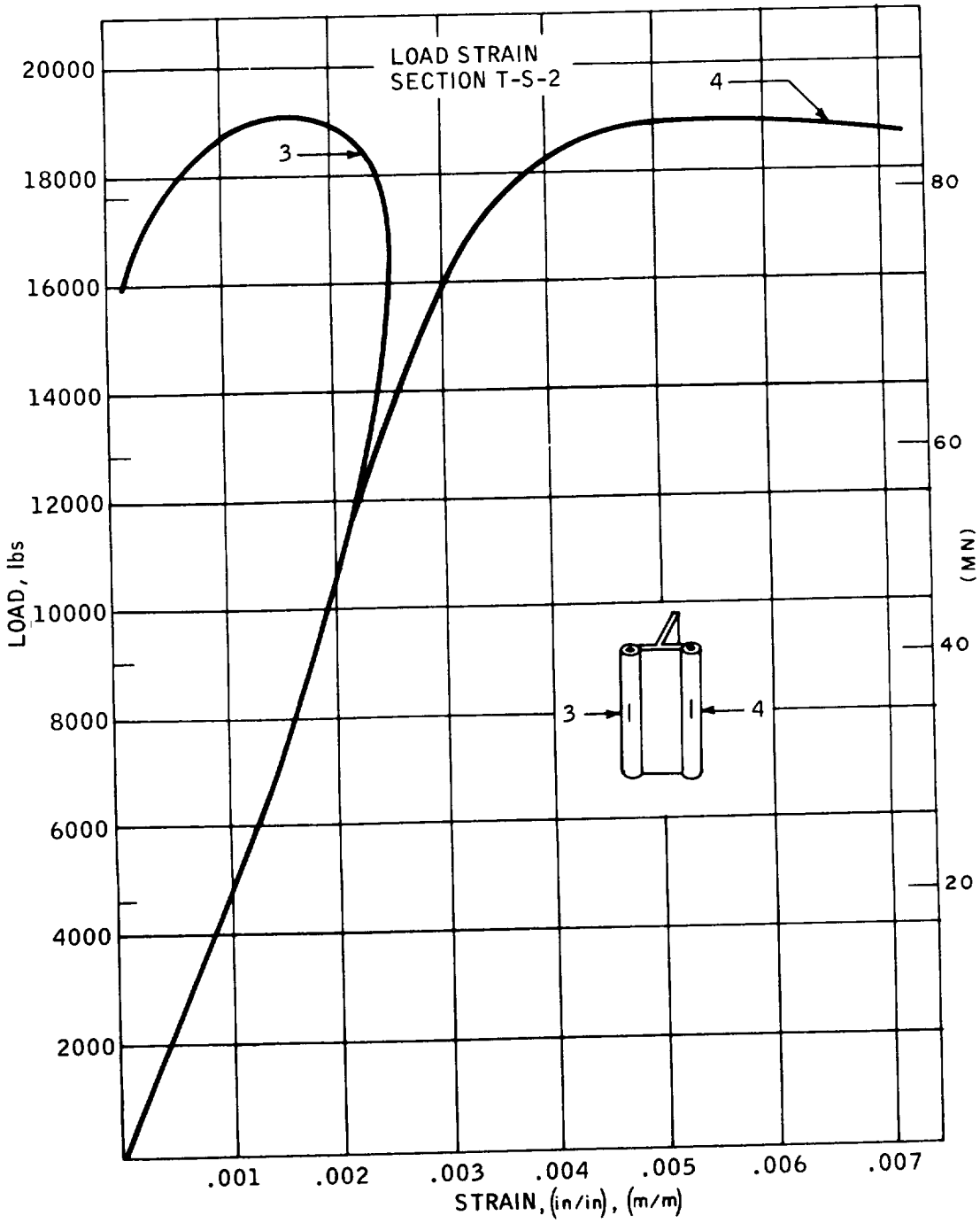

Figure 42 LOAD VERSUS STRAIN - SPECIMEN T-S-2

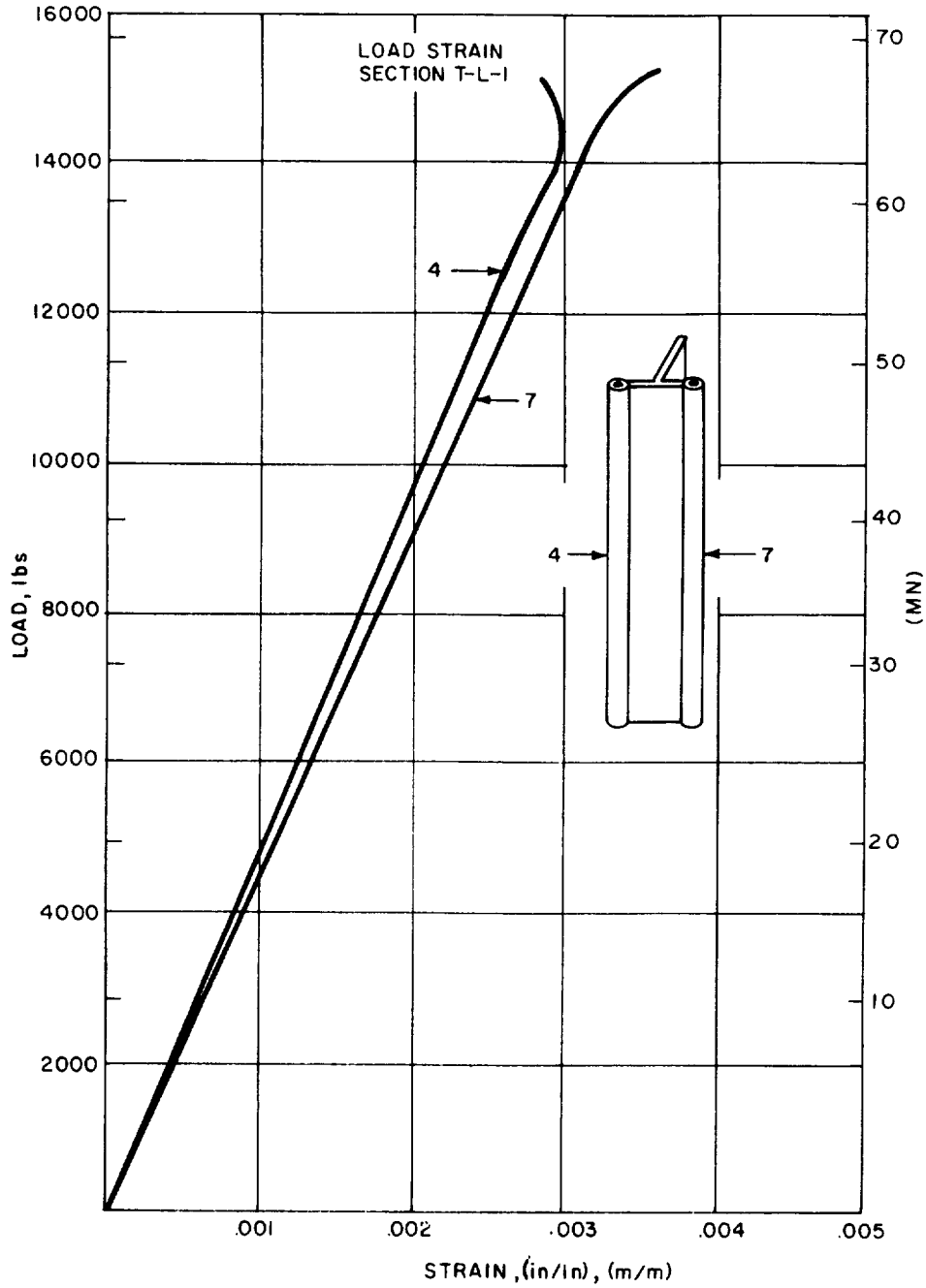

Figure 43 LOAD VERSUS STRAIN - SPECIMEN T-S-2

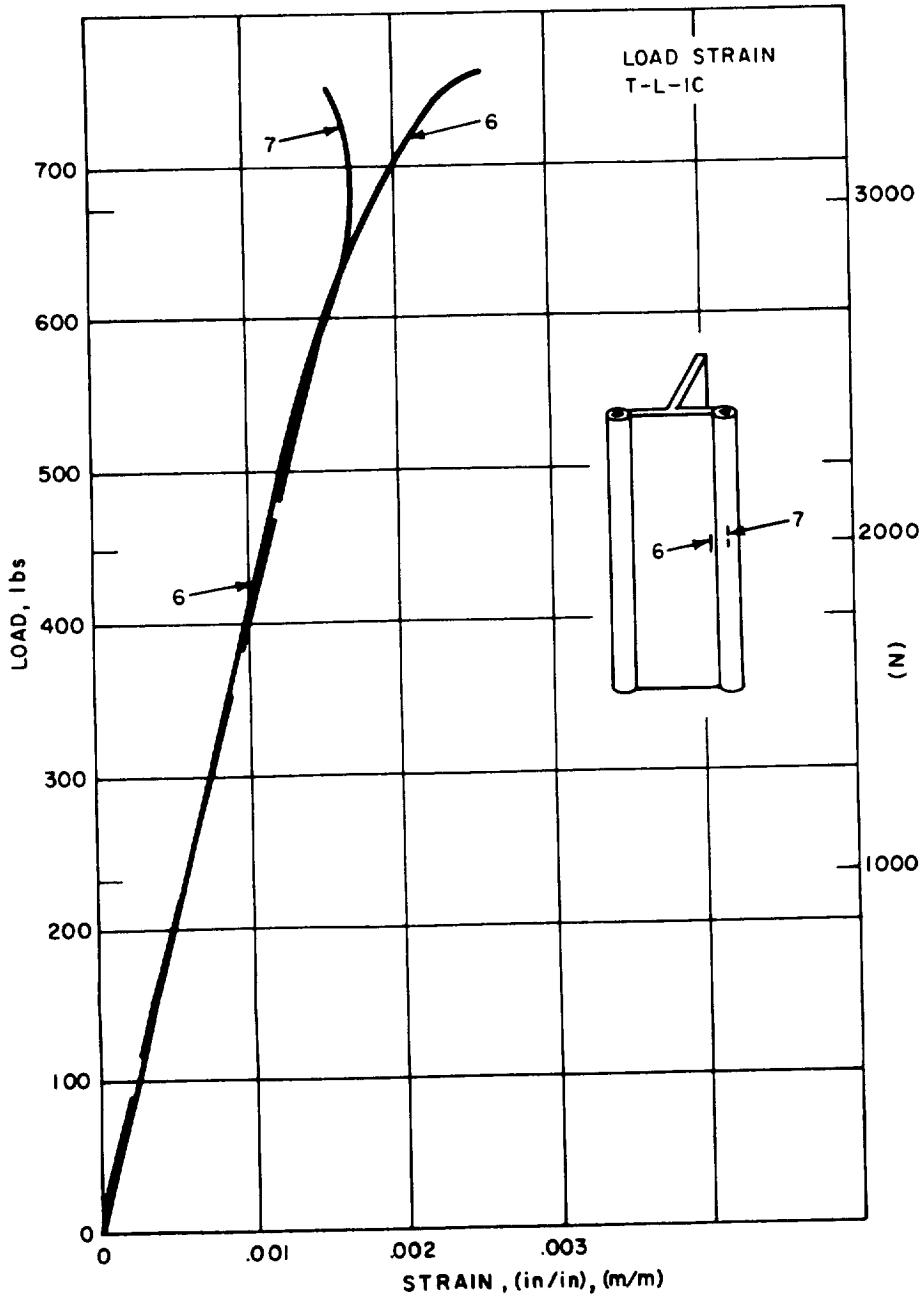

Figure 44 LOAD VERSUS STRAIN - SPECIMEN T-L-1C

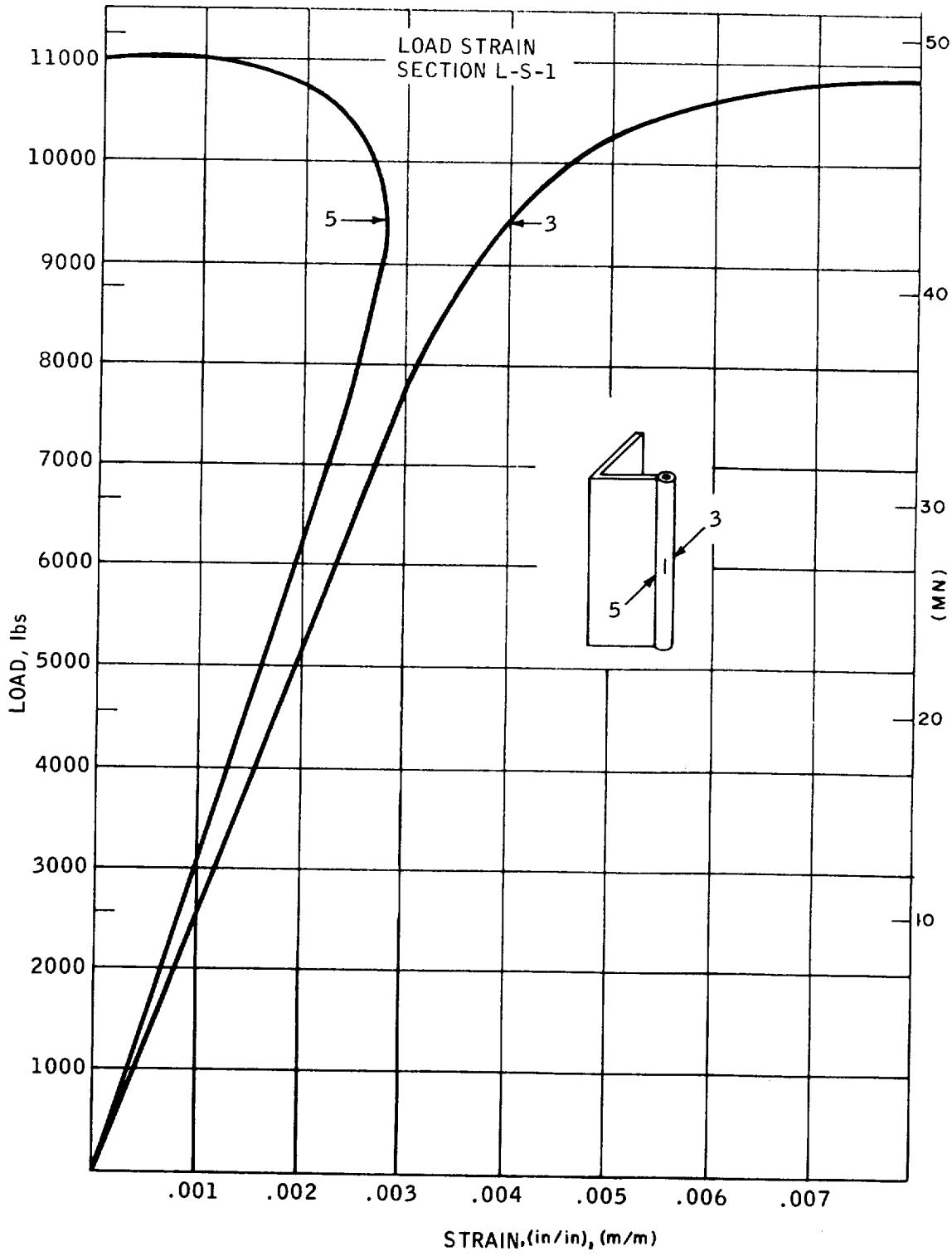

Figure 45 LOAD VERSUS STRAIN - SPECIMEN L-S-1

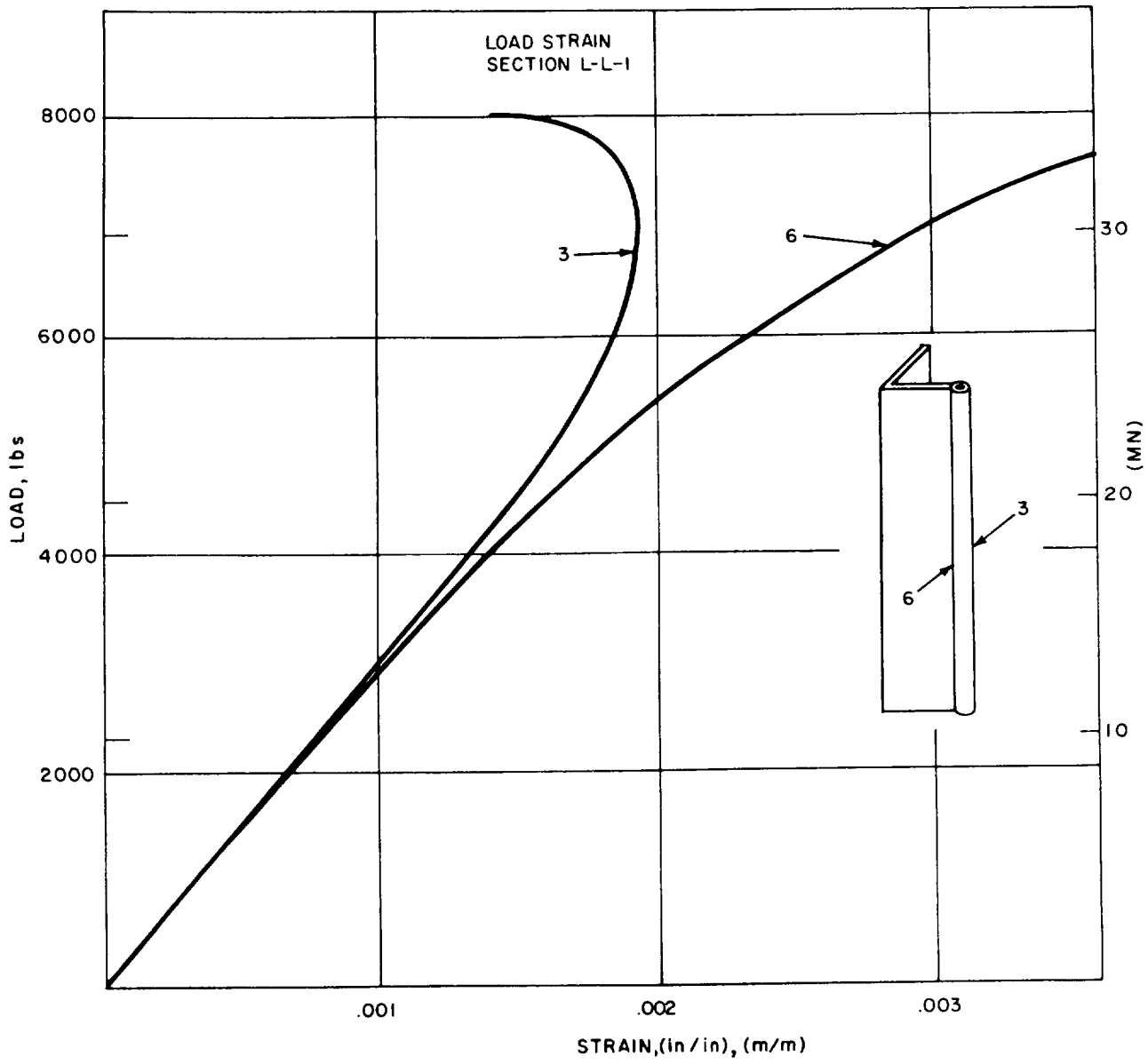

Figure 46 LOAD VERSUS STRAIN - SPECIMEN L-L-1

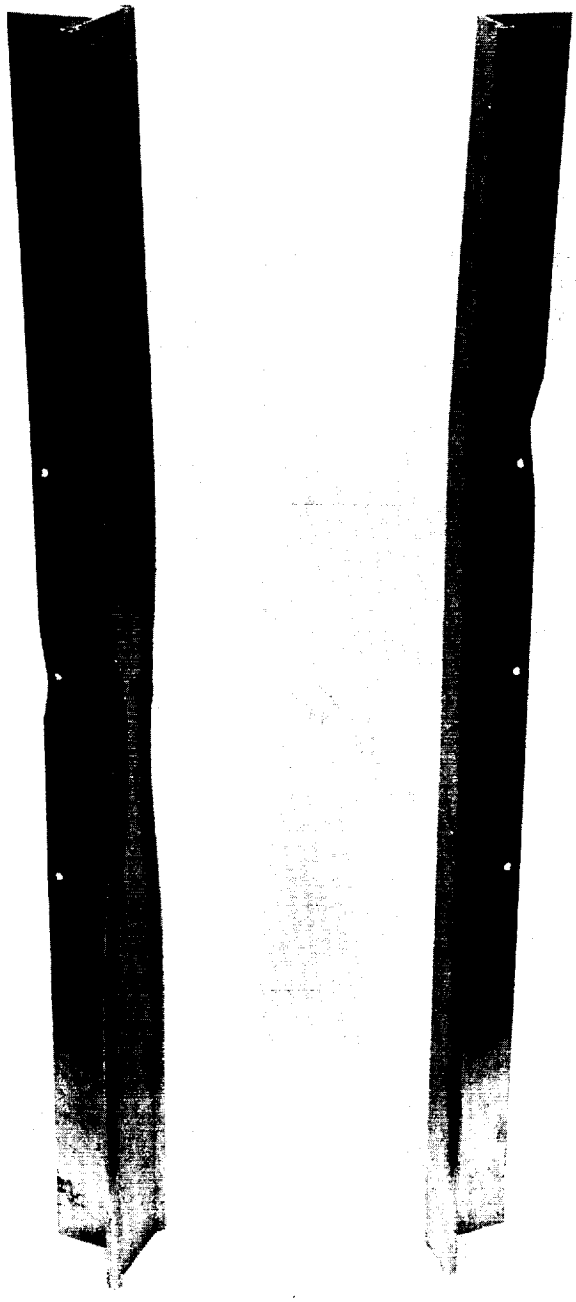

Figure 47 TYPICAL FAILURES FOR 24" "T" AND "L" SECTIONS SHOWING LOCAL FLANGE BUCKLING

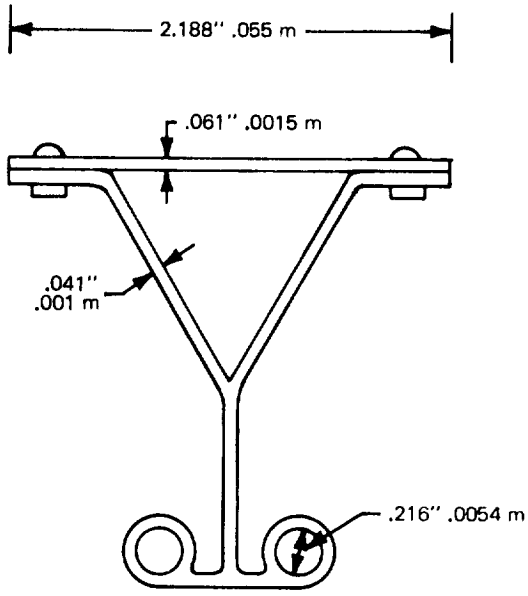

Figure 48 ELEMENTS NACA - Y-1, -2 and -3

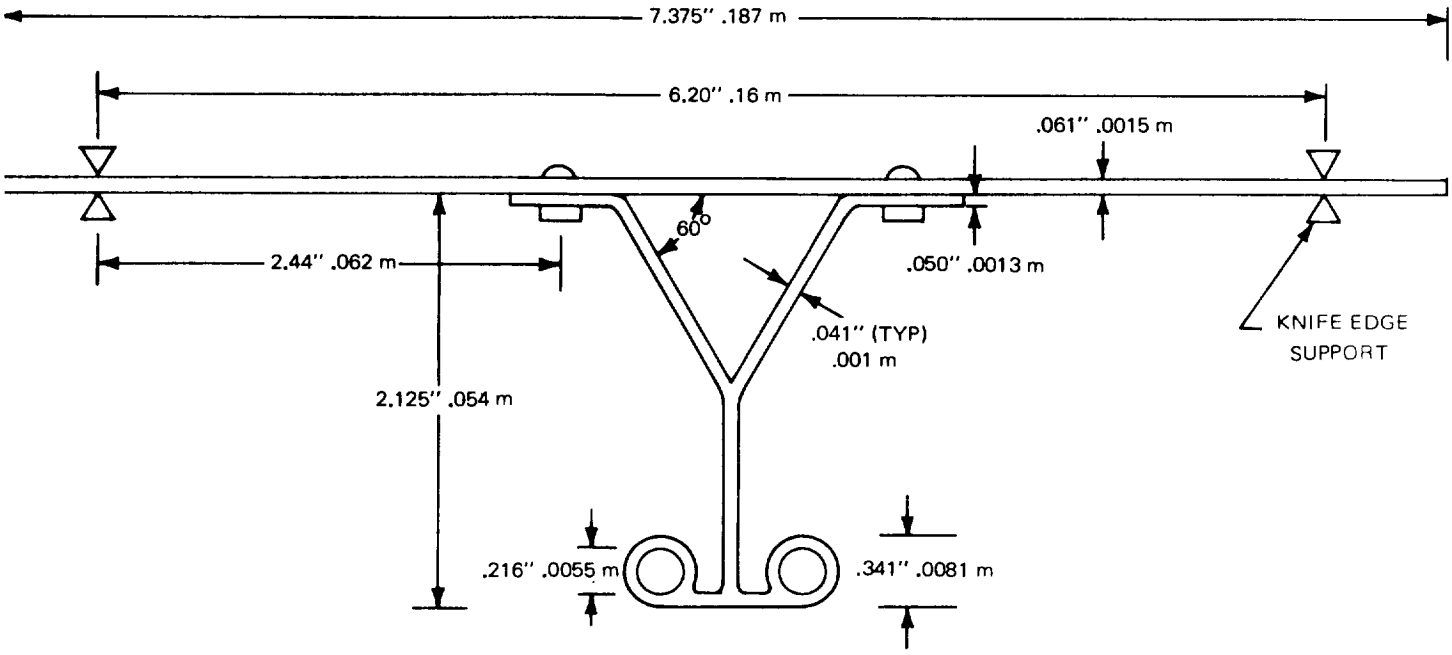

Figure 49 ELEMENT NACA - Y-4

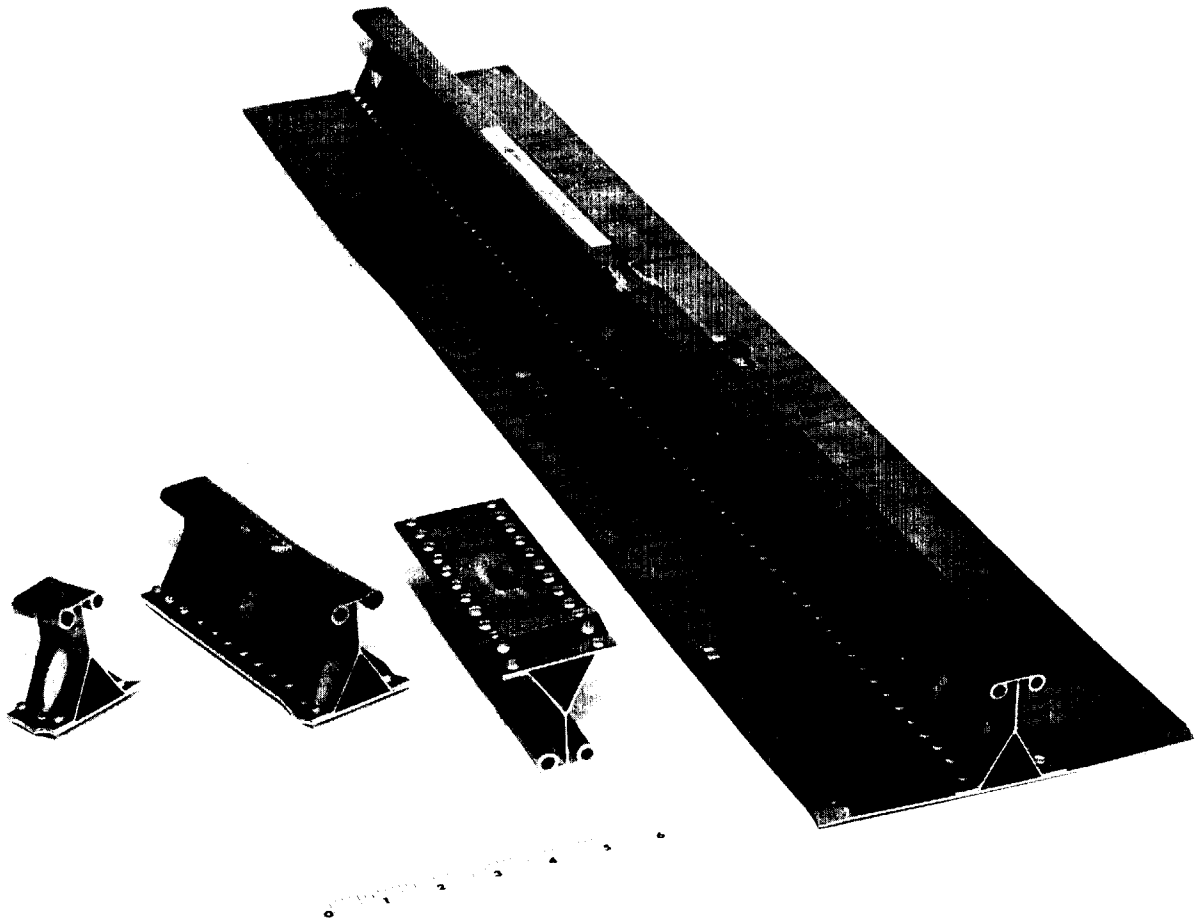

Figure 50 FAILED TEST SECTIONS

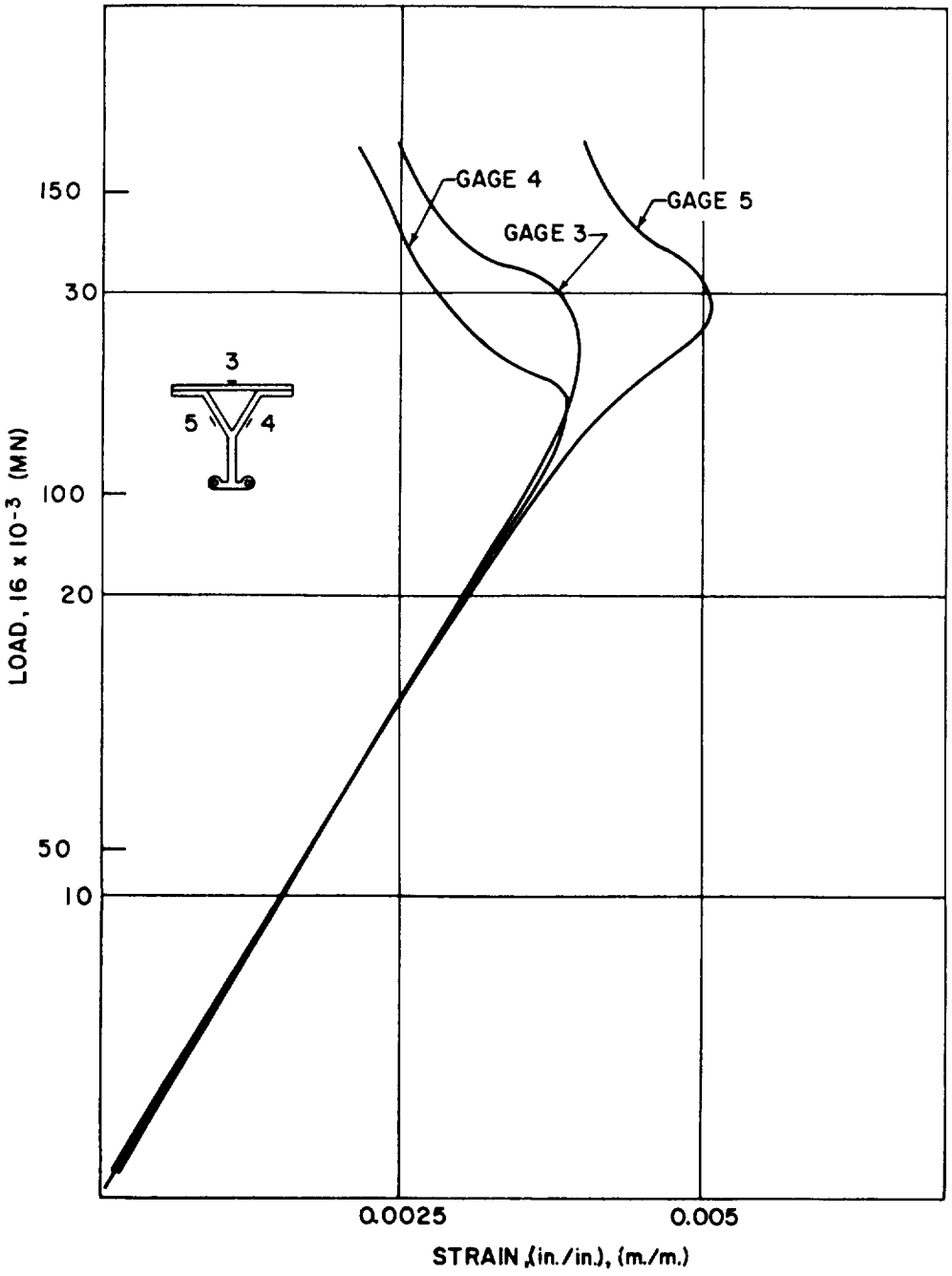

Figure 51 NACA - Y-2 LOAD-STRAIN CURVE

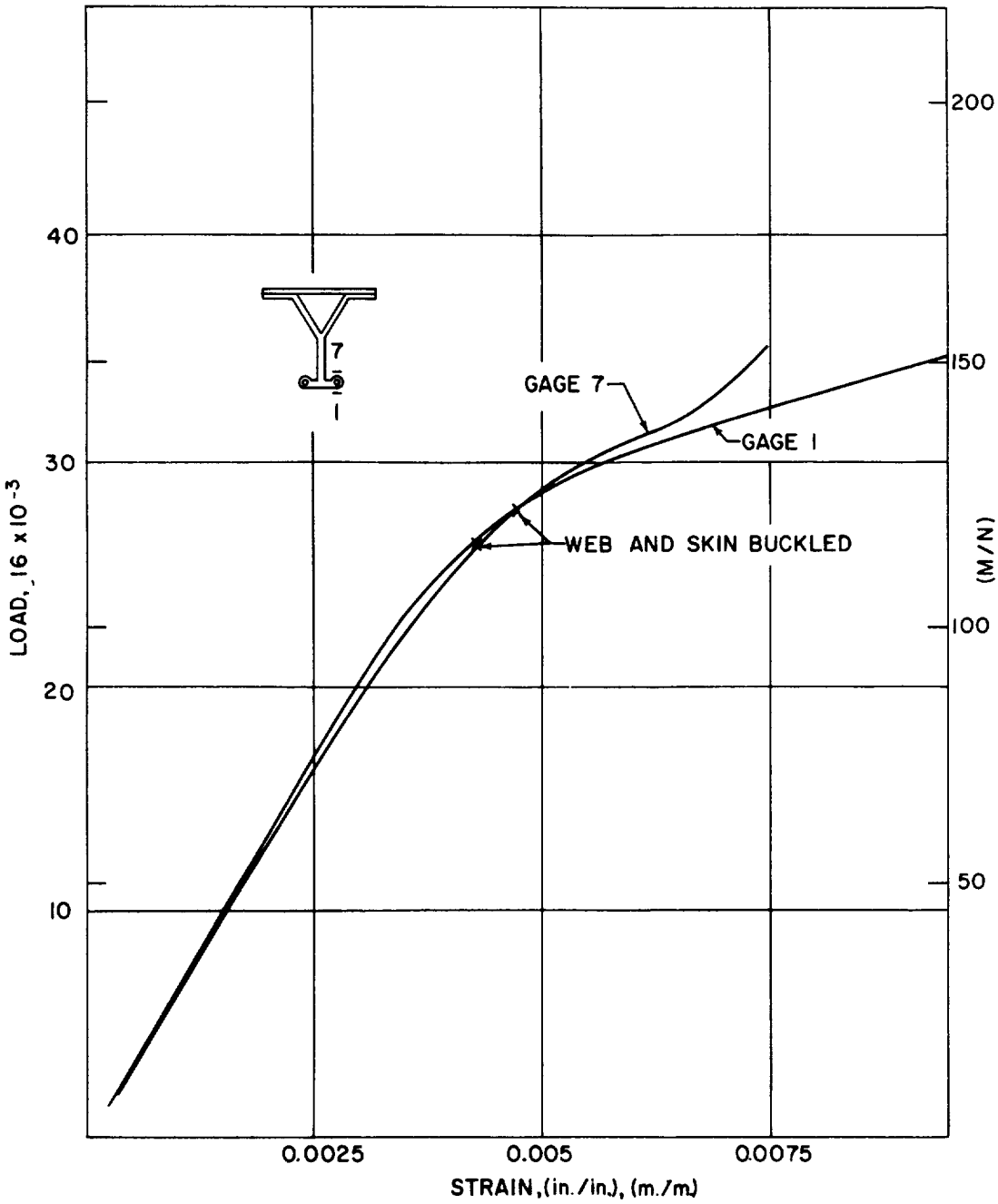

Figure 52 NACA - Y-2 LOAD-STRAIN CURVE

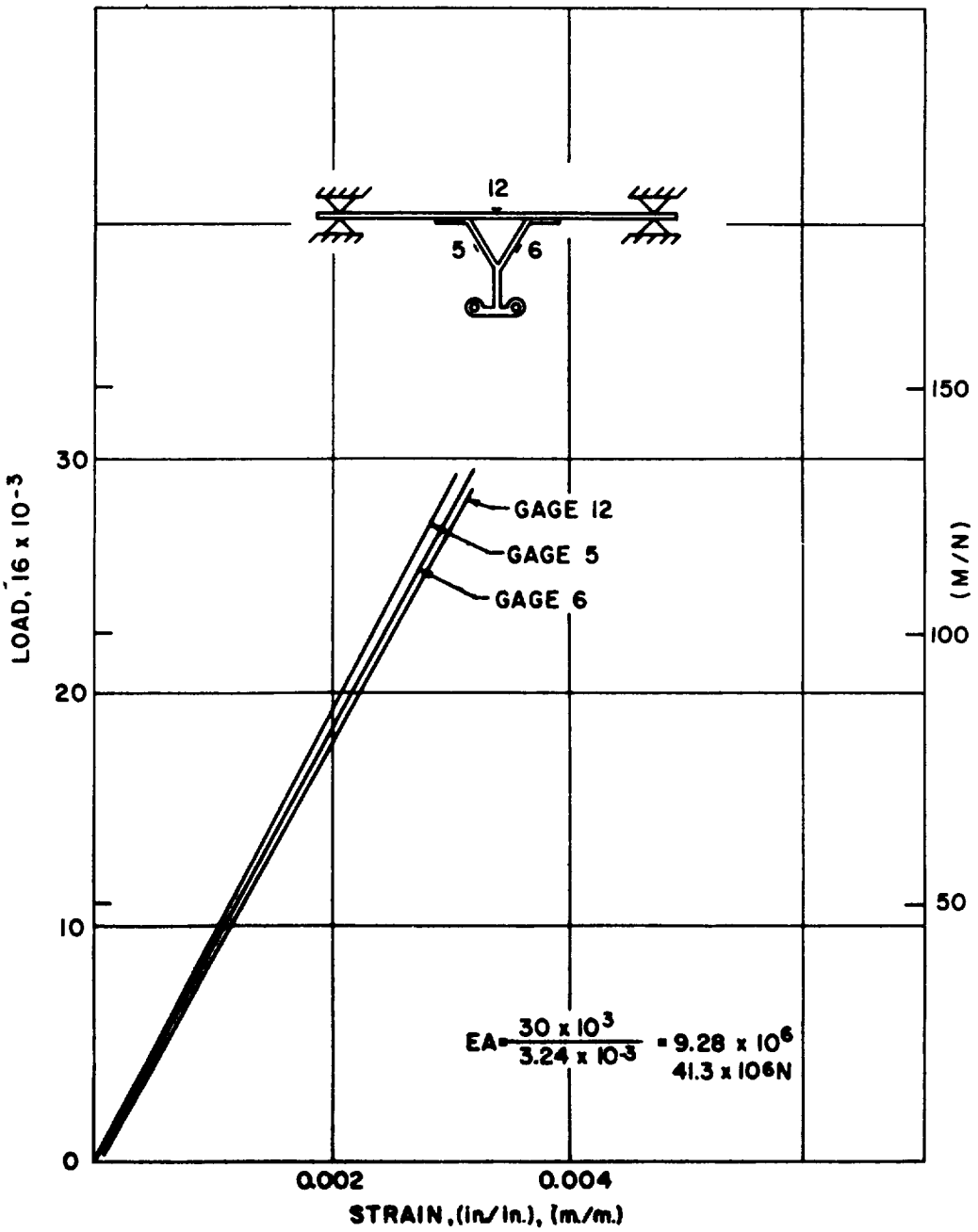

Figure 53 NACA - Y-3 LOAD-STRAIN CURVE

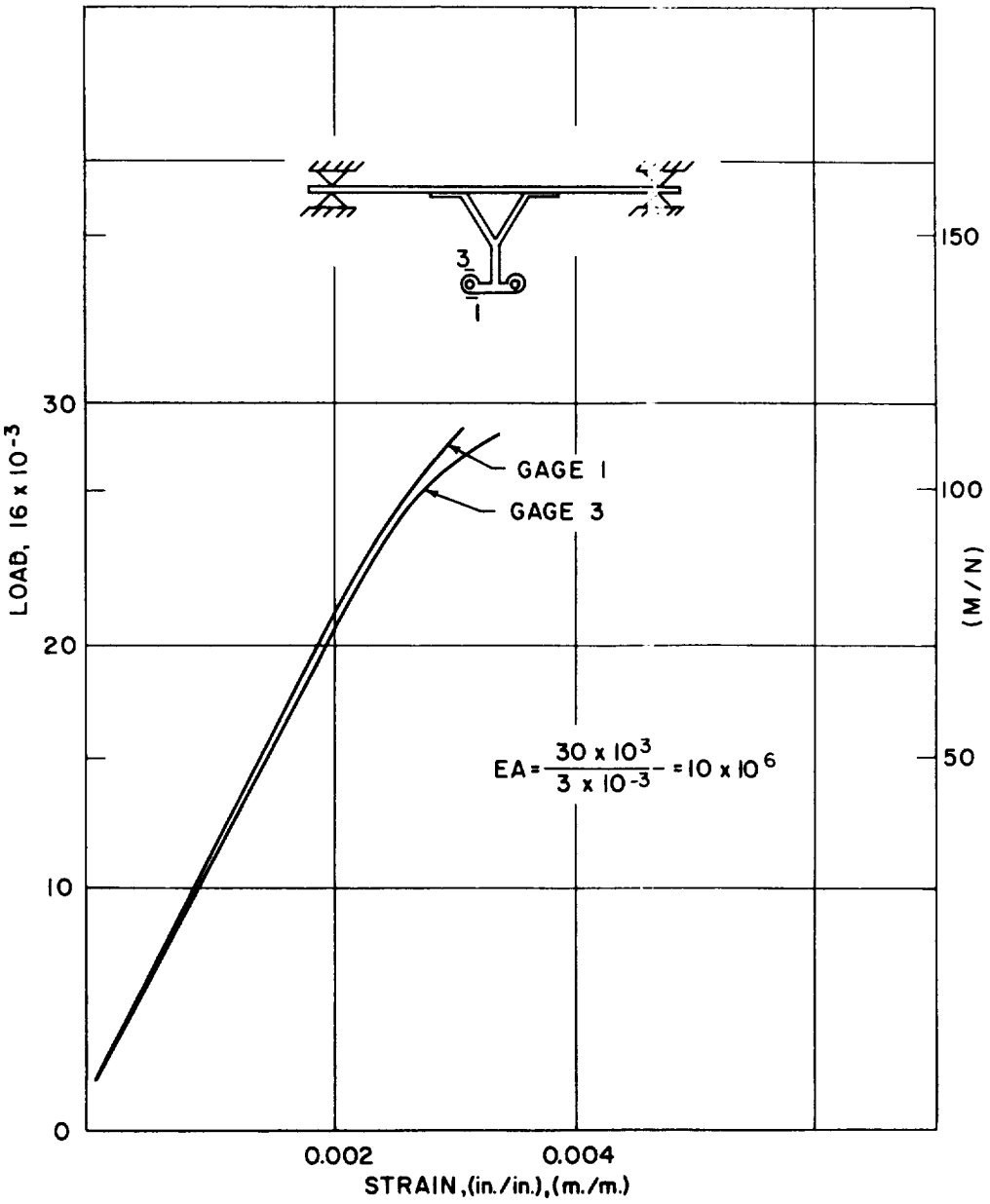

Figure 54 NACA - Y-4 LOAD-STRAIN CURVE

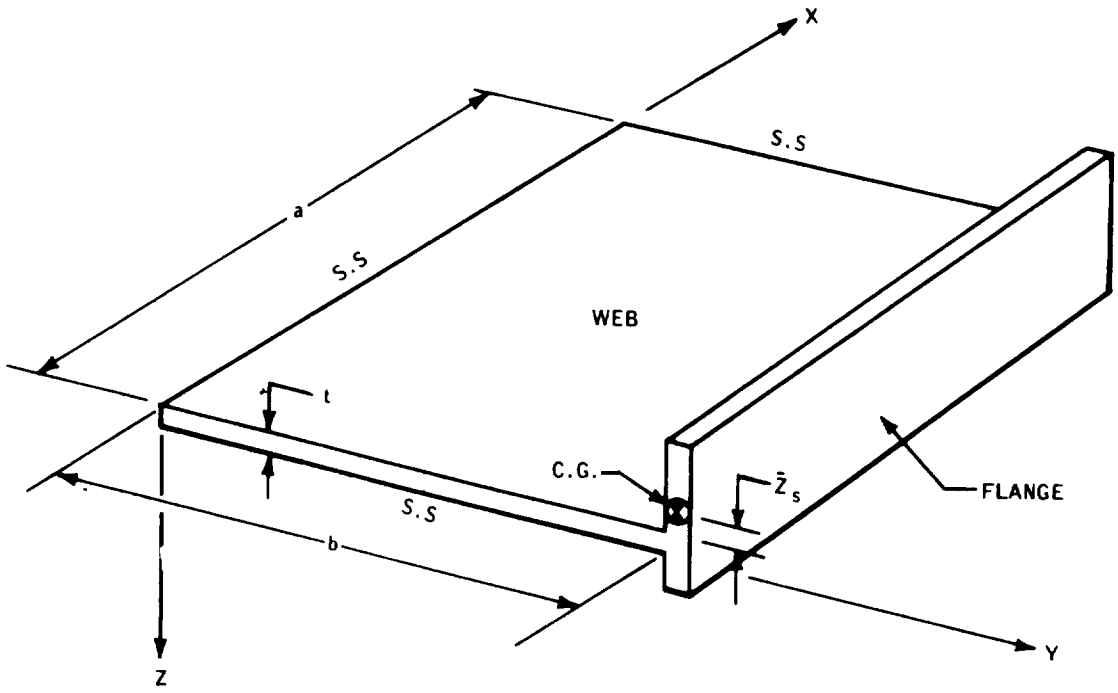

Figure A-1 ELASTICALLY SUPPORTED PLATE - STIFFENER MODEL

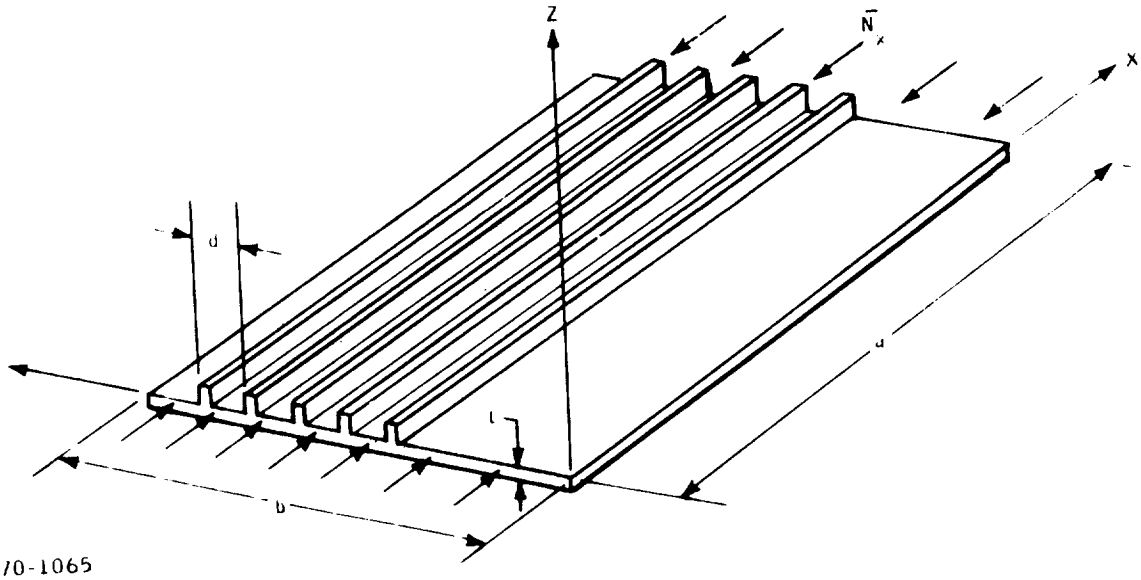

Figure B-1 PLATE GEOMETRY AND COORDINATE SYSTEM

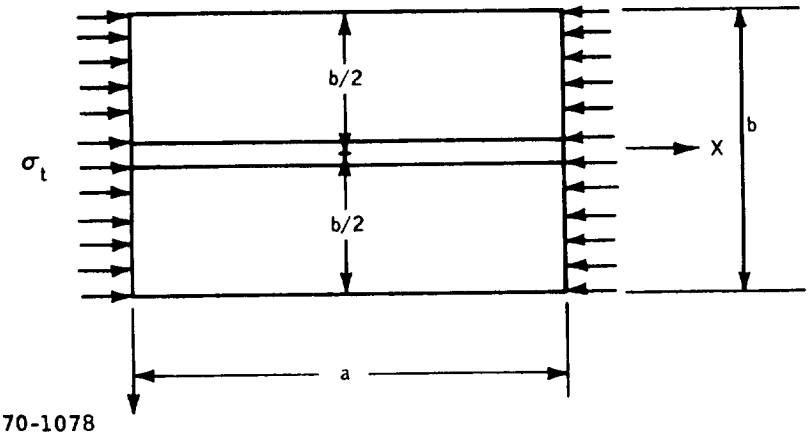

Figure C-1 PLATE - STIFFENER CONFIGURATION

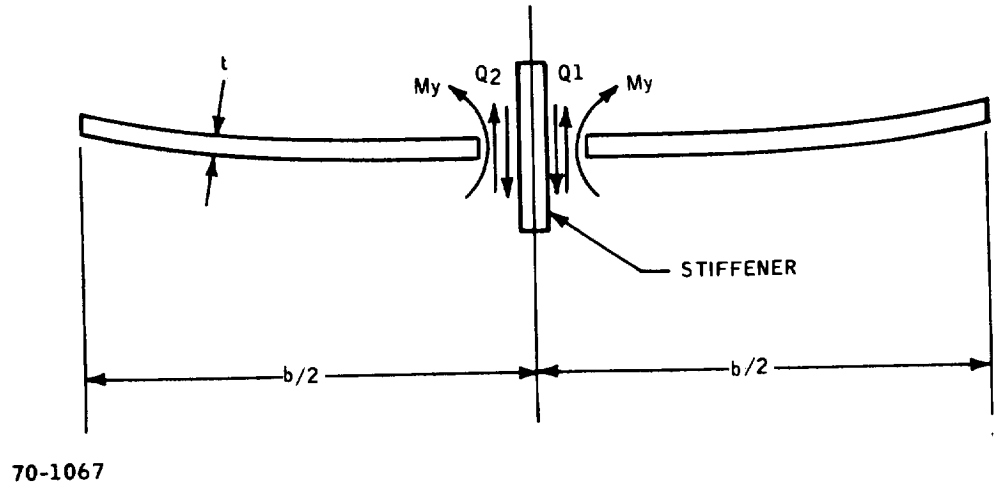

Figure C-2 PLATE - STIFFENER EQUILIBRIUM DIAGRAM